Role of SPFH proteins in aerobic respiration of *Escherichia coli*

Dissertation

zur Erlangung des Grades eines

Doktor der Naturwissenschaften

(Dr. rer.nat.)

des Fachbereichs Biologie der Philipps-Universität Marburg

Vorgelegt von

María Isabel Pérez López

Aus Bogotá D.C., Kolumbien

Marburg, 2023

Die vorliegende Dissertation wurde von September 2019 bis November 2023 am Max-Planck-Institut für terrestrische Mikrobiologie in Marburg unter Leitung von Prof. Dr. Victor Sourjik angefertigt.

Vom Fachbereich Biologie der Philipps-Universität Marburg (Hochschulkennziffer 1180) als Dissertation angenommen am _____

Erstgutachter: Prof. Dr. Victor Sourjik

Zweitgutachter: Prof. Dr. Martin Thanbichler

Weitere Mitglieder der Prüfungskommission:

Dr. Andreas Diepold

Prof. Dr. Lennart Randau

Tag der Disputation: _____

Contents

Abbreviations **8**

Zusammenfassung **10**

Summary **12**

1 Introduction **13**

1.1 SPFH membrane protein family 13

1.2 Eukaryotic SPFH proteins and lipid rafts 15

1.3 Discovery of lipid rafts/FMMs in bacteria 15

1.4 Constituent lipids of FMMs 17

1.5 SPFH proteins present in different bacterial species 18

1.6 SPFH proteins in Gram-positive bacteria 20

1.7 SPFH proteins in Gram-negative bacteria 20

1.8 SPFH proteins in *E. coli* 21

1.8.1 QmcA: quality control-related membrane complex 21

1.8.2 YqiK: flotillin inner membrane protein 21

1.8.3 HflK-HflC complex: high frequency of lysogenization 22

1.8.4 FtsH activity in *E. coli* 26

2 Aims **29**

3 Results **30**

3.1 Phenotypes of SPFH proteins in *E. coli* 30

3.1.1 Localization of SPFH proteins 30

3.1.1.1 Expression of GFP fusions under *trc* promoter 30

3.1.1.2 Expression under the native promoter 34

3.1.2 SPFH protein-protein interaction 36

3.1.2.1 Pull-down using protein extraction with Triton X-100 37

3.1.2.2 Pull-down using protein extraction with SMALP-30010P polymer 40

3.1.3 Phenotypic characterization of single and multiple SPFH knockouts 42

3.1.3.1 Growth at different temperatures 42

3.1.3.2 Growth under osmotic stress 45

3.1.3.3 Membrane fluidity 47

3.1.3.4 Growth under the influence of antibiotics 50

3.1.3.5 Biofilm assay 52

3.1.3.6 Growth under high aeration conditions 55
3.2 Characterization of HflKC complex in *E. coli* 58
3.2.1 Growth of *ΔhflKC* under different oxygen supply 58
3.2.2 Proteomics of Δ*hflKC* in different conditions 60
3.2.3 Proteomics of *ΔhflK* and *ΔhflC* individual deletions 65
3.2.4 Lipidomic profile of *ΔhflKC* strain 67
3.2.5 Effect of *ΔhflKC* on motility 69
3.2.6 Effect of *ΔhflKC* on MEP pathway 70
3.2.7 Oxygen consumption by *ΔhflKC* cells 71
3.2.8 *ΔhflKC* phenotype is restored with expression of IspG, an enzyme in the MEP pathway 73
3.2.9 *ispG* knockdown phenocopies *ΔhflKC* effects 75
3.2.10 Role of ArcAB system in *ΔhflKC* strain 77
4 Discussion 80
4.1 Phenotypes of SPFH proteins 80
4.1.1 SPFH fluorescent fusion proteins show similar localization patterns 80
4.1.2 Challenges in membrane protein extraction for pull-down analysis of SPFH proteins 81
4.1.3 Exploring the impact of SPFH proteins on growth, responses to temperature variations, and osmolality 83
4.1.4 Lack of SPFH protein reduces membrane fluidity at high temperature 84
4.1.5 Biofilm formation defect of SPFH proteins in *E. coli* 85
4.1.6 Tolerance of SPFH quadruple knockout to antibiotics 86
4.2 Regulation of aerobic respiration by HflKC complex 87
4.2.1 Lack of HflKC complex is important for *E. coli* growth under high aeration 87
4.2.2 Reduced levels of IspG account for the respiratory phenotype of *ΔhflKC* strains 88
4.2.3 Functional asymmetry of HflK and HflC in the regulation of FtsH activity 90
4.2.4 Cardiolipin and phosphatidylglycerol levels decrease in *ΔhflKC* strain 91
4.2.5 Lack of the HflKC complex affects the abundance of motility proteins 91
4.2.6 ArcAB system is active in *ΔhflKC* strain 92
4.2.7 What is the cause of the strong reduction of the IspG levels in *ΔhflKC* cells? 93
4.2.8 SPFH proteins and aerobic respiration in more complex organisms 94
4.2.9 Concluding remarks 95
5 Materials and methods 97
5.1 Reagents and kits used 97

5.2 Media and buffer solutions 98
5.3 Antibiotics and inducers 101
5.4 Molecular biology methods 101
5.4.1 Polymerase chain reaction (PCR) 101
5.4.2 DpnI treatment 102
5.4.3 Agarose gel electrophoresis 102
5.4.4 Gibson assembly 103
5.5 List of bacterial strains 103
5.5.1 Keio collection and P1 transduction 104
5.5.2 Lambda red 104
5.5.3 IspG knockdown 105
5.6 List of plasmids 105
5.6.1 Chemical competent cells with calcium chloride 106
5.6.2 Transformation 106
5.6.3 sfGFP-constructs: *trc* and native promoter 107
5.6.4 Sodium dodecyl sulfate-polyacrylamide gel electrophoresis (SDS-PAGE) 107
5.6.5 Western blot 108
5.6.6 Protein solubilization with Triton X-100 109
5.6.7 Protein solubilization with SMALP-30010P 110
5.6.8 Pull-down 110
5.7 Microbiology culture methods 111
5.7.1 Growth curve 111
5.7.2 Membrane fluidity with Di-4-ANEPPDHQ 111
5.7.3 Chemical library screening 112
5.7.4 Biofilm assay 112
5.7.5 Motility assay 113
5.7.6 Complemented phenotype of *ΔhflK*C 113
5.7.7 Measurements of Oxygen consumption 113
5.7.8 Measurement of reactive oxygen species (ROS) 113
5.7.9 Determination of membrane potential (MP) 114
5.8 Microscopy 114
5.8.1 Epifluorescence 114
5.8.2 Structured Illumination Microscopy (SIM) 114

5.8.3 Total internal reflection fluorescence (TIRF) Microscopy 115
5.9 Proteomics, metabolomics, and lipidomics 116
5.9.1 Abundance of proteins 116
5.9.2 Abundance of isoprenol substrate, Me-cPP 116
5.9.3 ATP measurements and energy change calculation 117
5.9.4 Lipid extraction and annotation 118
5.9.5 Abundance of ubiquinone-8 and uniquinol-8 120
References 121
Supplementary tables 131
Acknowledgements 151
Erklärung 153

Abbreviations

4-HB	4-hydroxybenzoate
ADP	Adenosine diphosphate
AMP	Adenosine Monophosphate
ATP	Adenosine Triphosphate
aTC	Anhydrotetracycline
BnOH	Benzyl Alcohol
CL	Cardiolipin
CoQ	Coenzyme Q
DCF	Dichlorodihydrofluorescein
$DiOC_2(3)$	3,3'-diethyloxacarbocyanine iodide
DMAPP	Dimethylallyl diphosphate
DMK	Demethylmenaquinone
DNP	Protonophore dinitrophenol
DRMs	Detergent-resistant membranes
DSM	Detergent-sensitive membrane
ETC	Electron transport chain
FMM	Functional Membrane Microdomains
FPP	Farnesyl diphosphate
GMM	Gaussian Mixture Modelling
GP	Generalized polarization
HMBPP	Hydroxymethylbutenyl 4-diphosphate
IPP	Isopentenyl diphosphate
ISPG	Isopropyl β-D-1-thiogalactopyranoside
LB	Luria-Bertani
Me-cPP	2C-methyl-D-erythritol 2,4-cyclodiphosphate
MEP	Methylerythritol phosphate pathway
MK	Menaquinone
MS	Mass spectrometry
NaCl	Sodium chloride

OD_{600}	Optical density
PC	Phosphatidylcholine
PG	Phosphatidylglycerol
ROS	Reactive oxygen species
SD	Standard deviation
SDS-PAGE	Sodium dodecyl sulfate-polyacrylamide gel electrophoresis
sfGFP	super folder Green Fluorescent Protein
SIM	Structured illumination microscopy
SPT	Single particle tracking
TB	Tryptone broth
TIRF	Total Internal Reflection Fluorescence Microscopy
WB	Western blots
WT	Wildtype

Zusammenfassung

SPFH ist eine Familie von Membranproteinen, die 1999 erstmals durch phylogenetische Analyse von Stomatinpoteinen von Tavernarakis und Kollegen entdeckt wurde. Der Name dieser Familie leitet sich von den Anfangsbuchstaben der dazugehörigen Proteine ab: Stomatin, Prohibitin, Flotilline und HflK-HflC. Alle Mitglieder dieser Protein-Familie teilen eine konservierte evolutionäre Domäne, die als SPFH-Domäne bekannt ist und auch als PHB (Prohibitin) Domäne bezeichnet wird. Seit ihrer Identifizierung wurden zahlreiche SPFH-Proteine in Organismen aller drei Lebensdomänen identifiziert. Interessanterweise zeigen alle Mitglieder dieser Familie eine hohe Ähnlichkeit in ihren Aminosäuresequenzen und Domänenstrukturen, was auf eine gemeinsame Funktion in Eukaryoten, Archaeen und Prokaryoten hindeutet.

In *Escherichia coli* gibt es vier Proteine, die die SPFH-Domäne enthalten. Dazu gehören QmcA, ein Stomatin-Protein, das mit einem membrangebundenen Qualitätskontrollkomplex assoziiert ist; YqiK, das zur Gruppe der Flotilline gehört und dessen Funktion unbekannt ist; sowie das Komplex HflK-HflC (HflKC), der die Aktivität der Metalloprotease FtsH moduliert. Überraschenderweise wurden SPFH-Proteine in *E. coli* bisher wenig erforscht, und wenig ist über ihre Funktionen in diesem Modellorganismus bekannt. In dieser Studie beabsichtigen wir, SPFH-Proteine systematisch mit verschiedenen Ansätzen zu charakterisieren, die die Lokalisierung, Proteininteraktionen, die biophysikalischen Eigenschaften der Membran und das Wachstum unter verschiedenen Stressbedingungen sowie andere Techniken umfassen.

Durch diese Analysen haben wir eine interessante Beobachtung gemacht: Das Fehlen des HflKC-Komplexes verursacht einen Wachstumsdefekt, der von der Atmung abhängig ist. Daher haben wir uns auf dieses Phänomen konzentriert, um seine Mechanismen genauer zu verstehen. Wir haben festgestellt, dass das Fehlen des HflKC-Komplexes die Menge an IspG beeinflusst, einem essentiellen Enzym im Isoprenoid-Biosyntheseweg. Wir konnten einen direkten Zusammenhang zwischen dem aeroben Wachstumsdefekt und dem Mangel an IspG nachweisen, was zu reduzierten Mengen an Ubichinon führt, einem Molekül, das eine wichtige Rolle als Elektronentransporter in aeroben Atmungsketten spielt. Infolgedessen weist der *hflKC*-Deletionsstamm eine reduzierte Atmung, niedrigere ATP-Spiegel und eine Abnahme des Membranpotenzials auf. Wir vermuten, dass das Fehlen des IspG-Proteins auf die Aktivität der FtsH-Protease zurückzuführen ist. In Abwesenheit des Schutzkäfigs, den der HflKC-Komplex bietet, ist IspG leichter zugänglich und wird schneller abgebaut. Wir schlagen ebenfalls vor, dass diese Regulation

der aeroben Atmung über die Isoprenoid-Biosynthese und Ubichinon-Spiegel in eukaryotischen Prohibitinen konserviert sein könnte. Dies könnte den zuvor berichteten Mangel an Atmung in Zusammenhang mit Prohibitin-Mutationen in Säugetier- und Hefezellen erklären.

Summary

SPFH is a family of membrane proteins initially discovered in 1999 through phylogenetic analysis of stomatin proteins by Tavernarakis and colleagues. The name of this family is derived from the initials of its constituent protein groups: stomatins, prohibitins, flotillins, and HflK-HflC. All members within this protein family share a conserved evolutionary domain known as the SPFH domain, also referred to as the PHB (Prohibitin) domain. Since its identification, numerous SPFH proteins have been found in all three domains of life. Interestingly, all members of this family exhibit a high degree of similarity in their amino acid sequences and domain structures, which could suggest a common function across eukaryotes, archaea, and prokaryotes.

In *E.* coli, there are four proteins that contain the SPFH domain. These include QmcA, a stomatin protein associated with a quality control-related membrane complex, YqiK, which belongs to the flotillin group and whose function remains unknown, and the complex HflK-HflC (HflKC), responsible for modulating the activity of FtsH metalloprotease. Surprisingly, SPFH proteins have been little explored in *E. coli* and little is known about their functions in this model organism. In this study, we aim to systematically characterize SPFH proteins using different approaches that include localization, protein interactions, biophysical properties of the membrane, and growth under different stress conditions, among other techniques. Through these analyses, we made an interesting observation: The absence of The HflKC complex causes a growth defect that is dependent on aeration. Therefore, we focused on this phenotype to further understand its origins.

We found that the absence of HflKC complex affects the abundance of IspG, a crucial enzyme in the isoprenoid biosynthesis pathway. We elucidated a direct link between the aerobic growth defect and lack of IspG, which leads to reduced levels of ubiquinone, a molecule that plays an important role as an electron transporter in aerobic respiratory chains. Consequently, the *hflKC* deletion strain exhibits reduced respiration, lower ATP levels, and a decrease in membrane potential. We hypothesize that lack of IspG protein is due to FtsH protease activity. In absence of the protective cage provided by HflKC complex, IspG is more accessible, resulting in faster degradation. Further, we propose that this regulation of aerobic respiration via isoprenoid biosynthesis and ubiquinone levels might also be conserved in eukaryotic prohibitins, which could explain previously reported lack of respiration associated with prohibitin mutations in mammalian and yeast cells.

1 Introduction

1.1 SPFH membrane protein family

In 1999, Tavernarakis and collaborators identified a novel family of proteins found in all three domains of life. The study performed a phylogenetic analysis using the Position-Specific Iterative-BLAST (PSI-BLAST) and stomatin protein sequences as reference due to their abundance in the membranes of human erythrocytes, but little was known about their function *in vivo*. The results of the analysis showed a common region that was highly similar to the prohibitin family of mitochondria proteins, the flotillins (reggie or caveolae), the bacterial plasma-membrane proteins HflK and HflC, and several proteins in archaea (**Figure 1.1**) [1]. This conserved region was named the SPFH domain, an acronym derived from the initials of the related protein families: stomatins, prohibitins, flotillins, and HflK/C, but also received the name of PHB domain. A common characteristic among all members of this family is their status as integral membrane proteins, with the SPFH domain located near the membrane-associated region [2].

The widespread conservation of the SPFH domain suggests that this motif could have a crucial function. However, recent phylogenetic analysis had some difficulties revealing their common ancestry and thus providing new insight about their functions. Some of the most relevant challenges arise from factors like lateral gene transfer or mixture of orthologs and paralogs genes [3] [4]. On the other hand, an interesting fact about SPFH proteins is that all members of this family share high similarity in amino acid sequence and domain organization, which could suggest a common function across eukaryotes, bacteria, and archaea. For instance, some of the most studied proteins in eukaryotic are the stomatins which share 29% of identity and 67% of similarity with QmcA in *E. coli*, and human flotillin exhibits 37% identity and 74% similarity with *B. subtilis.*

Importantly, SPFH proteins have been extensively studied in eukaryotic cells, while very little is known about their function in prokaryotic cells. Most of the known eukaryotic SPFH family members that have been investigated are involved in the scaffolding of proteins and specific lipids in membrane microdomains [2], suggesting that the SPFH domain may constitute a lipid recognition motif [5]. It wasn't until recently, with the discovery of the role of flotillins in lipid microdomains in *B. subtilis*, that increase the interest in studying SPFH proteins in prokaryotes. Significant progress has been achieved in Gram-

positive bacteria, where, for instance, FloT (formerly known as YuaG) is considered a marker for microdomains in *B. subtilis* [6], [7], and FloA is involved in the assembly of microdomains in *S. aureus* [8]. However, very little is known about the function of these proteins in Gram-positive bacteria.

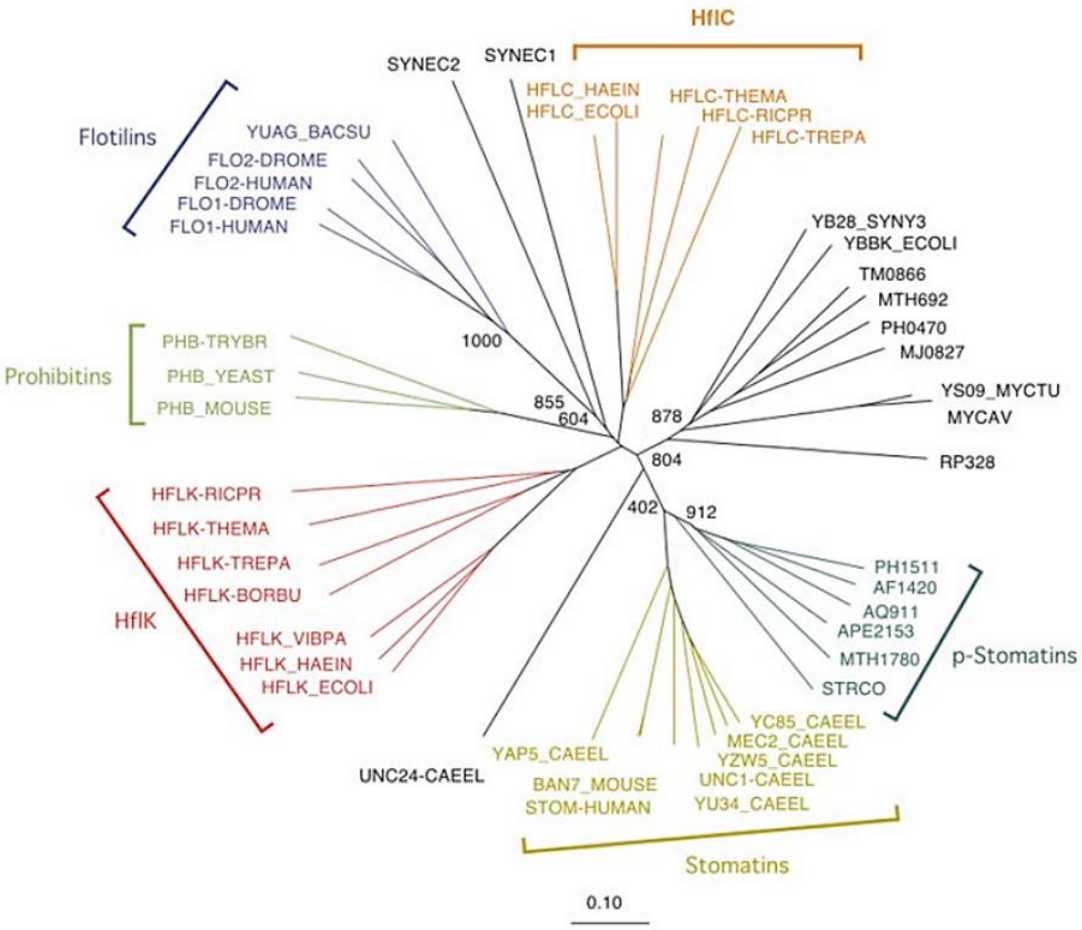

Figure 1.1 A dendrogram showing distance relationships between most of the SPFH protein family members. The phylogenetic analysis was constructed with the neighbor-joining method, based on pairwise distance estimates of the expected number of amino acid replacements per site (0.10 in the scale bar). Figure adapted from Tavernarakis N. et al., 1999 [1].

1.2 Eukaryotic SPFH proteins and lipid rafts

SPFH domain-containing proteins are known as lipid raft proteins due to their enrichment in detergent-resistant membranes (DRMs) fraction [9]. Lipid rafts are specialized membrane microdomains with a high content of sterols and sphingolipids, making them insoluble in non-ionic detergents and resulting in DRM and detergent-sensitive membrane (DSM) fraction [10], [11] [12]. These lipid rafts serve as platforms for various cellular processes, such as membrane transport, protein sorting, cholesterol and calcium homeostasis, and signal transduction [13].

SPFH can be found in diverse cellular locations, including the plasma membrane (PM), endosomes, Golgi apparatus, lipid droplets, mitochondria, and the endoplasmic reticulum (ER) [5], [9], [14]. These organelles contain high levels of glycosphingolipids (GSLs) and cholesterol, which are the primary components of lipid rafts, explaining the present of SPFH proteins in the DRMs [2]. In addition to their localization, SPFH proteins are considered key players in lipid microdomain formation, mediating the scaffolding of proteins and specific sterols within lipid rafts. Their association with lipid rafts appears to be facilitated by cholesterol binding, requiring the SPFH domain and specific sequences within the N-terminal hydrophobic domain [2].

Furthermore, SPFH proteins play roles in various biological processes, including the formation of specialized membrane structures, regulation of ion channels, chaperoning of membrane proteins, vesicle and protein trafficking, and membrane-cytoskeletal interactions, among others [5], [9], [15]. They are also associated with functions like inhibiting cell proliferation and neuronal regeneration, which have implications for diseases such as Alzheimer's and Parkinson's [2], [9], [15].

1.3 Discovery of lipid rafts/FMMs in bacteria

Lipid rafts or Functional Membrane Microdomains (FMMs) in bacteria were unexpectedly discovered during investigations of biofilm formation in *B. subtilis*. In 2009, Lopez D. and collaborators discovered that the sensor kinase KinC, responsible for triggering biofilm formation [16], became non-functional in a *ΔyisP* mutant unable to produce certain membrane-related polyisoprenoid lipids. However, when polyisoprenoid lipids were added to *ΔyisP*, KinC activity, and biofilm formation were restored [17]. YisP

acts as a phosphatase catalyzing the conversion of farnesyl diphosphate into farnesol [18]. The activity of several membrane-associated proteins is affected in *ΔyisP* mutant, including KinC [19], this leads to the hypothesis that bacteria could compartmentalize membrane-bound membrane-bound sensor kinases into FMMs with differing lipid compositions compared to the rest of the membrane.

The standard method developed for extracting eukaryotic lipid rafts is used to analyze the composition of FMMs in bacteria. This method is based on the unique lipid composition of lipid rafts, such as cholesterol in eukaryotes and cardiolipin in bacteria [20], which made them more compact and resistant to nonionic detergent treatment. The membrane fragments can be separated in a sucrose gradient experiment, resulting in DSM and DRM fractions. The analysis of protein composition in DSM and DRM fractions of *B. subtilis* and *E. coli* has revealed a diverse distribution of proteins, with many involved in cell signaling, transport, and protein secretion [17] [21].

Importantly, It has been shown that DRM fractions are enriched with homologues of the flotillin and prohibitin proteins found in eukaryotic cells, including FloT (previously named YuaG) and FloA (or YqfA) in *B. subtilis*, and HflKC and QmcA in *E. coli* [20]–[22]. While the exact function of these bacterial proteins in *E. coli* remains unclear, it has been demonstrated in *B. subtilis* that the absence of FloT leads to reduced sporulation efficiency due to defective activation of the signaling pathway for sporulation. This shows that FloT plays a significant role in the signaling pathways of *B. subtilis* [20].

It is important to mention that the existence of FMMs in bacteria remains a subject of debate since some contradictions have arisen around this topic. For instance, Lopez D. and collaborators demonstrated co-localization of FloT, FloA, and KinC in the DRM, and this co-localization disappears when cells are lacking polyisoprenoid lipids [17]. However, Dempwolff F. presented an alternative view, showing that FloT and FloA localize differentially and independently of each other [23]. In light of these different observations, the presence and role of FMMs in bacterial cells continue to be a subject of ongoing investigation, highlighting the need for further investigation.

1.4 Constituent lipids of FMMs

FMMs contain two crucial structural components consistently present under various experimental conditions. These components are the constituent lipids and the SPFH proteins, particularly flotillin which serve as markers of the presence of FMMs in bacteria membranes [2].

Genetic and biochemical investigations in *B. subtilis* have identified farnesol-derived polyisoprenoid lipids as key constituent lipids within FMMs [18]. While other lipids likely participate in FMM assembly, there is no precise notion of their molecular structure, which probably varies from one species to another. Extensive discussions have been done around the similarities and differences between FMMs and the structure of lipid rafts (**Figure 1.2 A, B**).

For instance, certain bacterial species produce cyclic polyisoprenoid lipids called hopanoids, which are structurally similar to eukaryotic cholesterol, a primary component of lipid rafts in eukaryotes [24]. In both Gram-negative and Gram-positive bacteria, hopanoids play crucial roles in maintaining membrane integrity, adapting to stress conditions, facilitating signal transduction, and contributing to cell division [25], [26]. Non-cyclic polyisoprenoid membrane lipids like carotenoids share similar chemical properties to hopanoids [27] and also regulate bacterial membrane rigidity [27], [28]. In *Staphylococcus aureus*, the absence of carotenoids leads to the mislocalization of flotillin proteins and FMMs [17], suggesting a structural role for carotenoids in FMM assembly. Additionally, carotenoids have two long fatty acid chains that potentially help in stabilizing FMMs within bacterial membranes [29].

Furthermore, Donovan and Bramkamp's study showed the formation of microdomains within *B. subtilis* membranes using the lipophilic dye NAO, which has an affinity for negatively charged phospholipids such as phosphatidylglycerol (PG) or cardiolipin (CL) [20]. Their research also demonstrated that flotillins and cardiolipin co-localize and both components can also be co-purified, indicating that cardiolipin has a potential role as one of the constituent lipids of FMMs.

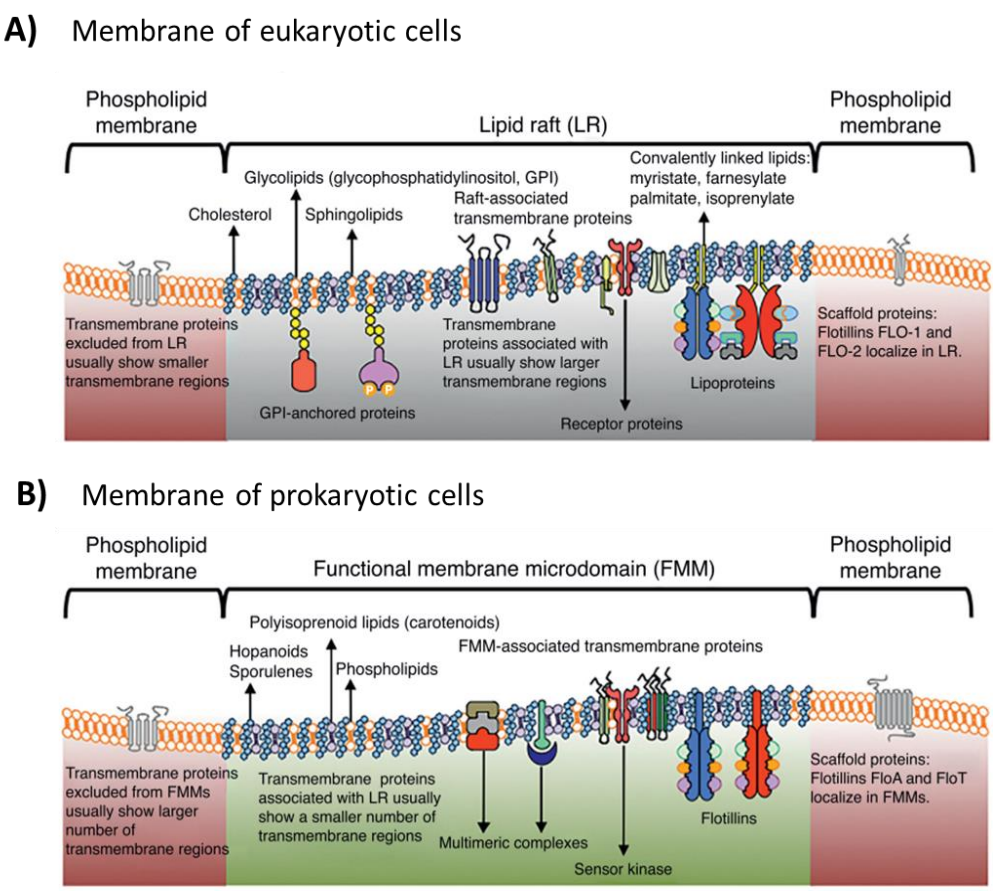

Figure 1.2 Scheme of the structural similarities and differences between eukaryotic and prokaryotic lipid domains.

(A, B) Lipid rafts composition in eukaryotic cells (A). Functional membrane microdomains (FMM) composition in prokaryotic cells (B). Figure adapted from Lopez D. & Koch G., 2017 [30].

1.5 SPFH proteins present in different bacterial species

The study of SPFH proteins in bacteria is an increasing area of study, with the goal of investigating other bacterial species to determine whether the organization of FMMs is a universal feature of bacteria and whether there are fundamental differences between different species. Currently, the most robust preliminary approach for screening the existence of SPFH proteins and FMMs in diverse bacterial species involves the use of bioinformatics tools.

In a phylogenetic study conducted in 2009, which included 466 fully sequenced bacterial genomes and 1486 SPFH bacterial proteins, 12 subgroups of SPFH proteins in bacterial phyla were identified (**Table 1**). The four largest subfamilies corresponded to the already mentioned stomatins, flotillins, HflK, and HflC, which collectively corresponded to 75% of all identified sequences. These subfamilies share two common structural features: at least one hydrophobic domain, likely representing transmembrane domains at the N-terminal of the protein, and a coiled-coil domain essential for oligomerization located in the C-terminal section [3].

The SPFH3a/b subfamily, which contains the HflKC proteins, is the second-largest SPFH subfamily in bacteria. However, it is notably absent from archaeal genomes and eukaryotes [3]. Despite being absent in eukaryotes, HflKC proteins could be considered functionally analogous to prohibitins in eukaryotic cells due to similarities in the structure of the membrane complex and their function as modulators of m-AAA protease activity. Furthermore, a recent publication showed that the human prohibitin 1 (PHB-1) secondary structure generated by Alphafold2 is well aligned with HflK [31].

Table 1 Distribution of the SPFH family within different bacterial phyla*

Bacteria (*)\SPFH subgroup	1a	1b	2a	2b	2c	3a/b	4	5	6	7	8	9	10	11a/b	12
Actinobacteria (42)	32	-	14	-	2	-	-	-	11	5	4	2	5	-	2
Aquificae (1)	-	1	-	-	-	-	-	-	-	-	-	-	-	-	-
Bacteroidetes/Chlorobi (27)	2	6	4	1	5	1	14	5	5	10	6	1	1	-	-
Chlamydiae (8)	-	-	-	-	-	-	-	1	-	-	-	-	-	-	-
Chloroflexi (8)	-	8	-	-	-	-	5	-	-	-	2	-	-	4	-
Cyanobacteria (31)	19	-	8	-	-	-	30	-	-	-	1	5	-	-	4
Deinococcus-Thermus (2)	1	-	1	-	-	-	1	-	1	-	-	-	-	-	-
Acidobacteria (2)	-	2	2	-	-	-	-	-	-	-	1	1	-	1	-
Firmicutes (73)	14	2	24	-	-	7	4	23	19	11	14	1	-	-	2
Fusobacteria (3)	3	-	1	-	-	-	1	-	-	-	-	-	-	-	-
Planctomycetes (3)	-	-	1	-	2	-	-	3	1	-	3	2	-	1	-
Alphaproteobacteria (87)	54	10	-	15	-	81	3	-	15	-	22	3	4	-	2
Betaproteobacteria (40)	33	25	-	3	-	38	6		-	-	12	7	1	-	2
Deltaproteobacteria (21)	12	12	2	-	3	10	4	-	-	-	15	2	3	1	1
Epsilonproteobacteria (15)	3	-	-	-	-	-	15	-	-	-	-	-	-	-	-
Gammaproteobacteria (113)	75	31	-	16	8	104	15	-	7	2	3	8	1	-	-
Spirochaetales (7)	3	-	-	-	-	5	2	-	-	-	3	1	-	-	-
Thermotogae (6)	5	-	-	-	-	5	-	1	-	-	-	-	-	-	-
absolute numbers	**256**	**97**	**57**	**35**	**20**	**251**	**100**	**33**	**59**	**28**	**86**	**33**	**15**	**7**	**13**

*Table adapted from Hinderhofer M., et al. 2009 [3].

1.6 SPFH proteins in Gram-positive bacteria

The majority of research on SPFH proteins in bacteria has been performed on Gram-positive bacteria. Among different organisms, *B. subtilis* is the most studied model for studying bacterial SPFH, particularly flotillins. In *B. subtilis*, two different flotillins are expressed, known as FloA and FloT [23].

FloA and FloT have similar molecular structures, with a predicted transmembrane region adjacent to a PHB domain. Notably, FloA contains 331 amino acids while FloT has 509 amino acids, the larger structure is due to its extended C-terminal region spanning an additional 178 amino acids [29]. A distinct group of *Bacillus* species, known as the *Bacillus cereus* group, which includes species like *B. cereus*, *B. anthracis* (a human pathogen), and *B. thuringiensis* (an insect pathogen), encode a gene for FloT, but do not express FloA. The precise reasons behind the absence of the FloA gene in the *B. cereus* group remain unknown. It is unclear what factors lead to the expression of two different flotillins in one species, like *B. subtilis*, or only a single FloT-like flotillin in another, such as those within the *B. cereus* group [29].

In parallel, *S. aureus* also encodes a unique flotillin in its genome, FloA, with an 84% similarity to FloA in *B. subtilis*. Interestingly, it has been shown that FloA plays a crucial role in the disassembly of FMMs, which contributes to enhancing the bacterium's virulence by reducing its tolerance to antibiotic resistance [8], [32].

1.7 SPFH proteins in Gram-negative bacteria

The role of SPFH proteins and the study of FMMs in Gram-negative bacteria have not been extensively study. *Escherichia coli* belongs to the class Gamma-proteobacteria, along with *Salmonella* and *Pseudomonas*. *E. coli* has four SPFH proteins, QmcA, YqiK considering a flotillin, and HflK and HflC that are exclusively present in bacteria and are considered to be homologs of prohibitin protein in eukaryotic cells.

P. aeruginosa possesses two distinct flotillin-encoding genes within its genome, denoted PA3729 and PA0452. PA3729 encodes a 688-amino-acid flotillin characterized by an extensive C-terminal region, structurally resembling FloT in *B. subtilis*. In contrast, PA0452 encodes a 264-amino-acid flotillin protein with a smaller C-terminal region, making it structurally similar to FloA in *B. subtilis*. In the genome of *Caulobacter crescentus*, there is a gene, CC3375, which encodes a flotillin similar to FloA in *B. subtilis.*

1.8 SPFH proteins in *E. coli*

1.8.1 QmcA: quality control-related membrane complex

In 2006, Chiba and colleagues studied a new *E. coli* membrane protein with an SPFH domain, and it was annotated as QmcA or also referred to as YbbK [33]. Protease accessibility assays were performed to determine QmcA orientation in the membrane. These experiments showed that QmcA has a type I (N_{OUT} -C_{IN}) topology, with its N-terminus oriented to the periplasm and a large cytoplasmic domain This topology is similar to some eukaryotic PHB proteins, such as stomatin [20][35].

QmcA knockout was grown at different temperatures, but no growth effects were observed. Additionally, disrupting *qmcA* or overproducing QmcA had no apparent impact on the degradation of membrane proteins like SecY and YccA, both of which are substrates of FtsH [33].

Remarkably, Chiba's study demonstrated that QmcA forms an oligomeric complex, with sizes ranging from 500 to 1000 KDa. Pull-down experiments confirmed that QmcA physically interacts with FtsH. However, it remains unclear whether QmcA can modulate the proteolytic activity of FtsH similarly to HflKC (see below). It remains possible that QmcA regulates FtsH action on substrates that are not affected by HflKC [33]. Furthermore, Chiba's study, found no observable effects of QmcA knockout on the lysogenic state of phage λ, in contrast to the HflKC disruption that markedly enhanced the lysogenic state [34]. This finding suggests that the function of QmcA and the HflK-HflC complex may not entirely overlap and they might have unique cellular roles.

Fluorescent microscopy showed that *E. coli* QmcA-GFP form a punctate foci on the membrane distributed throughout the cell body, with 96% of the cells harboring 5 foci or more [36]. In the same study, it was shown that lack of cardiolipin causes mis-localization of QmcA.

1.8.2 YqiK: flotillin inner membrane protein

E. coli has another member of the SPFH family, an inner membrane protein known as YqiK. The topology of YqiK on the membrane has been predicted using bioinformatics tools and homology comparisons with previously reported PHB family proteins. In 2019, a study revealed that YqiK has an N-terminus transmembrane region adjacent to the PHB domain and a large C-terminus region, the same study indicated that YqiK gen code a protein with 553 amino acids [37]. However, no depth structural analysis

has been conducted on this protein, thus limiting our understanding of its detailed structure and localization in the membrane.

The motivation to study the biological functions of YqiK comes from its intriguing similarity to other proteins. Specifically, YqiK exhibits a 45% similarity and a 26% amino acid identity with FloT in *B. subtilis*. Notably, this similarity becomes even more significant when compared to a flotillin found in a Gram-negative bacterium, *Pseudomonas aeruginosa*, where YqiK shares an impressive 90% similarity [29].

In 2009, Hinderhofer and colleagues conducted a study on YqiK's biological function and deletion defects in *E. coli*. Their findings indicated that YqiK is not induced by general cellular stress factors like oxidative growth conditions or changes in osmolarity. However, they observed an enhanced swimming behavior in *yqiK* mutants which could favor chemotaxis. In overall, deletion mutants did not exhibit growth defects under standard or the above mentioned stress conditions, suggesting that YqiK might function under very specific, as yet unknown conditions [3].

Regarding YqiK's cellular localization, it has been reported that overexpression of YqiK displays a punctate localization within the *E. coli* membrane [17]. In contrast, when a native promoter is used for its expression, the protein is poorly visible [36]. Moreover, overexpression of YqiK shows a marked effect on cell morphology, bacteria that overexpress YqiK are larger than wild-type cells and contain opaque cellular inclusions suggesting potential lipid overproduction [3].

1.8.3 HflK-HflC complex: high frequency of lysogenization

E. coli's HflK and HflC are considered to be part of the SPFH superfamily because they both have the evolutionarily conserved domain PHB (prohibitin homology) domain [25],[26]. HflK and HflC are regulators of FtsH function for the lysogenic decision of λ phage by protecting cII lysogenic protein for the degradation of FtsH [34], [38]. Moreover, the HflKC complex inhibits the SecY-degrading activity of FtsH, possibly helping quality control of integral membrane proteins [39]. FtsH is an ATP-dependent zinc metalloprotease for both cytoplasmic and membrane proteins, and it has a large list of substrates involved in different cellular processes [40].

Cryo-EM analysis revealed very interesting features for the HflKC-FtsH (KCH) complex that provided new insights into the understanding of the role of this complex *E. coli*. The overall structure of the KCF complex resembles an inverted circular cage on the membrane, with the cup wall formed by circularly arranged 12

copies of HflK–HflC dimers and four FtsH hexamers to form a higher order complex of about 2.7MDa [41] Consistent with the previously determined topology of these proteins [34] most sequences of HflK/C locate in the periplasm, whereas the two-layered catalytic domains of FtsH are anchored on the cytoplasmic side of the membrane (**Figure 1.3 A, B**).

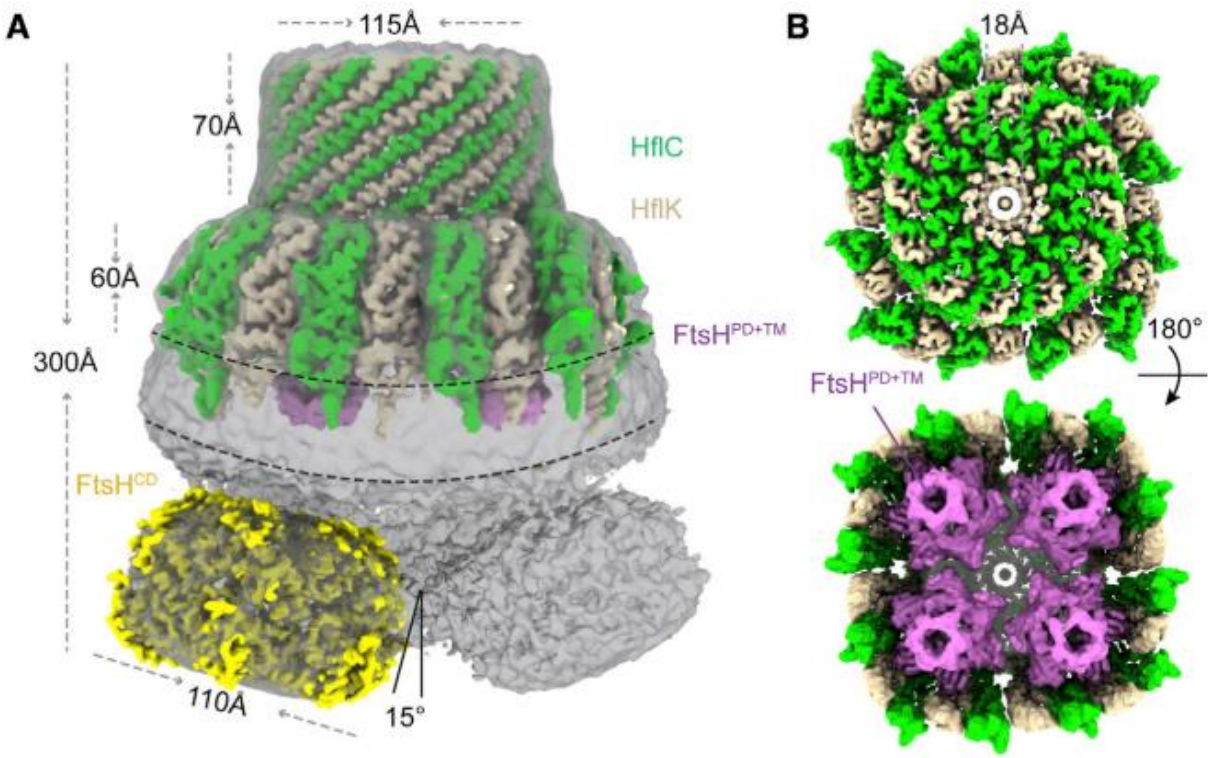

Figure 1.3 Cryo-EM map of the HflKC-FtsH complex.
(A, B) Overall 3D-reconstructed map of the HflKC- FtsH complex. Side view of the complex (A). Top and bottom view of the complex (B). $FtsH^{CD}$: cytoplasmic domain, $FtsH^{PD+TM}$: periplasmic domain + transmembrane helices. Figure adapted from Ma C. et al., 2022 [31].

Both HflK and HflC are type II membrane proteins, with a single N-terminal transmembrane helix (TM helix). Despite their significant sequence divergence, with only a 13% sequence identity, they share a highly conserved three-dimensional structure [31], [41]. Following the TM helix (α1), both proteins can be

divided into four distinct domains: two conserved SPFH domains (SPFH1 and SPFH2), coiled-coil domains (CC1 and CC2), and a C-terminal domain (CTD) (**Figure 1.4 A**, **B**).

An interesting discovery pertains to the SPFH1 domains of HflK and HflC, which consist of five antiparallel β-strands (β1–β5) and contain several hydrophobic residues, indicating their crucial role in membrane insertion. The structures of SPFH2 domains are very similar to previously reported fragment structures of other SPFH family members, displaying an α/β-fold with three β-strands and four α-helices [42]. The following coiled-coil domains of HflK and HflC are long α-helices (94 residues), which are divided into two pieces, CC1 (α6) and CC2 (α7) [31], [41].

HflK and HflC differ from each other in several insertion sequences: I) HflK possesses an additional N-terminal extension (NTE, residues 1–78) which contains 23 glycine residues. II) HflC contains two insertions in its SPFH1 and SPFH2 domains: a short β-hairpin between β2 and β3 of the SPFH1 domain, and an insertion in the α5 of the SPFH2 domain. III) The sequences and structures of the C-terminal domains (CTDs) of HflK and HflC are sharply different. The CTD of HflC starts with a short β-strand (β9), followed by a helix (α8), with the C-terminus exposed in the periplasmic space. In contrast, the CTD of HflK is characterized by an additional β-strand (β10) following β9, which turns around and places the C-terminal extension (CTE, residues 351–419) of HflK inside the KCF complex [31], [41].

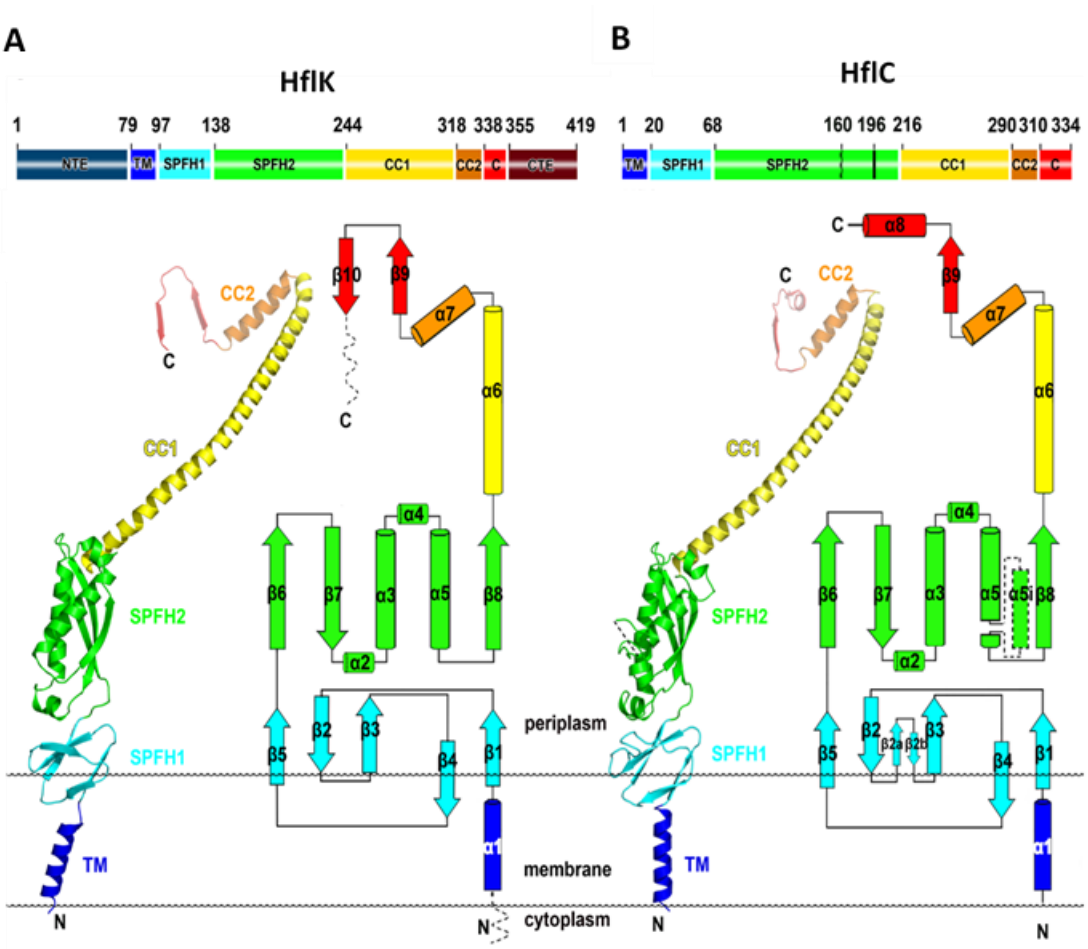

Figure 1.4 Structure and domain organization of HflK and HflC proteins.

(A, B) Schematic illustration of the domain organization of HflK (A) and HflC (B) with the atomic model and the secondary structure topology. Domains are separated by different colors. Figure adapted from Ma C. et al., 2022 [41].

Ma C. and colleagues proposed that FtsH interacts exclusively with HflK [41]. This observation was later validated by Qiao and colleagues, who noted that the hexameric FtsH periplasmic domain establishes connections with two HflK proteins separated by a single HflC. In one FtsH subunit, the b2-b3-turn loop, composed of residues K61, D62, and S63, forms strong interactions with b4 in HflK (**Figure 1.5**) [31]. Another interesting finding is the similarity of the 3D structure of the HflK-FtsH with the eukaryotic PHB1 and its metalloprotease AFG3L2. In the study, the model predicted by Alphafold2 of the PHB domain of human prohibitin 1 aligns well with HflK in *E. coli* [31] suggesting a possible common role of these SPFH proteins.

Based on the architecture of the KCF, Ma C. and collaborator suggests a straightforward model where HflK and HflC limit the substrate access to FtsH hexamers by confining the enzyme in a laterally segregated space. The HflKC complex therefore represents an additional layer of regulation on the proteolytic activity of FtsH. Similar to HflKC, loss of PHB1 or PHB2 in yeast also accelerated proteolysis of non-assembled mitochondrial inner membrane proteins by m-AAA proteases [43].

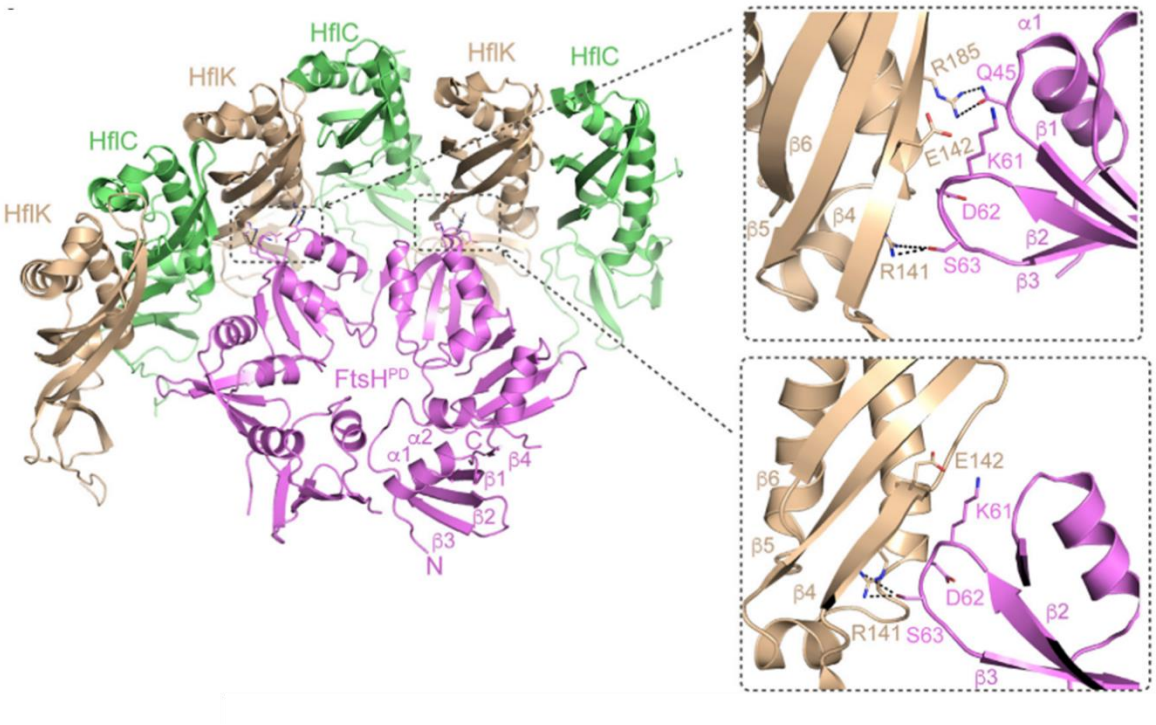

Figure 1.5 Interactions of HflK and FtsH.

The FtsH^{PD} hexamer interacts with the HflKC complex. The residues involved in the interaction are labeled and shown in sticks. Figure adapted from Ma C. et al., 2022 [31].

1.8.4 FtsH activity in *E. coli*

Many regulatory circuits or metabolic pathways are controlled by proteolysis to facilitate the immediate responses to external influences. Furthermore, proteases are crucial for cellular quality control. *E. coli* has

five AAA+ proteases: ClpXP, ClpAP, HslUV, Lon, and FtsH. All these proteases serve important cellular functions, but only FtsH is essential for the viability of *E. coli* [44].

FtsH is conserved in bacteria, mitochondria, and chloroplasts, and plays a role in many cellular pathways through regulated proteolysis of certain proteins [44]. One function of bacterial FtsH is, as a component of stress response, to degrade cytosolic proteins including the heat-shock transcription factor σ^{32}, a key enzyme LpxC in lipid A biosynthesis, and a phage transcription factor λCII which regulates lysis/lysogeny decision of phage λ [45]. Its mitochondrial homologs form two types of FtsH-related AAA- proteases (m-AAA and i-AAA proteases), both of which are anchored to the mitochondrial inner membrane. While the m-AAA protease has a similar topology as bacterial FtsH, the i-AAA protease exposes its enzymatic domains in the intermembrane space [46].

FtsH ATPase and proteolytic activity reside on a single poly- peptide that is ~650 aa in length. N- terminal part of the polypeptide chain is anchored to the lipid bilayer and has two transmembrane (TM) helices. A small periplasmic region is located between the two TM helices. The membrane-spanning part is connected to the AAA module via a glycine-rich linker of ~15–20 aa in length. The AAA module contains the characteristic sequence motifs of the AAA family, namely Walker A and B as well as the pore residues and the second region of homology (SRH) fingerprint [44]. The characteristic zincin HEXXH motif (HEAGH) identifies the protease active center. At the C-terminus, there is a leucine-rich motif that has been implicated in co- recognition of certain substrates [47].

For FtsH activity, the region required for the degradation initiation can be located at either end of the substrate. Recognition of the substrate is sequence-independent and requires exposed N or C terminus of approximately 20 or 10 aa in length [48]. Although it is not certain whether such a site indeed represents the position of degradation initiation, the simplest interpretation would be that FtsH can catalyze the degradation of proteins in either direction depending on the substrate. Then, some commitment steps allow the entry of the substrate into the hexamer cavity pore region of the ATPase domain. The conserved coiled-coil region in the C-terminal region of FtsH might also contribute to the substrate binding since alterations of a leucine residue here affect the FtsH binding to cII [49]. It is important to note that membrane protein substrates and cytoplasmic protein substrates may be recognized by FtsH by a different mode of interaction (**Figure 1.6 A, B**). After the bindings step, ATP hydrolysis triggers conformational changes in the AAA+ ring resulting in a pulling of the substrate towards the narrow pore, eventually resulting in unfolding and cleaving in the protease domain. Proteins are degraded into small peptides of ~6–25 aa in length [44], [45].

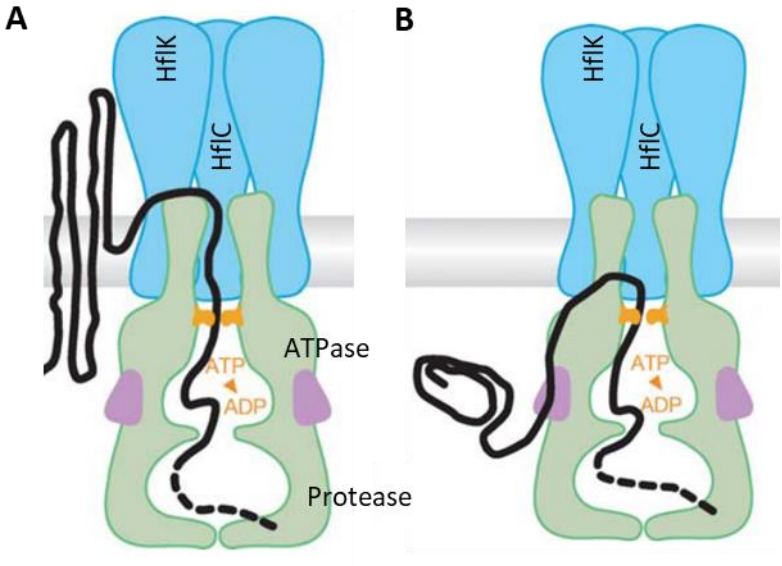

Figure 1.6 Possible entry route for FtsH substrates.

(A, B) Membrane protein substrates (A), and cytoplasmic protein substrates (B). Figure adapted from Ito K. & Akiyama Y, 2005 [45].

2 Aims

The SPFH membrane protein family is found across different species from eukaryotes to prokaryotes. Interestingly, all members of this family share high similarity in amino acid sequence and domain organization, which could suggest a common function in all three domains of life. While extensive work has been carried out to elucidate their function in Gram–positive bacteria such as *B. subtilis* and *S. aureus*, very little is known about their role in Gram-negative bacteria. This work aimed to answer some questions about the function of SPFH proteins in *E. coli.*

At first, we aimed to characterize all four SPFH proteins HflK, HflC, QmcA, and YqiK, by using different approaches including localization studies, protein-protein interaction analysis, testing biophysical properties in the membrane, and screening growth under different conditions. We then focused on a function of the HflKC complex, following our observation that absence of these proteins has a growth defect dependent on aeration.

We further investigated this phenotype, and collectively our data led us to conclude that the absence of HflKC complex causes a decrease in the abundance of the isoprenol enzyme IspG, and consequently a decrease of ubiquinone levels. Since ubiquinone plays a crucial role as an electron transporter molecule in aerobic respiratory chains, there was a strong decrease in respiration of *E. coli* lacking the HflKC complex and changes in expression of respiratory proteins. This enabled us to postulate a novel function for the HflKC complex in the regulation of aerobic respiration.

3 Results

3.1 Phenotypes of SPFH proteins in *E. coli*

3.1.1 Localization of SPFH proteins

3.1.1.1 Expression of GFP fusions under *trc* promoter

In this study, we investigated the expression and cellular localization of the SPFH proteins HflK, HflC, QmcA, and YqiK. Gibson assembly was used to create fusion constructs with super folder GFP (sfGFP) at both C-terminus and N-terminus. sfGFP was chosen as the fluorescent tag due to its brightness and rapidly folding kinetics in comparison to the standard EGFP [50]. We used pTrc99A plasmid as a vector given its strong *trc* promoter, which is inducible by isopropyl β-D-1-thiogalactopyranoside (IPTG), facilitating the control of the expression of proteins of interest. All SPFH fusion proteins have a flexible linker sequence (Gly-Gly-Gly-Gly-Ser) that connects with sfGFP. All SPFH fusions were verified by sequencing and then transformed into *E. coli* MG1655.

The integrity and stability of SPFH fusions were validated by sodium dodecyl sulfate-polyacrylamide gel electrophoresis (SDS-PAGE) and immunoblotting with anti-GFP antibody. All strains were cultivated in LB medium, induced with 2µM IPTG, and collected at an optical density of 0.4-0.6 measured at 600nm. *E. coli* MG1655 carrying the pTrc99A_sfGFP was used as a control. Notably, C-terminus-tagged SPFH proteins exhibited a dominant band corresponding to the expected molecular mass of the full-length fusion, sfGFP (26.8 KDa), HflK-sfGFP (72.3 KDa), HflC-sfGFP (64.4 KDa), QmcA-sfGFP (60.4 KDa), YqiK-sfGFP (87.5 KDa). Multiple bands were detected for HflK-sfGFP and HflC-sfGFP, which could be explained by partial degradation of these proteins that result in fragments that appear as additional bands. On the other hand, N-terminus-tagged proteins were not expressed (**Figure 3.1 A**). Even though sfGFP is smaller than its standard molecular GFP, it may affect the proper localization of the membrane protein within the membrane. This effect could result in mislocalization and reduced stability, ultimately leading to complete protein degradation. Given that SPFH proteins C-terminus-tagged present good stability, our subsequent analyses focused exclusively on the C-terminus constructs.

We further performed microscopy experiments to study the distribution and localization of SPFH proteins in the membrane. All SPFH-sfGFP proteins expressed in pTrc99A were transformed into the corresponding SPFH knockout strain to ensure a unique copy of the gene. After growth in TB medium and 2μM IPTG induction, bacterial cells were spread on 1% agarose pads prepared in 1X PBS buffer. Fluorescent microscopy was performed with a Nikon Eclipse *Ti* and an oil immersion objective (100x). *E. coli* MG1655 carrying pTrc99A with sfGFP alone exhibited uniform cytoplasmic localization (**Figure 3.1 B**). On the contrary, SPFH-sfGFP fusion proteins displayed multiple spots distributed within or proximate to the cell membrane. HflK-sfGFP, HflC-sfGFP, and QmcA-sfGFP displayed spots at cell poles and lateral borders. YqiK-sfGFP exhibited a higher number of spots also located at cell poles and lateral borders.

Structured illumination microscopy (SIM) was used to enhance the visualization of SPFH-sfGFP spots and to study their dynamics. We did time-lapse imaging consisting of 50 frames with continuous acquisition every 110 milliseconds per frame. SIM time-lapse corroborated the membrane localization of SPFH proteins C-terminus sfGFP-tagged (**Figure 3.1 C**). Similar protein distribution is observed for HflK-sfGFP, HflC-sfGFP, and QmcA-sfGFP, with bigger immobile spots located at the cell pole and smaller mobile spots distributed along the membrane, while YqiK-sfGFP exhibited mostly big and relatively dynamic spots.

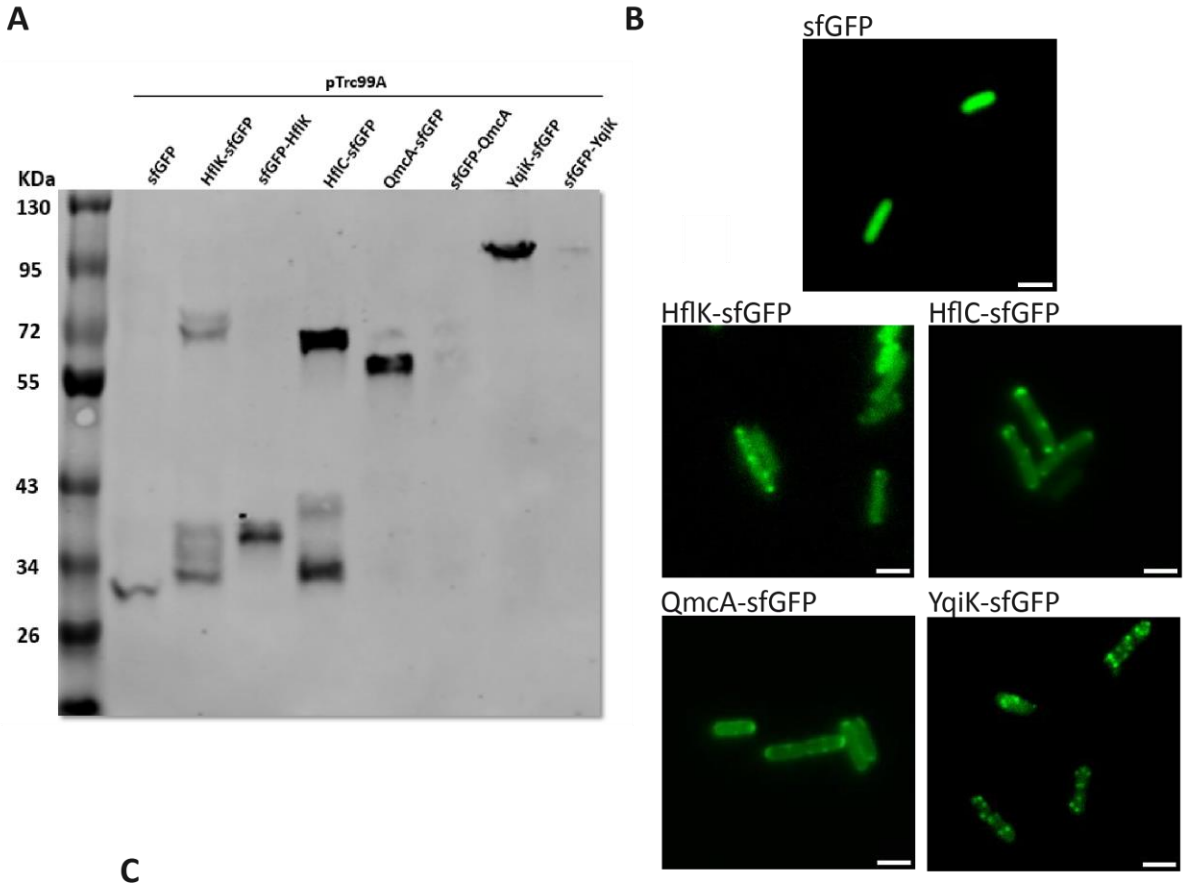
A
pTrc99A
sfGFP
HflK-sfGFP
sfGFP-HflK
HflC-sfGFP
QmcA-sfGFP
sfGFP-QmcA
YqiK-sfGFP
sfGFP-YqiK
KDa
130
95
72
55
43
34
26
B
sfGFP
HflK-sfGFP
HflC-sfGFP
QmcA-sfGFP
YqiK-sfGFP
C
HflK-sfGFP
7.8 sec
14.4 sec
21.6 sec
28.8 sec
36 sec
43.2 sec
50.4 sec
57.6 sec
HflC-sfGFP
7.8 sec
14.4 sec
21.6 sec
28.8 sec
36 sec
43.2 sec
50.4 sec
57.6 sec

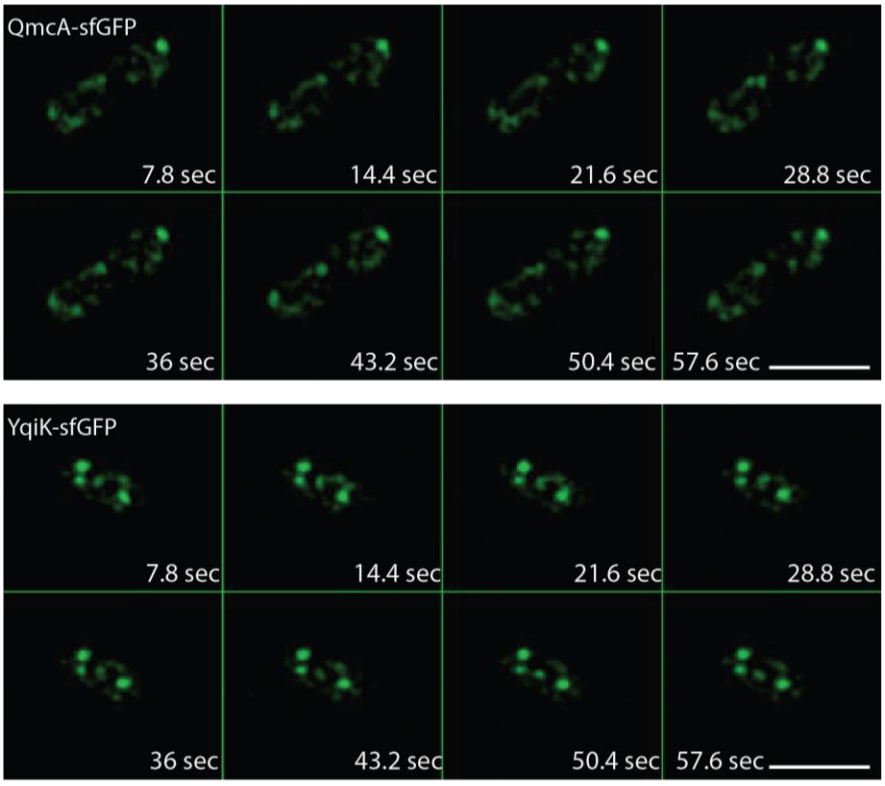

Figure 3.1 Expression and membrane localization of SPFH-sfGFP fusion integrated into pTrc99A.

(A) Western blots (WB) of fluorescent protein fusions, using a primary antibody specific for GFP. Lanes: 1) Proteins ladder. 2) *E. coli* MG1655 carrying pTrc99A_sfGFP empty vector used as a control. 3) *E. coli* MG1655 carrying pTrc99A_*hflK-sfGFP*. 4) *E. coli* MG1655 carrying pTrc99A_*sfGFP-hflK*. 5) *E. coli* MG1655 carrying pTrc99A_*hflC-sfGFP*. 6) *E. coli* MG1655 carrying pTrc99A_*qmcA-sfGFP*. 7) *E. coli* MG1655 carrying pTrc99A_*sfGFP-qmcA.* 8) *E. coli* MG1655 carrying pTrc99A_*yqik-sfGFP*. 9) *E. coli* MG1655 carrying pTrc99A_*sfGFP-yqiK*. Proteins were probed using a 1:10000 dilution of anti-GFP primary antibody (JL-8 monoclonal, mouse, Takara) and anti-mouse secondary antibody (IRDye® 800CW Rabbit anti-mouse IgG) equally 1:10000 diluted in 5% TBS-T milk.

(B) Localization by epifluorescence of SPFH C-terminus tagged sfGFP. *E. coli* MG1655 carrying pTrc99A_sfGFP empty vector used as a control. Cells grown in TB medium at 220 rpm and 37°C. Scale bars: 2 µm.

(C) Structured illumination microscopy imaging of SPFH proteins. Montange of movies with SIM reconstruction for SPFH-sfGFP proteins. Cells grown in TB medium at 220 rpm and 37°C. 2uM of IPTG was added as inducer. Z-stacks resulting from the sfGFP channel were merged and projected into tomographic representations. 110 ms acquisition time. 50 frames. The scale bar is 2 µm.

3.1.1.2 **Expression under the native promoter**

To study the localization and distribution of SPFH proteins within *E. coli* under their native expression levels, we integrated sfGFP DNA fragments at the C-terminus of SPFH proteins in the *E. coli* MG1655 genome through lambda red homologous recombination. PCR validation confirmed the precise genomic insertion sites. The stability and molecular mass of the resulting SPFH fusions were verified by SDS-PAGE and immunoblotting using an anti-GFP antibody (**Figure 3.2 A**). All insertions were correctly positioned within the genome and exhibited molecular masses consistent with full-length sfGFP fusions. In contrast to the *trc* promoter-driven expression, all constructs under native expression conditions had a single band, except for YqiK which expression was too low to be detected. Notably, HflK and HflC showed lower abundance, QmcA displayed higher abundance, and YqiK remained undetectable, even upon doubling the sample loading volume (20 µl).

Images acquired with a Nikon Eclipse *Ti* microscope, show membrane-localized spots for three of the SPFH proteins (**Figure 3.2 B**). HflK and HflC displayed both small and large spots, difference in size could be because these two proteins form a complex of 12 proteins each. Thus, small spots might correspond to the formation of the complex, while large spots may denote the aggregation of more than two complexes. Regarding QmcA, this protein exhibited numerous spots distributed along cell poles and lateral borders. In contrast to *trc* promoter-driven expression, YqiK under native expression exhibited few visible spots, consistent with low expression of this protein under our experimental growth condition.

To study the dynamics of SPFH proteins under native promoter, we performed Total Internal Reflection Fluorescence Microscopy (TIRF) in collaboration with the group of Dr. Peter Graumann at Marburg University. We performed SPT (Single Particle Tracking) to quantify changes in protein dynamics at a single molecule level, using an experimental setup that has been described before [51]. For quantification of the particle trajectories, we employed Gaussian Mixture Modelling (GMM) (**Figure 3.2 C**), which allowed us to directly compare molecule dynamics between different proteins. It aims to distinguish subpopulations with different diffusion constants (D), and then to identify the population size of molecules with a given D (**Table 2**). GMM allows to distinguish if the probability density function of observed step sizes can be explained by a single Gaussian function, and thus by the presence of a single population of molecules having the same value for D, or by two different populations, which is tested by an r^2 analysis. The results show that HflK-sfGFP, HflC-sfGFP and QmcA-sfGFP (excluding YqiK-sfGFP due to its low expression) have particles with two different dynamics, mobile and not mobile. Specifically, HflK

and HflC exhibited a large proportion of mobile particles, 76% ± 1.1 and 89% ± 2.2 of their respective populations. In contrast, only 29% of the QmcA proteins were mobile.

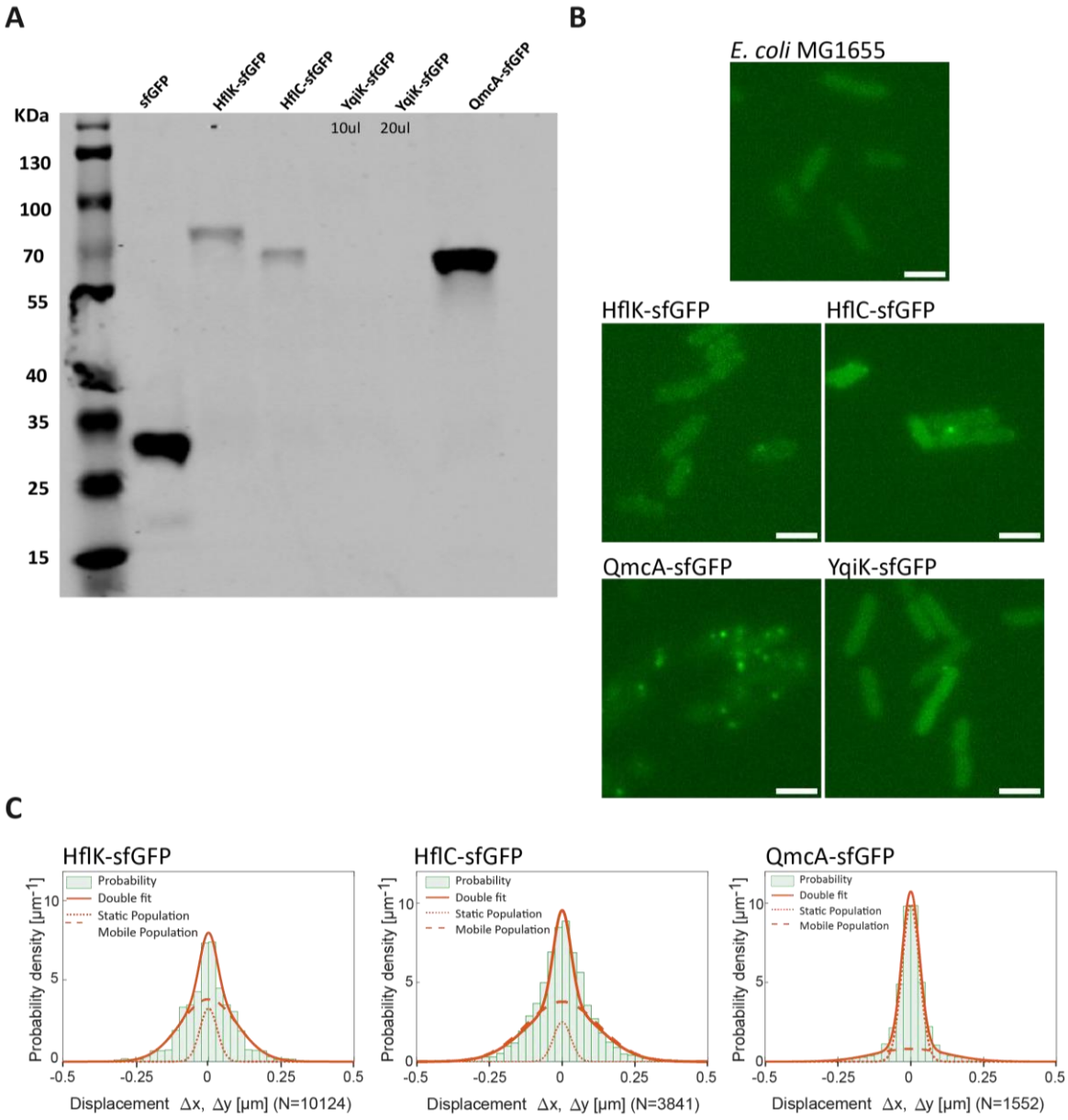

Figure 3.2 Native expression and localization of SPFH proteins.

(A) Western blots (WB) of fluorescent protein fusions, using primary antibody specific for GFP. Lanes: 1) Proteins ladder.2) *E. coli* MG1655 carrying pTrc99A-sfGFP induced with 2μM of IPTG. 3) *E. coli* MG1655 HflK-sfGFP 4) *E. coli* MG1655 HflC-sfGFP. 5 and 6) *E. coli* MG1655 YqiK-sfGFP 7) *E. coli* MG1655 QmcA-sfGFP. For all SPFH proteins, 10 μl of the whole cell lysate was loaded onto the gel, and when indicated 20 μl for YqiK. The cells were cultivated in TB medium at 220 rpm and 37°C. Proteins were probed using

a 1:10000 dilution of anti-GFP primary antibody (JL-8 monoclonal, mouse, Takara) and anti-mouse secondary antibody (IRDye® 800CW Rabbit anti-mouse IgG) equally 1:10000 diluted in 5% TBS-T milk.
(B) Localization by epifluorescence of SPFH native expression. *E. coli* MG1655 was used as a negative control. Cells were grown in TB medium at 220 rpm and 37°C. Scale bars: 2 µm.
(C) Diffusion of SPFH proteins using TIRF Microscopy. Gaussian mixture model (GMM) analyses of frame-to-frame displacements in x- and y-directions. HflK, HflC and QmcA orange lines represent the sum of the two Gaussian distributions. Dotted and dashed lines represent the single Gaussian distributions corresponding to the static and mobile fractions, respectively.

Table 2 Diffusion constants and percentages of static and mobile molecule fractions

Strain	# tracks	D_1	F_1	D_2	F_2
HflK-sfGFP	10124	0.011 ± 0.0007	24±1.1	0.12 ± 0.024	76±1.1
HflC-sfGFP	3841	0.012 ± 0.004	11±2.2	0.18 ± 0.0069	89±2.2
QmcA-sfGFP	1552	0.011 ± 0.011	71±4.2	0.29 ± 0.011	29±4.2

D_1, diffusion constant of static fraction ($\mu m^2 \cdot s^{-1}$). F_1, percentage of static molecules (%).

D_2, diffusion constant of mobile fraction ($\mu m^2 \cdot s^{-1}$). F_2, percentage of mobile molecules (%).

3.1.2 SPFH protein-protein interaction

Given the limited understanding of protein–protein interactions of SPFH proteins in bacteria, specifically for *E. coli*, we decided to study the protein interaction network of SPFH using pull-down technique with GFP-Trap magnetic beads. To identify optimal conditions for enhancing the solubility of SPFH membrane proteins, we used two different methods. One method involved the use of detergent triton X-100, while the other utilized the polymer SMALP-30010P. For these experiments, we used SPFH-sfGFP proteins integrated into pTrc99A. This selection was based on their higher expression levels compared to the expression achieved using the native promoter. For the negative control, we used sfGFP alone and the membrane protein Tar-sfGFP, which has been extensively studied in our laboratory. To induce protein

expression, we used 2µM of IPTG at 37°C and in LB medium. After protein extraction with both methods, we performed pull-down and mass spectrometry (MS) to identify proteins.

3.1.2.1 **Pull-down using protein extraction with Triton X-100**

Triton X-100, a commonly used detergent in the extraction of membrane protein, acts by disrupting lipid-lipid and protein-lipid associations. This disruptive action aids in solubilizing membrane proteins, making them easier to extract into a solution. In this experiment, we used the lysis buffer detailed in section 5.6.6 of Materials and Methods. Bacteria cultures were collected and resuspended in lysis buffer and incubated for a 3-hour in a rotating shaker. After that step, 1 min sonication was performed to enhance membrane disruption. Microscopy images of the whole lysate were taken after the 3 hours of lysis treatment and after 1 min sonication to assess the efficacy of both steps in the membrane disruption (**Figure 3.3 A, B**). Cells poorly lyse after treatment with the lysis buffer. For some samples, there was a loss of rod-shaped morphology in the cells, which is indicative of cell wall disruption. Nevertheless, membrane aggregation and protein agglutination were still observed. Sonication significantly improved the disruption of membrane aggregation; however, it was not as effective as expected.

We tested different sonication times to identify an optimal condition for membrane disruption: 30 seconds, 1 minute, 3 minutes, and 4 minutes. Given some concerns about potential damage during prolonged sonication and its impact on protein stability, SDS-PAGE and immunoblotting analyses were conducted to evaluate both stability and efficiency. We observed that there was a high abundance of the proteins throughout all sonication times, with a slight increase in protein solubility after 4 minutes of sonication for YqiK and Tar (**Figure 3.3 C**). Notable, HflK-sfGFP bands were very weak, pointing out the poor expression of the protein for this particular experiment. Besides this, certain samples have multiple bands, possibly by degradation and/or denaturation during sonication.

For determining the solubilized protein fraction, both supernatant and pellet fractions of the samples were assessed (**Figure 3.3 D**). For sfGFP alone, most of the sample was present in the supernatant, with increased protein abundance following 4 minutes of sonication. On the other hand, for HflC-sfGFP and QmcA-sfGFP, a significant portion of the sample remained associated with the membrane even after a 4-minute sonication. In the cases of YqiK-sfGFP and Tar-sfGFP, the abundance in both supernatant and pellet fractions was equal. As a result, we decided to use the soluble fraction from the 4-minute sonication for subsequent pull-down experiments.

Results from pull-down and mass spectrometry analyses revealed an elevated count of peptides for each of the tagged proteins (**Table 3**). The interaction between HflK-HflC and FtsH proteins was detected, aligning with prior reports. However, enrichment for other potential candidates was notably minimal. Moreover, these interactors were present across all samples, including both control sfGFP and Tar-sfGFP, which could indicate an artifact interaction.

Given the poor outcomes of these results, we used an alternative protein extraction using polymer SMALP-300P (see the next section 3.1.2.2).

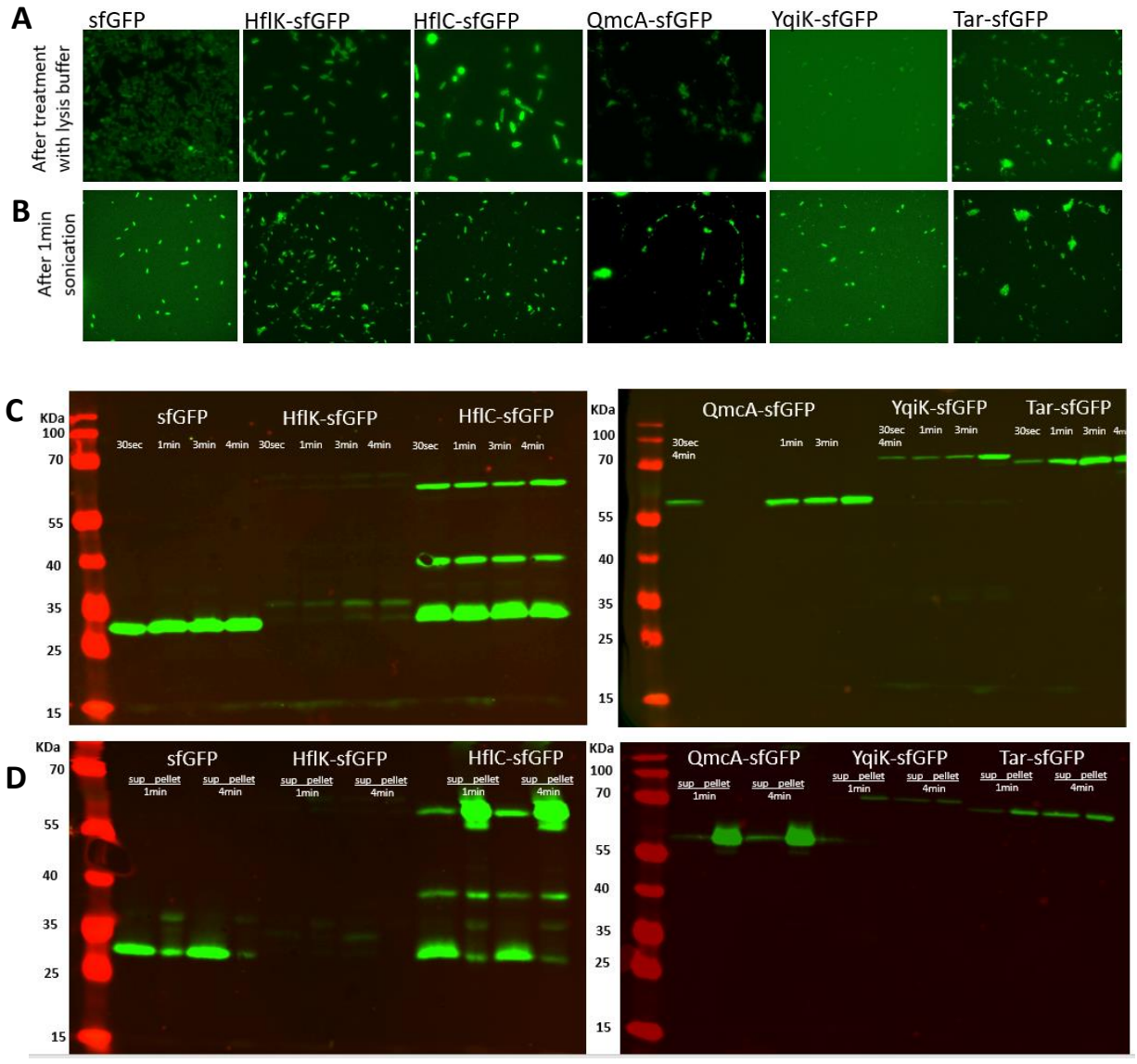

Figure 3.3 Solubility analysis of SPFH-sfGFP fusion expressed from pTrc99A using extraction with Triton X-100.

(A, B) Epifluorescence of whole cell lysate of SPFH-sfGFP fusion after lysis buffer treatment with 2% of Triton X-100 (A). After 1min sonication (B). Cells were cultured in LB medium until reaching an OD_{600} of 0.4-0.6, 2µM IPTG was used for induction.

(C) Western blots (WB) of the whole cell lysate of SPFH-sfGFP fusion after different sonication times. Anti-GFP primary antibody (JL-8 monoclonal, mouse) was used for specific labeling of sfGFP-tagged proteins.

(D) WB of supernatant (sup) and pellets of SPFH-sfGFP fusion after 1 min and 4 min of sonication. Anti-GFP primary antibody (JL-8 monoclonal, mouse) was used for specific labeling of sfGFP-tagged proteins.

Table 3 Interactome of SPFH protein extracted with Triton X-100

Sample / Proteins ID	HflK-sfGFP	HflC-sfGFP	QmcA-sfGFP	YqiK-sfGFP	Tar-sfGFP	sfGFP
HflK	**365**	284	5	17	32	12
HflC	35	**234**	1	2	16	3
QmcA	0	0	**54**	19	5	0
YqiK	0	0	0	**136**	33	0
Tar	0	1	0	0	**456**	0
FtsH	**15**	**73**	0	0	11	0
GFP	110	171	37	48	86	**58**
DnaK	186	50	3	14	59	11
AceF	12	33	6	8	69	10
AceE	12	33	1	3	79	6
GroL	68	18	6	26	110	27
FtsZ	8	2	4	0	5	0
HemB	7	25	0	0	4	2
FliC	3	14	5	8	0	46
GLPK	34	45	55	36	31	16
TufA	24	36	15	15	71	17
GapA	22	36	8	21	83	27
HisB	19	38	2	8	27	11
HtpG	11	5	0	0	21	2
SdaC	10	5	12	8	13	1
Lpp	9	29	0	1	26	6
SdhA	9	1	4	6	23	6
RpsE	7	9	0	1	13	0
TreB	7	4	6	5	9	0

FusA	6	15	15	12	42	7
SecD	6	1	1	0	6	0
OmpC	5	35	10	5	29	8
SecA	5	2	0	0	0	0
AtpA	4	9	3	2	32	5
RplF	4	7	0	0	9	0
SucB	4	3	0	0	20	2
LysU	4	2	0	0	9	0
HslU	4	1	1	1	8	0
SrlE	4	0	0	0	1	0
PflB	3	7	2	0	27	5

3.1.2.2 **Pull-down using protein extraction with SMALP-30010P polymer**

SMALP-30010P polymer is a styrene maleic acid copolymer recently used for the extraction of membrane proteins. This polymer can encapsulate membrane proteins from native membranes, operating without the need for detergents. SMALP polymer achieves this action by enveloping a section of the lipid bilayer, forming a disc-like particle or nanodisc [52]. In this experiment, we used 5uM concertation in 50ml of bacteria sample.

Notable, the polymer exhibited remarkable efficiency across all samples, effectively lysing the cells and showing minimal membrane aggregation (

Figure 3.4). Post-centrifugation, we separated the pellet from the supernatant fraction and used the soluble fraction for pull-down and mass spectrometry analysis. While all SPFH target samples yielded a substantial count of peptides (**Table 4**), all other candidate proteins, previously identified in triton X-100 extraction, show a minimal enrichment in comparison to the results accomplished using triton X-100. Notably, the interaction between HflK-HflC and FtsH was absent in this experiment. We hypothesize that this observation may be attributed to the size of the nanodisc generated by the polymer, which has been reported to range between 6 to 30nm in diameter [52], while the HflK-HflC complex has a diameter of 20nm [41]. It is possible that the polymer might tend to generate small discs that could disrupt some protein-protein interactions.

In summary, the extraction of SPFH proteins demands the implementation of diverse strategies to ensure effective protein solubilization. This could potentially be attributed to the suggested localization of these proteins in lipid rafts, a factor that could increase the challenges associated with membrane disruption.

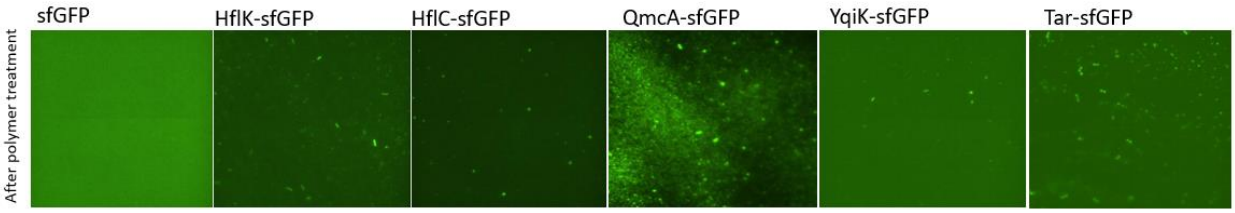

Figure 3.4 Images of whole cell lysates of SPFH sfGFP fusion after treatment with SMALP-30010P polymer

Table 4 Interactome of SPFH protein extracted with SMALP-30010P

Sample / Proteins ID	HflK-sfGFP	HflC-sfGFP	QmcA-sfGFP	YqiK-sfGFP	Tar-sfGFP	sfGFP
HflK	**416**	27	9	2	4	8
HflC	1	**150**	18	2	4	0
QmcA	13	6	**591**	47	41	6
YqiK	43	34	27	**107**	107	5
Tar	12	3	16	3	**301**	14
FtsH	**0**	**0**	1	1	0	0
GFP	104	59	234	28	59	**35**
DnaK	1	0	7	2	6	2
AceF	0	0	3	1	2	1
AceE	0	0	4	2	6	5
GroL	7	3	19	9	18	13
FtsZ	0	0	1	0	0	0
HemB	0	0	0	0	0	0
FliC	0	0	57	34	6	23
GLPK	7	4	18	2	10	1
TufA	13	12	42	5	51	7
GapA	2	1	13	3	9	2
HisB	0	0	0	0	0	0
HtpG	0	0	0	0	0	0
SdaC	0	0	13	2	2	3
Lpp	54	13	53	38	74	9
SdhA	0	0	4	4	4	1

RpsE	1	1	6	3	8	0
TreB	0	0	27	10	3	2
FusA	4	1	13	1	15	2
SecD	1	0	2	0	0	0
OmpC	13	12	81	39	59	18
SecA	2	0	1	0	0	0
AtpA	1	2	17	9	16	3
RplF	0	0	7	2	11	1
SucB	0	0	0	0	0	0
LysU	0	0	0	0	0	0
HslU	0	0	0	0	0	0
SrlE	0	0	3	0	0	0
PflB	2	0	7	1	2	0

3.1.3 Phenotypic characterization of single and multiple SPFH knockouts

3.1.3.1 Growth at different temperatures

SPFH proteins form a large homo-oligomeric complex within the cellular membranes. Some of these SPFH proteins have been identified within detergent-resistant membranes (DRMs), leading to speculation that SPFH proteins are integral components of FMM and could potentially influence membrane structure and organization. Changes in membrane organization have the potential to affect growth in response to temperature changes. Consequently, we studied the effect of different temperatures on the growth of SPFH knockouts.

To assess the growth of SPFH knockouts, we first used 96-well plates as the experimental platform. Overnight cultures were inoculated at an initial OD_{600} of 0.01 in both LB and TB media. Each well contained 150 µl of culture and the plate was covered with the lid provided by the producer and further sealed with parafilm to prevent evaporation but allow air exchange. Plates were incubated at different temperatures (37°C, 42°C, 30°C, and 25°C) with continuous shaking, alternating between 150s orbital and 150s linear, in a Tecan Infinite® 200 PRO plate reader.

Our initial observations show that SPFH knockouts exhibited some growth differences in LB and TB media. At 37°C, SPFH knockout *ΔhflC*, *ΔhflKC*, and *ΔhflKC ΔqmcA* grow similar compared to the WT in both LB and TB media. Nevertheless, *ΔhflK*, *ΔqmcA*, *ΔyqiK*, and *ΔhflKC ΔqmcA ΔyqiK* exhibited slightly higher growth rates than the wildtype during the late exponential phase also in both media (**Figure 3.5 A, B**). Subsequently, we increased the incubation temperature to 42°C, and similar to the observations at 37°C, *ΔhflK*, *ΔqmcA*, *ΔyqiK*, and *ΔhflKC ΔqmcA ΔyqiK* showed slightly higher growth rates compared to the wildtype in LB. However, in TB medium all the strains exhibited poor growth, with *ΔhflKC* being the most affected under this condition (**Figure 3.5 C, D**).

At the lower temperature of 30°C, the quadruple knockout exhibited slower growth in both LB and TB mediums when compared to the wildtype, and no significant growth effects were observed in the other SPFH knockouts (**Figure 3.5 E, F**). To further investigate the impact of lower temperatures on the quadruple knockout, we reduced the temperature to 25°C. Interestingly, the quadruple knockout strain exhibited even slower growth in LB medium. Nevertheless, the growth effect in TB medium was not as pronounced as at 30°C (**Figure 3.5 G, H**).

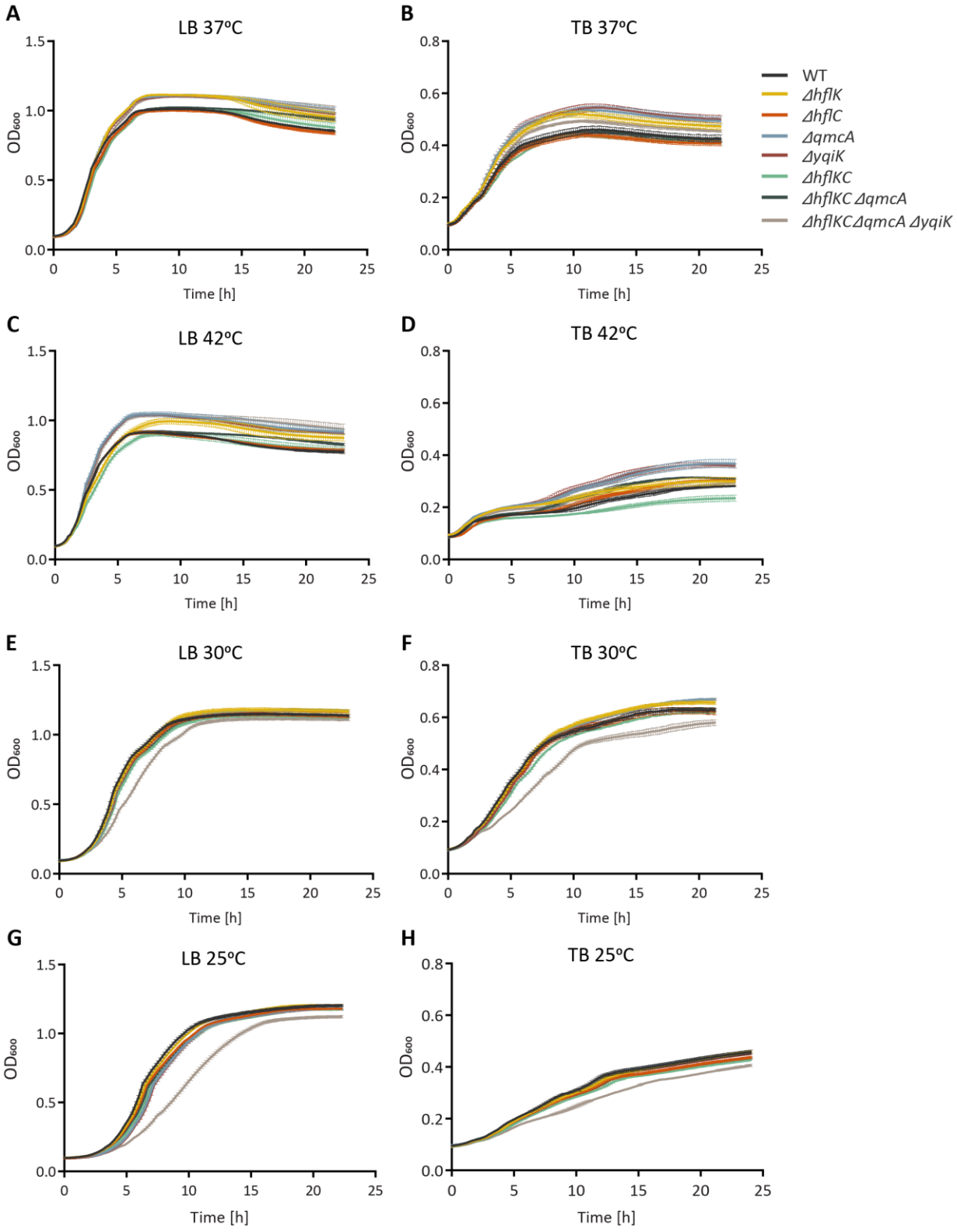

Figure 3.5 Effect of temperature on the growth of SPFH knockouts.

(A – H) Growth curve of SPFH knockouts and corresponding wildtype (WT) MG1655 in LB and TB media with continuous shaking, alternating between 150s orbital and 150s linear, in a Tecan Infinite® 200 PRO plate reader. (A and B) Growth curve at 37°C. (C and D) Growth curve at 42°C. (E and F) Growth curve at 30°C and (G and H) Growth curve at 25°C. For all growth curves, data represent the mean value and standard deviation (SD) for three independent cultures grown in the same representative experiment.

3.1.3.2 **Growth under osmotic stress**

To study the physiological relevance of SPFH proteins in membrane integrity, we decided to evaluate the response of SPFH knockout to osmotic stress induced by sodium chloride (NaCl) and sucrose. To assess this, strains were cultivated in LB medium enriched with either NaCl or sucrose, with concentrations ranging from 0.25 to 1 M. Strains were grown in 96-well plates and cultivated in a Tecan Infinite® 200 PRO plate reader as described 5.7.1.

Growth curves in LB medium were used as the standard grow of SPFH knockouts and wildtype (**Figure 3.6 A**). We observed a similar growth behavior described in **Figure 3.5 A**, which highlights the reproducibility of the growth phenotype. Regarding the osmotic conditions, we consistently observed a reduction in growth as the high concentration of NaCl. Notably, at 0.25 M NaCl, no substantial differences were detected between the SPFH knockout strains and the wildtype (WT) (**Figure 3.6 B**). However, at higher NaCl concentrations, both SPFH knockout strains and the wildtype exhibited growth irregularities during the stationary phase, particularly stronger at 0.7M (**Figure 3.6 C, D**). Importantly, we excluded the possibility of aggregation as the cause of these growth irregularities, and we also eliminated mechanical issues with the plate reader, as consistent results were obtained from two different devices. Therefore, it was reasonable to attribute these irregularities to the osmotic stress itself. Finally, it is important to note that all tested strains barely grew in the presence of 1 M NaCl (**Figure 3.6 E**).

Similar to NaCl osmotic stress, we observed a decrease in growth as the concentration of sucrose increased. Notably, there were no visible differences in growth between the SPFH knockouts and the wildtype at 0.25 M and 0.5 M of sucrose (**Figure 3.6 F, G**). Nevertheless, all SPFH knockouts grew slightly higher compared to the wildtype at 0.75 M sucrose (**Figure 3.6 H**), this behavior is less strong at higher osmotic stress (**Figure 3.6 I**).

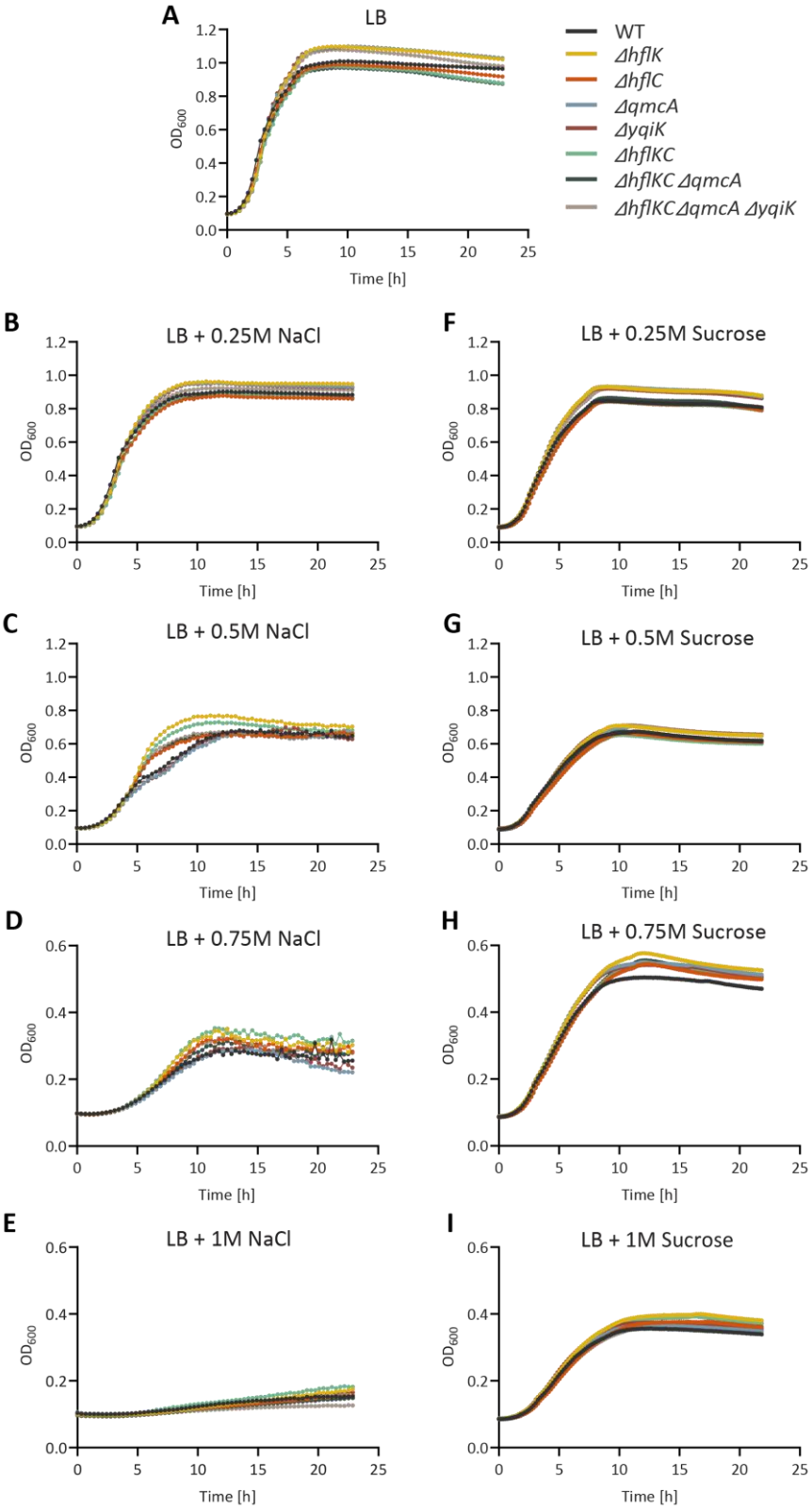

Figure 3.6 SPFH knockouts under osmotic stress induced by NaCl or sucrose.

(A-I) Growth curves of single and multiple knockout strains and corresponding wildtype MG1655 in LB medium at 37^0C with continuous shaking, incubated in a Tecan Infinite® 200 PRO plate reader. (A) Strains grown in LB medium without osmotic stress. (B - E) Strains grown in LB supplemented with different concentrations of NaCl. (F – I) Strains grown in LB supplemented with different concentrations of sucrose. For all growth curves, data represent the mean value and standard deviation (SD) for three independent cultures grown in the same representative experiment.

3.1.3.3 **Membrane fluidity**

Several studies have shown that SPFH proteins are part of the membrane microdomains in both eukaryotic and prokaryotic cells. Microdomains are regions in the membranes with specific lipid composition and elevated structural organization that influence the overall fluidity of cell membranes. As SPFH proteins are components of these microdomains, their potential role in membrane organization and fluidity dynamics has been hypothesized.

Here we used the fluorescent probe di-4-ANEPPDHQ (**Figure 3.7 A**) to measure the membrane fluidity of SPFH knockouts and thus elucidate the potential influence of these proteins on the lipid membrane order. Di-4-ANEPPDHQ is a lipophilic dye that is incorporated into cell membranes; its fluorescent properties are sensitive to changes in the physical state of the lipid bilayer, specifically the polarity, a property correlated with membrane fluidity. In a more fluid membrane environment, such as in regions with high lipid mobility and more hydrophilic, the probe has red-shifted emission. In rigid or ordered membranes, water molecules penetrate less deep into the membrane, and the probe's conformation changes, leading to a green-shifted emission (**Figure 3.7 B**). The shift in emission between the disordered and ordered phases allows a quantitative assessment of the generalized polarization (GP) value. Low GP values indicate a less ordered membrane (more fluid) and high values indicate more ordered or rigid membranes [53].

Recently developed techniques allowed the measurement of membrane fluidity in living cells, although their efficiency requires optimization to specific organisms and growth conditions. Several critical factors must be considered when employing this technique, including cell density, dye concentration, and incubation time. We tested different conditions for all three critical steps, and we determined that maintaining a cell density between 0.4 and 0.6 $O.D_{600}$, using 5 µM di-4-ANEPPDHQ, and 30 minutes of incubation at 37°C yielded optimal results for imaging acquisition. This specific combination facilitated

efficient cell separation and segmentation, ensured optimal dye intensity for both fluorescent channels, and allowed sufficient time for the dye to permeate and equilibrate within the cellular membrane. We used TIRF microscopy and the analysis of imagined described by Owen D. in 2006 [53]. Roughly 100 cells were processed for each condition to calculate the GP Value, and illustrative acquisition of images is shown in **Figure 3.7 C**.

For fluidity positive control, we used Benzyl Alcohol (BnOH), a fluidizer that enhances membrane hydration and thereby increases the membrane disorder [54]. We observed a reduction in GP value when the wildtype was treated with different concentrations of BnOH (**Figure 3.7 D**), indicating a decrease in membrane order. This allowed us to differentiate between liquid-ordered and liquid-disordered membranes within living cells. Furthermore, we proceeded to calculate the GP values for all SPFH knockouts when grown in LB at 37^{o}C. All SPFH knockout showed a slight reduction in GP values, visible as a leftward shift in the Gaussian curve relative to the wildtype (**Figure 3.7 E**).

Assuming that any effect in the single knockouts will be reflected in the multiple gene knockout, we decided to further characterize the quadruple SPFH knockout. We studied whether this knockout would respond to both lower and higher temperatures. At 25°C, the GP slightly shifts to the right, which represents an increase of GP value for both the wildtype and quadruple SPFH knockout, with the ΔGP registering 0.125 for the wildtype and 0.063 for *ΔhflKC ΔqmcA ΔyqiK* (**Figure 3.7 F**), leading to more rigid membranes in both strains. At the higher temperature of 42°C, both wildtype and *ΔhflKC ΔqmcA ΔyqiK* GP values decreased, denoting a less rigid membrane. The difference was more pronounced in the *ΔhflKC ΔqmcA ΔyqiK*, with a ΔGP of 0.157, and for the wildtype's ΔGP of 0.093. (**Figure 3.7 G**).

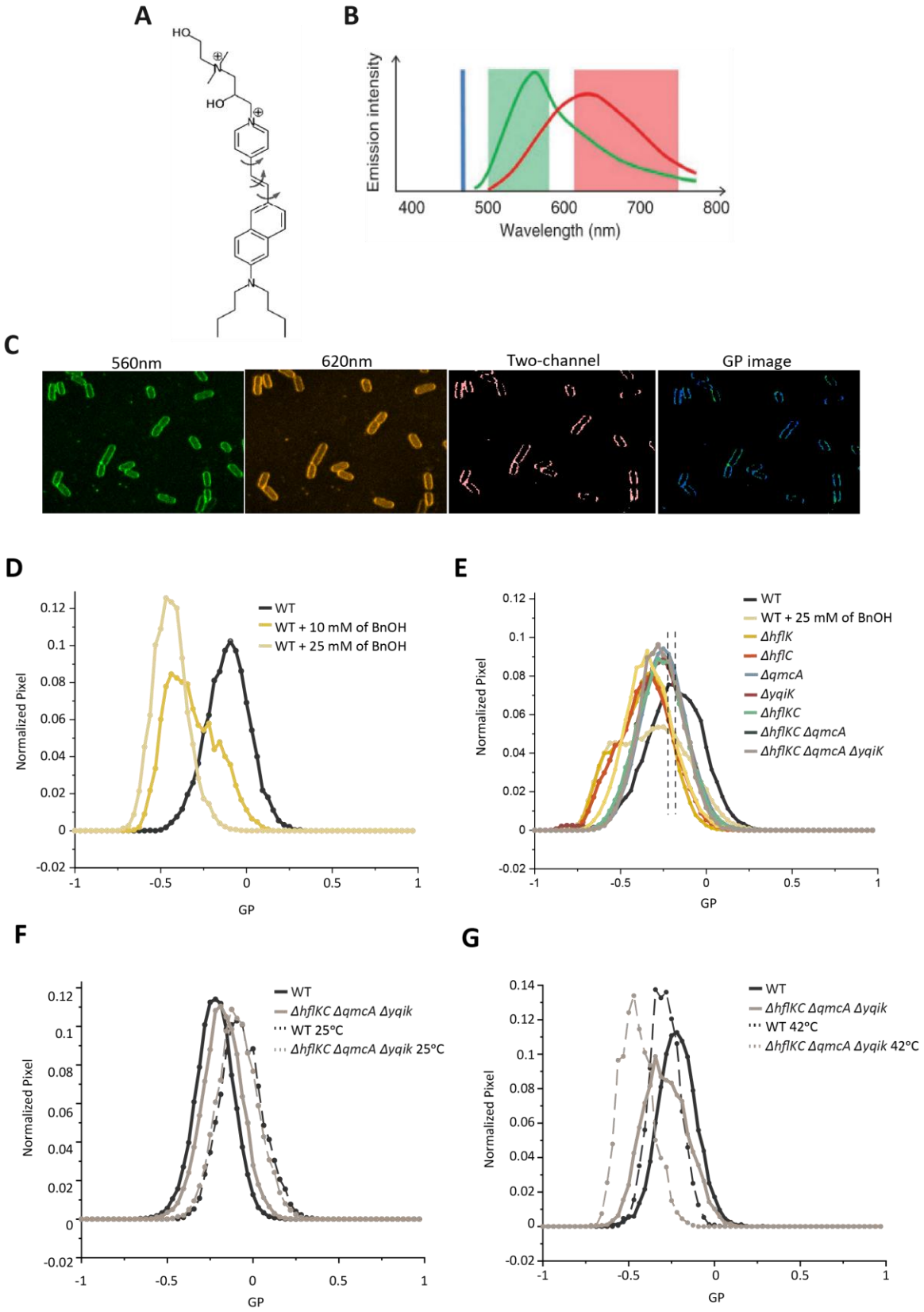

Figure 3.7 Measurement of membrane fluidity in SPFH knockout strains grown in LB medium.

(A) Structure of the probe di-4-ANEPPDHQ.

(B) Scheme of the fluorescence properties of di-4-ANEPPDHQ. The dye is excited at 488 nm (blue line). The dye fluoresces with a peak emission wavelength of ~560 nm (green) when residing in the ordered phase, and ~620 nm in the disordered phase (red). Two-channel acquisition was conducted in the wavelength bands indicated by shaded boxes. Figure from Owen D.M, 2012 [53].

(C) Di-4-ANEPPDHQ GP image of *E. coli* wildtype strain grown in LB medium in the presence of 25mM BnOH. GP = $(I_{500\text{-}580} - I_{620\text{-}750})/(I_{500\text{-}580} + I_{620\text{-}750})$. *I* represents the intensity in each pixel in the image acquired in the indicated spectral channel.

(D) Membrane fluidity in the presence of different concentrations of BnOH.

(E) Membrane fluidity measurement for all SPFH Knockout strains.

(F) Membrane fluidity of the wildtype and *ΔhflKC ΔqmcA ΔyqiK* at 25°C.

(G) Membrane fluidity of the wildtype and *ΔhflKC ΔqmcA ΔyqiK* at 42°C. For all experiment conditions approximately 100 cells were used to calculate the generalized polarization (GP) value.

3.1.3.4 **Growth under the influence of antibiotics**

We used the Prestwick chemical library to screen 1200 FDA-approved drugs to evaluate their potential to inhibit the growth of quadruple SPFH knockout (*ΔhflKC ΔqmcA ΔyqiK*) in comparison to the wildtype. OD_{600} was measured at specific time points (1h, 2h, and 3h) and data was normalized against positive (containing only cells) and negative (LB medium) control to produce scatter graphs. We considered important hits when the coefficient is upper or lower to the linear regression. These hits are highlighted in light and dark orange on the scatter plots (**Figure 3.8 A – D**).

The screening of the SPFH quadruple knockout against the wildtype yielded valuable observation, with 1 compound showing potential tolerance on the knockout strain (Meropenem: β-lactam antibiotic), while 4 compounds displayed slightly reduced tolerance characteristics. A detailed listing of these compounds is provided in **Table 5**. Notable, this group of compounds does not belong to a single category; instead, they include a diverse range of broad-spectrum antibiotics. Only two compounds (sarafloxacin and gatifloxacin) belong to the fluoroquinolone antibiotics, which are antibiotics used for the treatment of a wide spectrum of bacterial infections.

Table 5 Tolerance of SPFH quadruple knockout to Prestwick chemical library compounds

Plate 3	H5	Nimesulide
Plate 4	H6	Minocycline hydrochloride
Plate 14	**G7**	**Meropenem**
	F9	Sarafloxacin
Plate 15	G2	Gatifloxacin

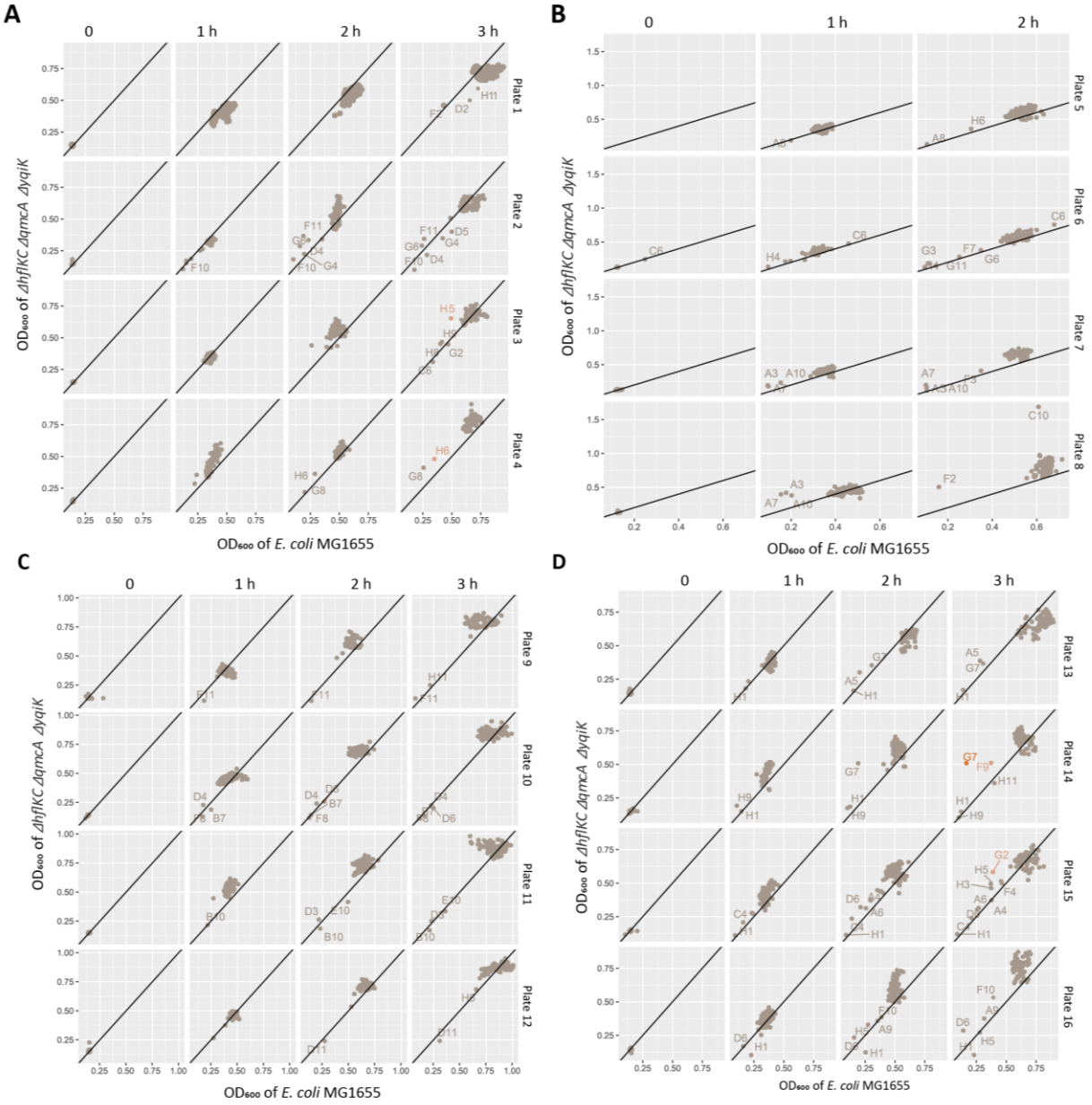

Figure 3.8 Screening of the Prestwick Chemical Library compounds in the SPFH quadruple knockout.

(A-D) The *ΔhflKC ΔqmcA ΔyqiK* and wildtype strains were grown in LB medium at 37°C in orbital shaking at 220rpm in the presence of 20uM of the chemical compounds. OD_{600} measurements were collected after 1 h, 2h and 3h of incubation. (A) Plates 1 to 4. (B) Plates 5 to 8. (C) Plates 9 to 12. (D) Plates 13 to 16. Data represents one biological replicate.

3.1.3.5 **Biofilm assay**

Several studies have shown that the absence of the SPFH protein FloT reduces biofilm formation in *Bacillus subtilis* [6]. Therefore, our objective was to investigate the effect of SPFH knockouts on biofilm production in *E. coli*. We used crystal violet staining to quantify biofilm formation of SPFH knockouts and wildtype strain in a 96-well plate. The use of microtiter plate allows for the formation of a biofilm on the wall and/or bottom of the well and the high throughput nature of the assay makes it useful for genetic screenings.

For our experiments, overnight cultures were inoculated in LB and TB medium within glass flasks and incubated at 37°C in an orbital shaking at 220 rpm. Once the strains reached an OD_{600} between 0.3 and 0.4, the samples were diluted to an OD_{600} of 0.04. Subsequently, the cultures were transferred to the 96-well plate and incubated for 24 hours without shaking. The biofilms were then stained with the crystal violet dye, which was then extracted in ethanol. Biofilm biomass was quantified by measuring the absorbance of the extract at 595 nm using a Tecan Infinite® 200 PRO plate reader, with LB and TB medium serving as blanks. The strain *ΔfliC* was used as a negative control since the deletion of this gene is known to reduce biofilm formation in *E. coli* [55].

As anticipated, *ΔfliC* formed less biofilm compared to the wildtype in both LB and TB medium. In LB medium, four out of the seven SPFH knockouts significantly reduced biofilm formation compared to the wildtype: *ΔhflK, ΔqmcA, ΔyqiK, and ΔhflKC ΔqmcA ΔyqiK* (**Figure 3.9 A**). On the other hand, in TB medium, the overall biomass of the biofilm was lower compared to that in LB. This difference could be attributed to the absence of yeast extract in TB, which typically contains amino acids, vitamins and other components known to enhance bacteria biomass. Additionally, we did not observe any significant differences in biofilm formation among the SPFH knockouts when they grow in TB medium (**Figure 3.9 B**).

During this experiment, we made an interesting observation regarding *ΔhflK* and *ΔhflKC*. These knockouts exhibited slower growth when incubated in TB medium in glass flasks and orbital shaking at 220 rpm. We observed that after 5 hours of incubation under these specific conditions, *ΔhflK* and *ΔhflKC* did not reach

the optimum optical density required to proceed with the experiment. Consequently, these knockout strains had to be excluded from this assay. However, to gain a more comprehensive understanding of this observation, we performed growth curves for SPFH knockouts within glass flasks and orbital shaking at 220 rpm. For a detailed analysis of the results obtained from these growth curves, please refer to section 3.1.3.6.

In addition to our study of biofilm formation, we used colony morphology analysis to have qualitative insights into the colony appearance by SPFH knockouts. To achieve this, we cultivated the strains on LB agar plates at 37°C for 24h, 48h, and 72h, followed by image acquisition using a PeqLab transilluminator. During our analysis, we carefully examined colony size, shape, color, and texture. Our analysis did not reveal any visible changes in colony morphology under these conditions for any of the SPFH knockout strains. The visual aspects of the colonies remained consistent across the incubation times (**Figure 3.9 C**). This result suggests that any potential alterations in biofilm formation or other colony characteristics may require more specialized assays or conditions to be effectively observed.

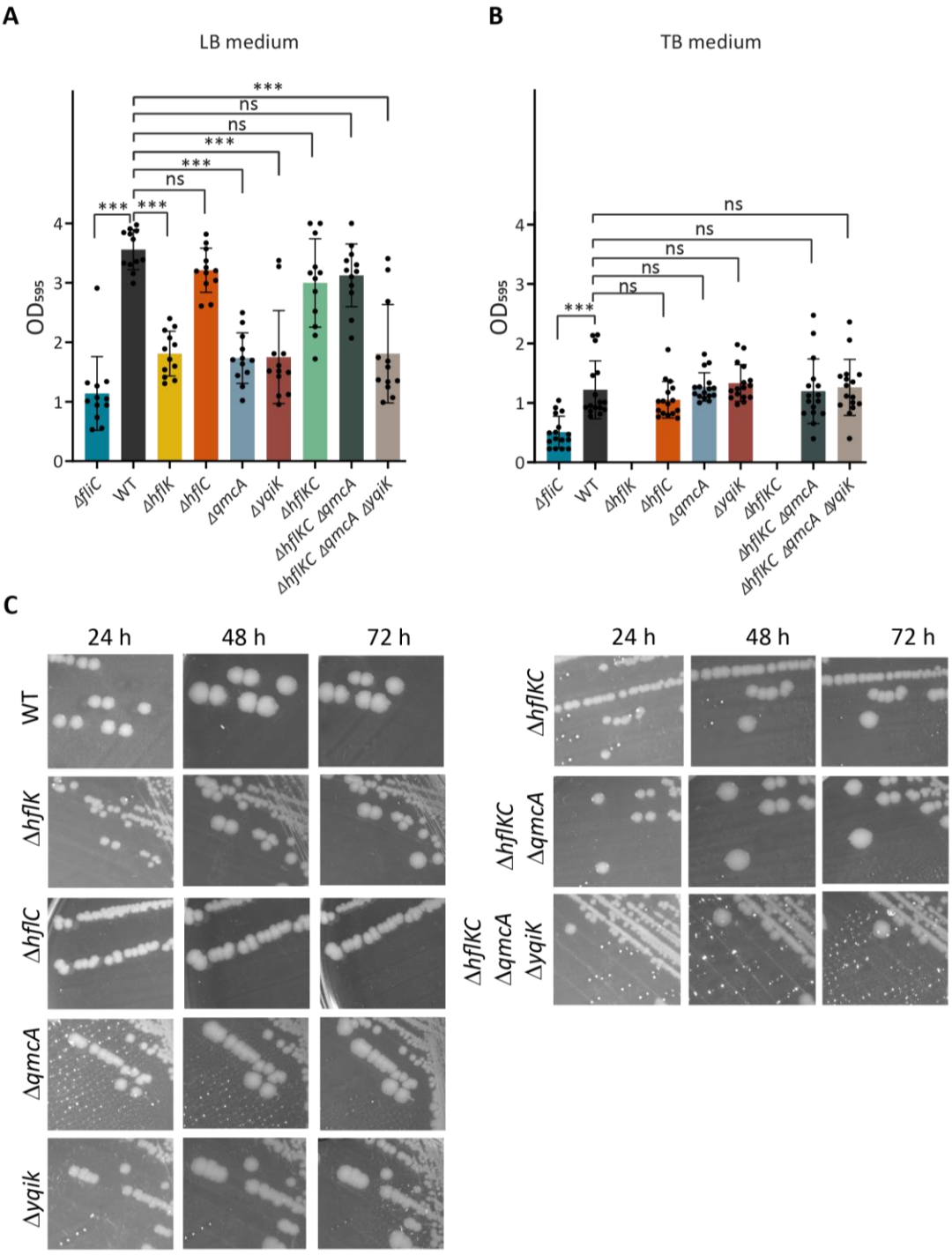

Figure 3.9 Biofilm and colony morphology of SPFH knockouts.

(A, B) Biofilm production of SPFH knockout strains and wildtype were incubated in LB (A) and TB (B) medium at 37°C for 24h. Data represent the mean value and standard deviation (SD) for twelve independent cultures grown in the same representative experiment. Significance of indicated differences between samples: ***p<0.001 and ns = not significant according to an unpaired *t*-test.

(C) Colony morphology of SPGH knockouts grown in LB medium at 37°C. Images were acquired using a PeqLab transilluminator at incubation times of 24h, 28h, and 72h.

3.1.3.6 **Growth under high aeration conditions**

To validate our initial observation of a reduced growth of *Δhflk* and *ΔhflKC* under the specific conditions of TB medium, glass flask, and orbital shaking at 220rpm, we performed growth curve analysis for SPFH knockouts at these specific conditions.

Our results show that SPFH knockouts did not exhibit growth defects when cultivated in LB medium (**Figure 3.10 A**). On the contrary, the knockouts *Δhflk*, *ΔhflKC*, and *ΔhflKC ΔqmcA ΔyqiK* have slower growth compared to the wildtype in TB medium (**Figure 3.10 B**). Notably, among these, the double mutant has the most pronounced growth defect. It should be noted that this growth phenotype was consistently observed in all knockout strains containing the *hflK* deletion, highlighting the essential role of the HflK protein in these specific growth conditions.

To further elucidate this growth phenotype, we performed a single-cell analysis to evaluate cell length and morphological changes at the single level. We collected samples from the SPFH knockout cultures after 4 hours of growth in LB and TB media and used phase-contrast images for subsequent cell segmentation. Through this method, we were able to measure the length of approximately 100 cells per sample.

Our analysis shows that the majority of SPFH knockouts did not have significant changes in cell length when growing in LB medium (**Figure 3.10 C**). However, only *ΔhflKC* has a higher cell length in this condition (**Figure 3.10 E**). On the contrary, in TB medium, *ΔhflKC* shows a reduction in cell length, corroborated by microscopy images that clearly show smaller cells in the double mutant compared to the wildtype. In the case of the single knockout *ΔhflK,* we did not detect changes in cell length; however, its cells are also smaller (**Figure 3.10 D, F**). In this condition, *ΔyqiK* and *ΔhflkC ΔqmcA* seem to have longer cells compared to the wildtype, however, microscopy images do not show a visible difference.

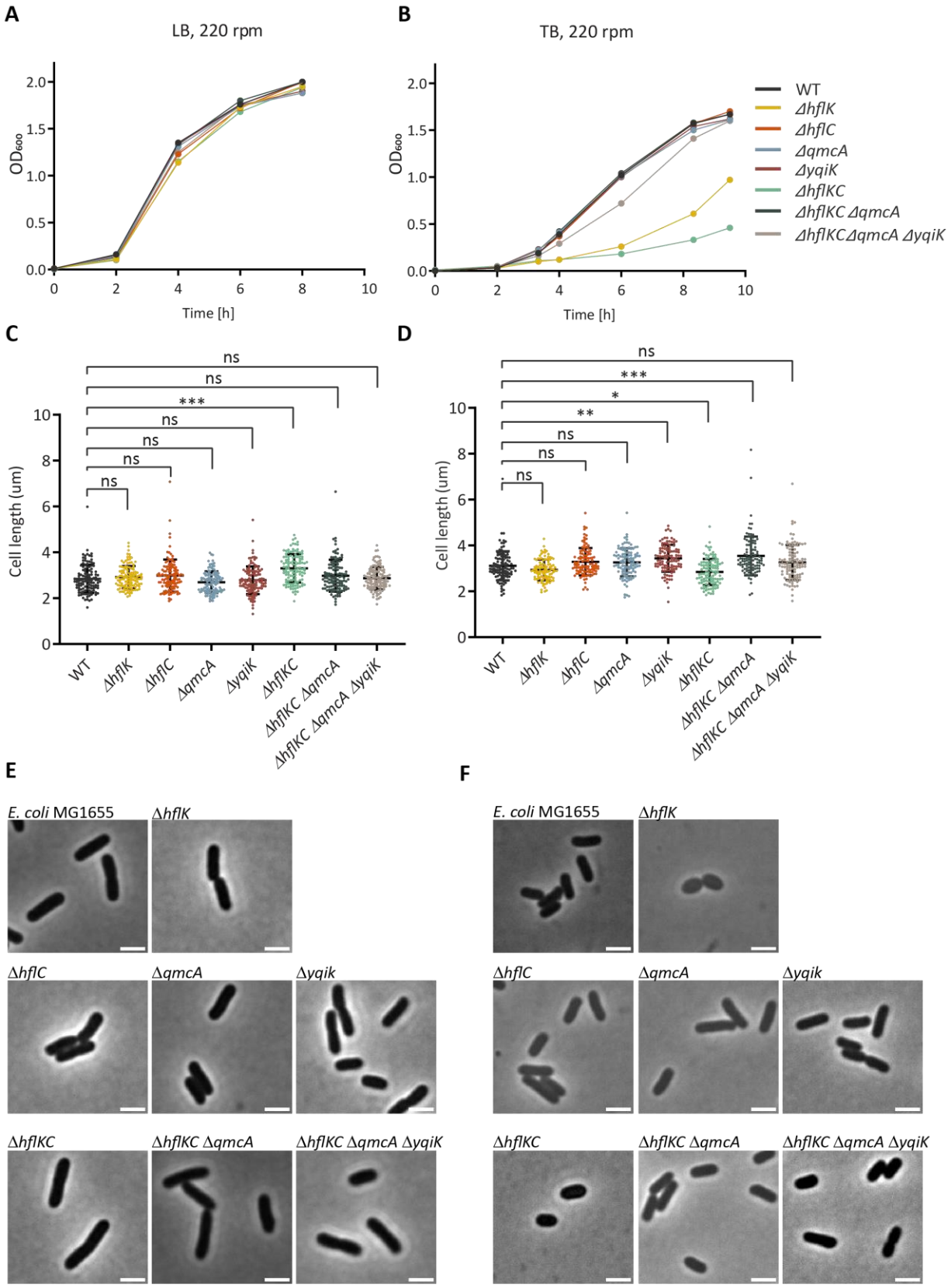
A
LB, 220 rpm
OD600
Time [h]
B
TB, 220 rpm
WT
ΔhflK
ΔhflC
ΔqmcA
ΔyqiK
ΔhflKC
ΔhflKC ΔqmcA
ΔhflKC ΔqmcA ΔyqiK
C
Cell length (um)
ns
***
D
*
**
E
E. coli MG1655
ΔhflK
ΔhflC
ΔqmcA
Δyqik
ΔhflKC
ΔhflKC ΔqmcA
ΔhflKC ΔqmcA ΔyqiK
F

Figure 3.10 Growth curve of SPFH knockouts in high aeration conditions.

(A, B) Growth curve of SPFH knockouts and corresponding wildtype (WT) MG1655 in LB (A) and TB (B) media in an orbital shaker at 37°C and 220 rpm.

(C, D) Cell length of SPFH knockouts in exponential phase. Segmentation was done using BacStalk for a sample size of 100 cells. In LB (C) and TB medium (D).

(E, F) Bright-field images of indicated strains. Scale bar is 2 μm.

3.2 Characterization of HflKC complex in *E. coli*

3.2.1 Growth of *ΔhflKC* under different oxygen supply

In the previous section (**3.1.3.6**), we observed growth defect dependent on aeration and medium composition in *ΔhflKC* strain. In this section, we further investigated this phenotype using different oxygen supplies and media. We observed that when *E. coli* was cultured in rich tryptone broth (TB) medium in an orbital shaker, growth of both individual and pairwise deletions of *hflK* and *hflC* genes at a low shaking rate was similar to that of the wildtype strain (**Figure 3.11 A**). However, at higher shaking rates the growth of the *ΔhflK ΔhflC* (= *ΔhflK*C) strains was markedly slower compared to the wildtype (**Figure 3.11 B-D**). Whereas growth of the wildtype expectedly increased with stronger aeration at higher shaking rates, that of the *ΔhflKC* mutant even decreased. A weaker but similar growth defect was apparent for the *ΔhflK* strain, whereas the *ΔhflC* strain showed no differences from the wildtype growth. The observed growth defect of the *ΔhflKC* strain was specific since it could be largely complemented by co-expressing *hflK* and *hflC* genes from a plasmid (**Figure 3.11 E, F**).

These results indicate that the lack of the HflKC complex, or of HflK, causes specific aeration-dependent growth phenotype. Interestingly, however, no growth defect was observed for the *ΔhflK* and *ΔhflKC* strains at high aeration in an even richer Luria-Bertani (LB) medium (**Figure 3.11 G, H**), which contains yeast extract in addition to tryptone and NaCl that are present in both LB and TB. We therefore tested whether the addition of a fermentable carbon source to TB might compensate the growth defect of the *ΔhflKC* mutant. However, while supplementing TB with glucose generally enabled faster growth, the difference between the *ΔhflKC* strain and the wildtype remained (**Figure 3.11 I, J**). The growth phenotype of the *ΔhflKC* strain further remained visible when cells were cultured at high aeration in M9 minimal medium containing glucose as a sole carbon source (**Figure 3.11 K, L**). Consistent with the aeration-dependence of the growth defect observed for the *ΔhflKC* strain, no difference in growth from the wildtype was observed in TB under anaerobic conditions (**Figure 3.11 M, N**).

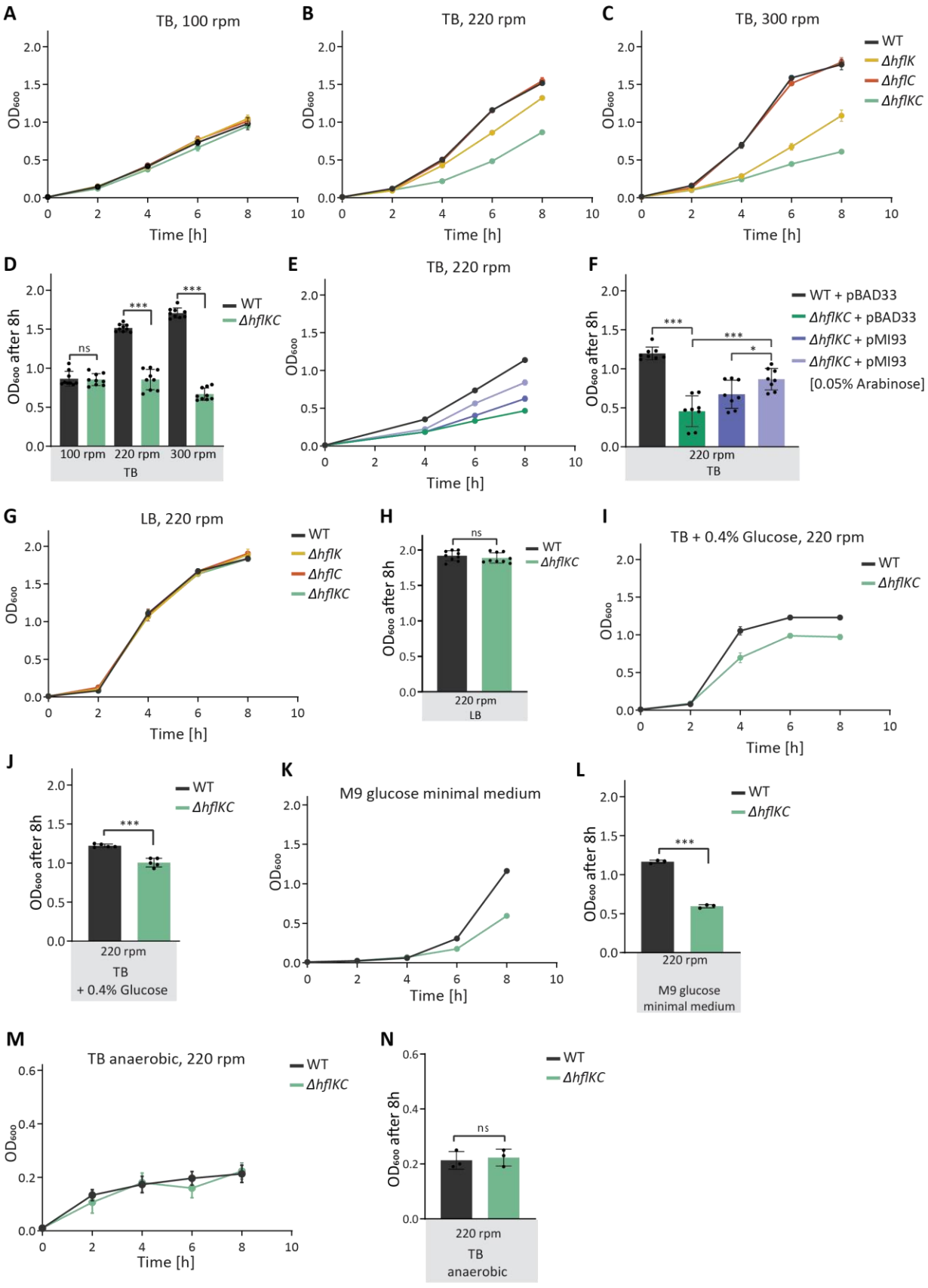
A
TB, 100 rpm
B
TB, 220 rpm
C
TB, 300 rpm
WT
ΔhflK
ΔhflC
ΔhflKC
OD600
Time [h]
D
OD600 after 8h
ns
***
***
100 rpm
220 rpm
300 rpm
TB
E
TB, 220 rpm
F
WT + pBAD33
ΔhflKC + pBAD33
ΔhflKC + pMI93
ΔhflKC + pMI93
[0.05% Arabinose]
*
220 rpm
TB
G
LB, 220 rpm
H
220 rpm
LB
I
TB + 0.4% Glucose, 220 rpm
J
220 rpm
TB
+ 0.4% Glucose
K
M9 glucose minimal medium
L
220 rpm
M9 glucose
minimal medium
M
TB anaerobic, 220 rpm
N
220 rpm
TB
anaerobic

Figure 3.11 Growth of *ΔhflKC, ΔhflK and ΔhflC* strains under different conditions.

(A-D) Time course of growth of *E. coli ΔhflK, ΔhflC* and *ΔhflKC* strains and corresponding wildtype (WT) MG1655 in TB medium in an orbital shaker at 100 rpm (A), 220 rpm (B), or 300 rpm (C), quantified using optical density at 600 nm (OD_{600}). Final OD_{600} after 8 h of growth in TB at indicated shaking rates for *ΔhflKC* and wildtype strains (D).

(E, F) Growth of *ΔhflKC* strain carrying either an empty vector (pBAD33) or pBAD33-derived expression plasmid pMI93 encoding *hflK* and *hflC*, in TB at 220 rpm (E), and corresponding final OD_{600} (F). Where indicated, 0.05% L-arabinose was added as inducer of expression. Wildtype strain carrying pBAD33 was used as a control.

(G, H) Growth of *E. coli ΔhflK, ΔhflC, ΔhflKC*, and wildtype (WT) strains in LB medium in an orbital shaker at 220 rpm (G) and corresponding final OD_{600} (H).

(I, J) Growth of *ΔhflKC* and wildtype (WT) in TB supplemented with 0.4% of glucose at 220 rpm (I) and corresponding final OD_{600} after 8 h of growth (J).

(K, L) Growth of *ΔhflKC* and wildtype (WT) strains in M9 minimal medium supplemented with 0.4% glucose (K) and corresponding final OD_{600} after 8 h of growth (L).

(M, N) Growth of *ΔhflKC* and wildtype (WT) strains in TB at 220 rpm under anaerobic conditions (M) and corresponding final OD_{600} after 8 h of growth (N).Growth curve data represent the mean and SD of three independent replicates cultures grown in the same representative experiment. Data of final OD_{600} represent the mean and SD of independent replicates indicated by symbols, grown in three different experiments. Significance of indicated differences between samples: *p<0.05, ***p<0.001, and ns = not significant according to an unpaired *t*-test.

3.2.2 Proteomics of Δ*hflKC* in different conditions

To identify possible origin of the observed growth defect, we first analyzed changes in protein levels caused by the deletion of *hflK* and *hflC* genes, for *E. coli* cultures grown with strong shaking in either LB or TB. Consistent with similar growth of the Δ*hflKC* and wildtype strains in LB (**Figure 3.11 G**), only a small number of proteins showed pronounced differences in abundance under these conditions (**Figure 3.12 A** and **Table 6**). In contrast, differences between TB-grown cultures, where the deletion strain exhibited growth defect at high aeration (**Figure 3.11 B**), were more much extensive (**Figure 3.12 B** and **Table S 1**).

Fewer differences in protein composition were again observed when the two strains were grown under anaerobic conditions (**Figure 3.12 C** and **Table S 2**), consistent with their similar growth (**Figure 3.11 M**).

Despite these dependencies on conditions of incubation, levels of several proteins showed consistent differences between the Δ*hflKC* and wildtype strains (**Figure 3.12 D**). Among proteins that were significantly perturbed in their abundance under aerobic conditions in both LB and TB, the most prominent were two cytochrome quinol oxidases, CyoABCD (bo_3) and CydAB (*bd*), that are respectively used by *E. coli* under aerobic (i.e., high O_2) or microaerobic (low O_2) conditions [57]. The levels of two cytochrome quinol oxidases showed opposite changes, with catalytic subunits CyoAB of the aerobic quinol oxidase bo_3 being reduced in the Δ*hflKC* strain, whereas the levels of microaerobic quinol oxidase CydAB being elevated. Expression of several other respiration-related proteins was also affected in LB (**Figure 3.12 E** and **Table 6**), and even more prominently in TB under aerobic conditions (**Table S 2**).

We further observed a strong reduction in the levels of two metabolic enzymes, UbiE and IspG, that are involved in the biosynthesis of electron carriers of the respiratory chain. UbiE methyltransferase is a part of the ubiquinone and menaquinone biosynthesis pathway [58]. IspG belongs to the methylerythritol phosphate (MEP) pathway and catalyzes the conversion of Me-cPP (2C-methyl-D-erythritol 2,4-cyclodiphosphate) into HMBPP (hydroxymethylbutenyl 4-diphosphate), a key substrate in the production of isoprenoids that are also required for the quinone biosynthesis (**Figure 3.16 A**) [59]. Reduced abundance of these two enzymes was observed even under anaerobic conditions, regardless of the respiration status of *E. coli* cells. Notably, although the change in the UbiE level was below the significance threshold in TB under aerobic conditions, its expression was nevertheless reduced (**Figure 3.12 B**).

In addition to the cluster of respiration-related proteins, significant changes in the Δ*hflKC* strain were also observed in the levels of other proteins. Most prominently, proteins involved in motility and chemotaxis were downregulated in LB (**Figure 3.12 E** and **Table 6**) and also in TB under both, aerobic and anaerobic conditions (**Table S 1** and **Table S 2**). Notably, the abundance of known FtsH substrates [60] and of FtsH itself was not significantly affected in either LB or TB (**Figure 3.12 F, G**), confirming that the Δ*hflKC* deletion does not lead to a general change of the FtsH activity.

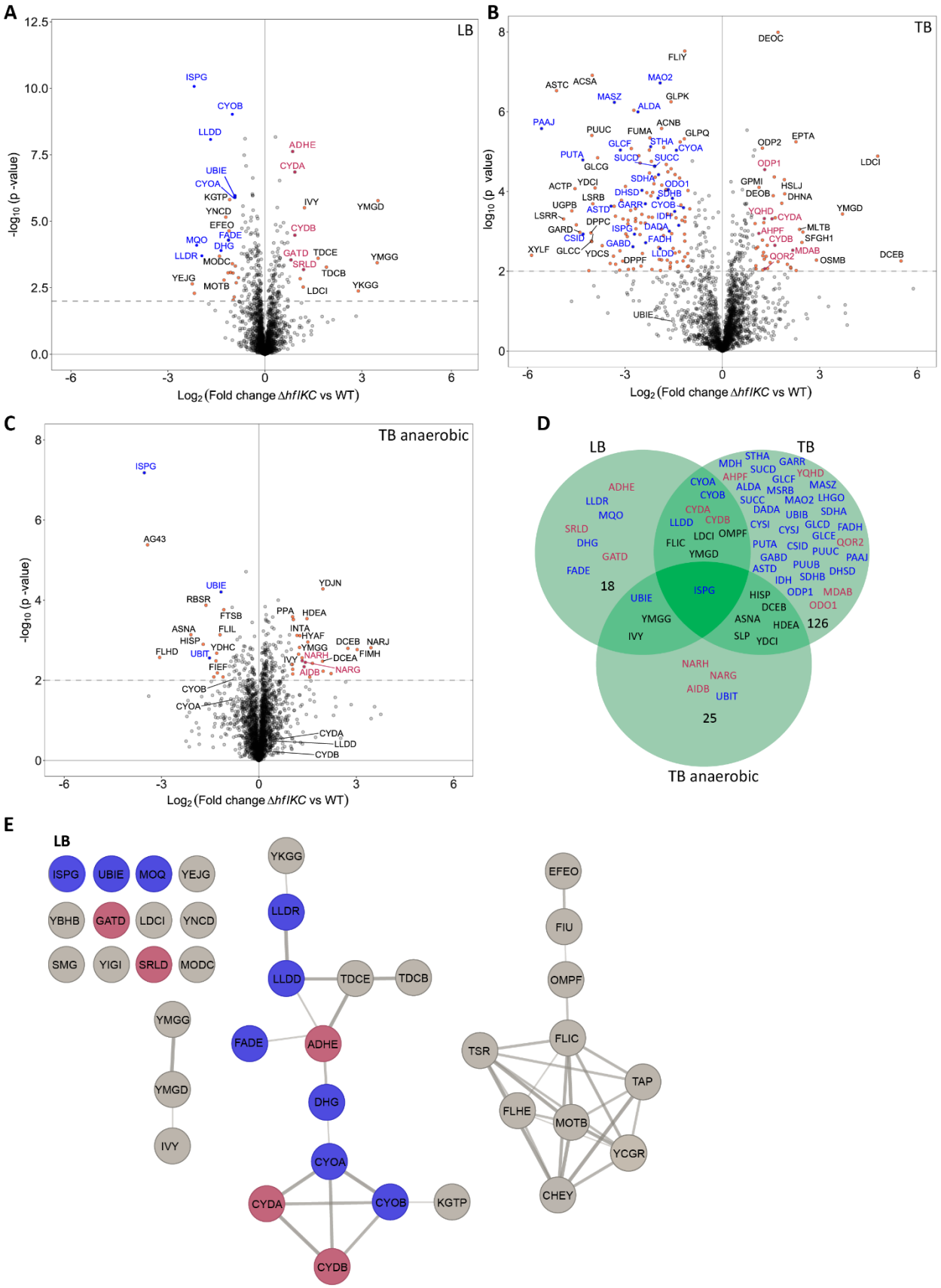
A
LB
-log10 (p -value)
Log2 (Fold change ΔhflKC vs WT)
B
TB
log10 (p value)
Log2 (Fold change ΔhflKC vs WT)
C
TB anaerobic
-log10 (p -value)
Log2 (Fold change ΔhflKC vs WT)
D
LB
TB
TB anaerobic
18
126
25
E
LB

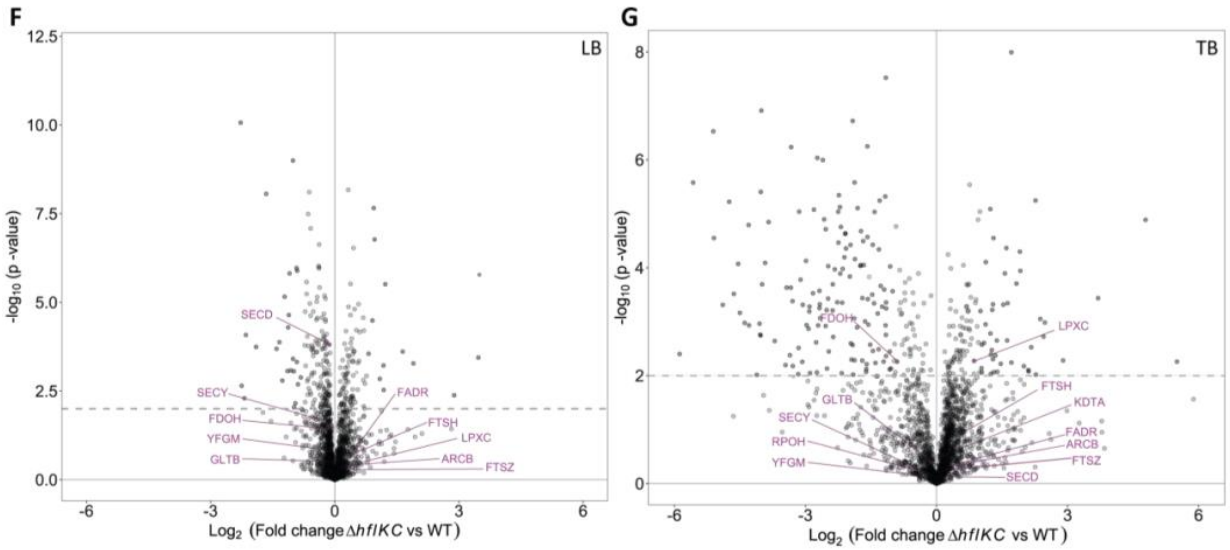

Figure 3.12 Changes in abundances of respiratory and other proteins in *ΔhflKC* deletion strain.

(A-C) Volcano plots showing difference in protein levels between *ΔhflKC* deletion and wildtype strains, for cultures grown for 4 h aerobically at 220 rpm in LB (A) or in TB (B), or anaerobically in TB (C). Data are for six (LB) or three (TB) independent replicates. Labeled proteins, with the p-value <0.05 and log2 of fold change >0.8 (LB) or >1 (TB), were considered to be significantly different between the two strains. Respiration-related proteins are highlighted in either blue (downregulated) or red (upregulated); other significantly affected proteins are shown with orange dots, and no significantly affected proteins are shown in black labels.

(D) Venn diagram showing commonalities and differences between proteins that are significantly up- or downregulated under different conditions. Colors are as in other panels; only respiration-related proteins and those affected under more than one conditions are shown by names. Numbers of other proteins affected under particular condition are indicated.

(E) STRING diagram showing proteins that are significantly up- or downregulated in *ΔhflKC* deletion strain, with links indicating relations between proteins. Proteins related to respiration are labeled in red (upregulated) or blue (downregulated).

(F-G) Abundance of known FtsH substrates in *ΔhflKC*. Same volcano plot in Figure 3.12 A, showing the FtsH substrates and FtsH itself being highlighted in purple. Strains cultures in LB (F) or in TB (G) at 220 rpm. Data are for six (LB) or three (TB) independent replicates. Proteins with the p-value < 0.05 and log2 of fold change > 0.8 (LB) or >1 (TB) are considered to be significantly different between the two strains.

Table 6 Proteins showing significant differences between *ΔhflKC*, *ΔhflK* or *ΔhflC* and wildtype strains during growth in LB

Protein	**Function**	**Log_2 (Fold change)[a]**		
Respiratory proteins		*ΔhflKC vs* WT	*ΔhflK* vs WT	*ΔhflC vs* WT
ISPG	Oxidoreductase involved in isoprenol biosynthesis	-2.28	-2.37	0.02
MQO	Malate: quinone oxidoreductase	-2.15	-1.84	-0.33
LLDR	L-lactate dehydrogenase operon regulator	-1.90	-2.26	-0.44
LLDD	L-lactate dehydrogenase	-1.66	-1.52	-0.38
DHG	Quinoprotein glucose dehydrogenase	-1.34	-1.26	-0.23
FADE	Acyl-CoA dehydrogenase	-1.13	-0.50	-0.78
CYOB	Cytochrome bo(3) ubiquinol oxidase subunit 1	-1.01	-1.01	-0.20
UBIE	Ubiquinone biosynthesis	-0.92	-0.93	-0.01
CYOA	Cytochrome bo(3) ubiquinol oxidase subunit 2	-0.91	-0.85	0.00
SRLD	Sorbitol-6-phosphate 2-dehydrogenase	1.18	1.44	-0.36
CYDA	Cytochrome bd-I ubiquinol oxidase subunit 1	0.96	0.85	-0.03
ADHE	Fused acetaldehyde-CoA dehydrogenase	0.94	0.89	-0.08
CYDB	Cytochrome bd-I ubiquinol oxidase subunit 2	0.91	0.68	-0.05
GATD	Galactitol-1-phosphate 5-dehydrogenase	0.82	1.12	0.28
DMSA	Dimethyl sulfoxide reductase subunit A	0.26	-0.95	0.40
Other proteins				
YEJG	Unknown function	-2.25	-1.27	-0.15
YIGI	Putative thioesterase	-2.18	-1.23	-0.14
IBPB	Small heat shock protein	-1.74	-1.10	-0.75
MODC	Molybdate ABC transporter ATP binding subunit	-1.41	-1.35	-0.07
MOTB	Flagellar rotation	-1.27	-1.55	-0.19
YNCD	Pyrroloquinoline quinone TonB-dependent	-1.21	-1.21	-0.11
TSR	Methyl-accepting chemotaxis protein I	-1.14	-1.12	-0.20
EFEO	Ferrous iron transport system protein	-1.11	-0.99	-0.12
KGTP	Alpha-ketoglutarate:H(+) symporter	-1.09	-1.07	-0.35
KGTP	Alpha-ketoglutarate:H(+) symporter	-1.09	-1.07	-0.35
FIU	Ion transport	-1.06	-1.29	-0.06
FLGI	Flagellar P-ring protein	-1.06	-2.15	-0.12
FLHE	Flagellar protein	-1.01	-0.86	-0.19
FLIC	Flagellar filament structural protein	-0.99	-1.27	-0.21
CHEY	Chemotaxis protein	-0.98	-0.84	-0.39
TAP	Methyl-accepting chemotaxis protein IV	-0.95	-1.11	-0.42
FLIZ	DNA-binding transcriptional regulator	-0.92	-1.75	0.19
OMPF	Outer membrane porin F	-0.92	-0.86	-0.22
SMG	Uncharacterized protein	-0.89	-0.12	-0.24
YCGR	Flagellar brake protein	-0.82	-0.86	-0.07
YHCH	N-acetylneuraminate anomerase	-0.80	-0.35	-1.07
MOTA	Motility protein A	-0.80	-1.05	0.10

FLGN	Flagellar biosynthesis protein	-0.79	-0.99	0.09
CHEA	Chemotaxis protein	-0.77	-0.91	0.03
CHEW	Chemotaxis protein	-0.75	-0.89	-0.06
FLGE	Flagellar hook protein	-0.70	-1.22	-0.16
DEAD	ATP-dependent RNA helicase	-0.58	-0.80	-0.01
YECR	Lipoprotein	-0.58	-1.03	-0.05
YMGD	Unknown function	3.49	3.91	0.39
YMGG	Unknown function	3.47	4.22	0.26
YKGG	Unknown function	2.88	1.10	0.50
TDCB	Catabolic threonine dehydratase	1.90	1.71	0.63
TDCE	Formate C-acetyltransferase	1.64	1.92	0.44
IVY	Inhibitor of vertebrate lysozyme	1.22	1.62	0.00
LDCI	L-lysine degradation	1.18	1.08	0.41
YDCY	Unknown function	1.13	1.19	0.94
YBHB	Putative kinase inhibitor	1.09	0.93	0.43
PTHA	Glucitol/sorbitol transport	0.77	1.02	-0.28
PTHB	Glucitol/sorbitol transport	0.72	0.97	-0.44
PTHC	Glucitol/sorbitol transport	0.71	1.22	-0.43
TNAA	Ttryptophanase	0.62	0.85	-0.15
AG43	Antigen 43	0.37	-3.04	-0.05
THID	Hydroxymethylpyrimidine kinase	0.22	0.53	0.81
FLGC	Flagellar basal-body rod protein	ND	-0.94	-0.02

[a]Values in grey indicate no significant change; ND: no detected

Data are from Figure 3.12 A and Figure 3.13 A, B.

3.2.3 Proteomics of *ΔhflK* and *ΔhflC* individual deletions

Although we primarily focused on the phenotype of the strain lacking the entire HflKC complex, we also assessed the individual effects of *hflK* and *hflC* deletions. Consistent with their growth, proteome profiles of the Δ*hflKC* and Δ*hflK* strains were similar, whereas Δ*hflK* showed disruption of several proteins (**Figure 3.13 A, C**), and the Δ*hflC* strain showed little changes in proteome composition compared to the wildtype (**Figure 3.13 B, D**). Thus, the phenotype observed in the Δ*hflKC* strains seems to be primarily due to the lack of HflK, whereas the lack of HflC can be tolerated by the cell and becomes discernable only in the background of the *hflK* deletion. Notably, both individual deletions of *hflK* and *hflC* caused a reduction in the level of the pair protein in the HflKC complex, but such reduction in the case of Δ*hflC* strain was apparently not sufficiently strong to cause the growth phenotype or impact on the proteome composition.

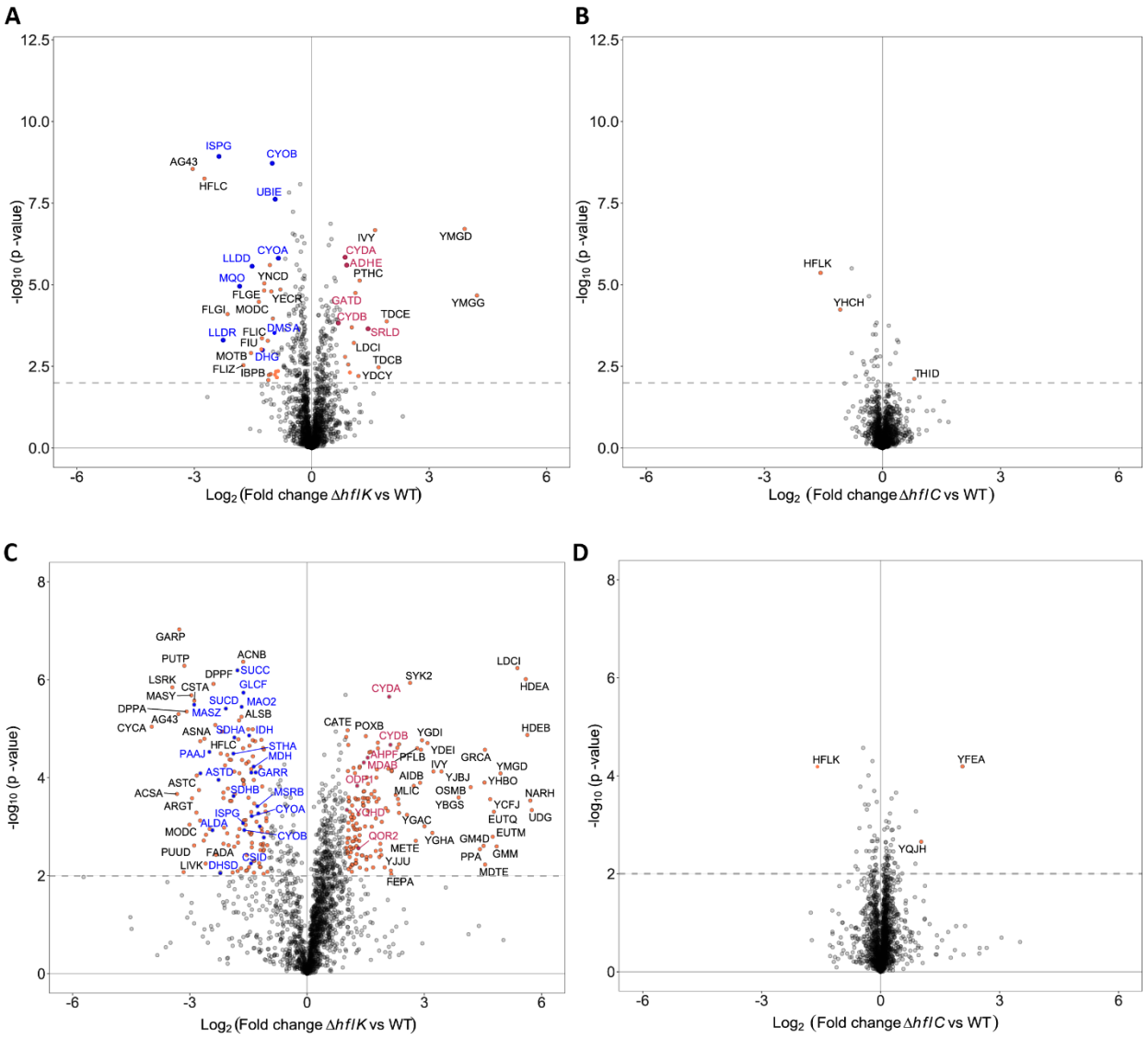

Figure 3.13 Protein abundances affected by the absence of HflK and HflC proteins.

(A, B) Volcano plots showing difference in protein levels in the *ΔhflK* (A) and *ΔhflC* (B) deletion strain and the wildtype, for cultures grown for 4 h aerobically at 220 rpm in LB. Data are for six independent replicates. Labeled proteins, with a p-value <0.05 and log2 of fold change >0.8, were considered to be significantly different between the two strains. Labels are as in Figure 3.12 A.

(C, D) Volcano plots showing difference in protein levels in the *ΔhflK* (C) and *ΔhflC* (D) deletion strain and the wildtype, for cultures grown for 4 h aerobically at 220 rpm in TB. Data are for three independent replicates. Labeled proteins, with the p-value <0.05 and log2 of fold change >1, were considered to be significantly different between the two strains. Labels are as in Figure 3.12 A.

3.2.4 Lipidomic profile of *ΔhflKC* strain

Given that SPFH proteins are known to localize within and facilitate the recruitment of other proteins into Functional Membrane Microdomains (FMM), which are regions characterized by a high content of cardiolipin (CL) and phosphatidylglycerol (PG) [20], the absence of SPFH proteins could potentially impact the levels of these specific lipids. Therefore, we decided to study changes in lipid composition in the *ΔhflKC* strain, with a particular focus on CL and PG.

Among the diverse lipids composition in bacteria membranes, phospholipids such as phosphatidylcholine (PC) and phosphatidylglycerol (PG) are the major components of the biological membranes and they form the structural basis of the membrane bilayer. There are other lipid classifications, such as the presence of double bonds (unsaturated) or their absence (saturated), as well as the length of the fatty acid chains, that can significantly influence the biophysical properties of the membrane. We used gas chromatography to obtain the lipid composition of membranes isolated from wildtype and *ΔhflKC* when grown in LB medium at 37^{o}C. **Table S 3** shows the abundance of the different acyl chain species present in both strains. We observed no difference in abundance of PC between the *ΔhflKC* and the wildtype strain. However, a significant decrease is noticed for PG in the mutant strain (**Figure 3.14 A**). Notably, there is no significant difference in the abundance of unsaturated and saturated lipids groups (**Figure 3.14 B**), and there is not difference in lipid chain length either (**Figure 3.14 C**). Interestingly, we did detect a significant reduction in the levels of cardiolipin within the double knockout strain (**Figure 3.14 D**).

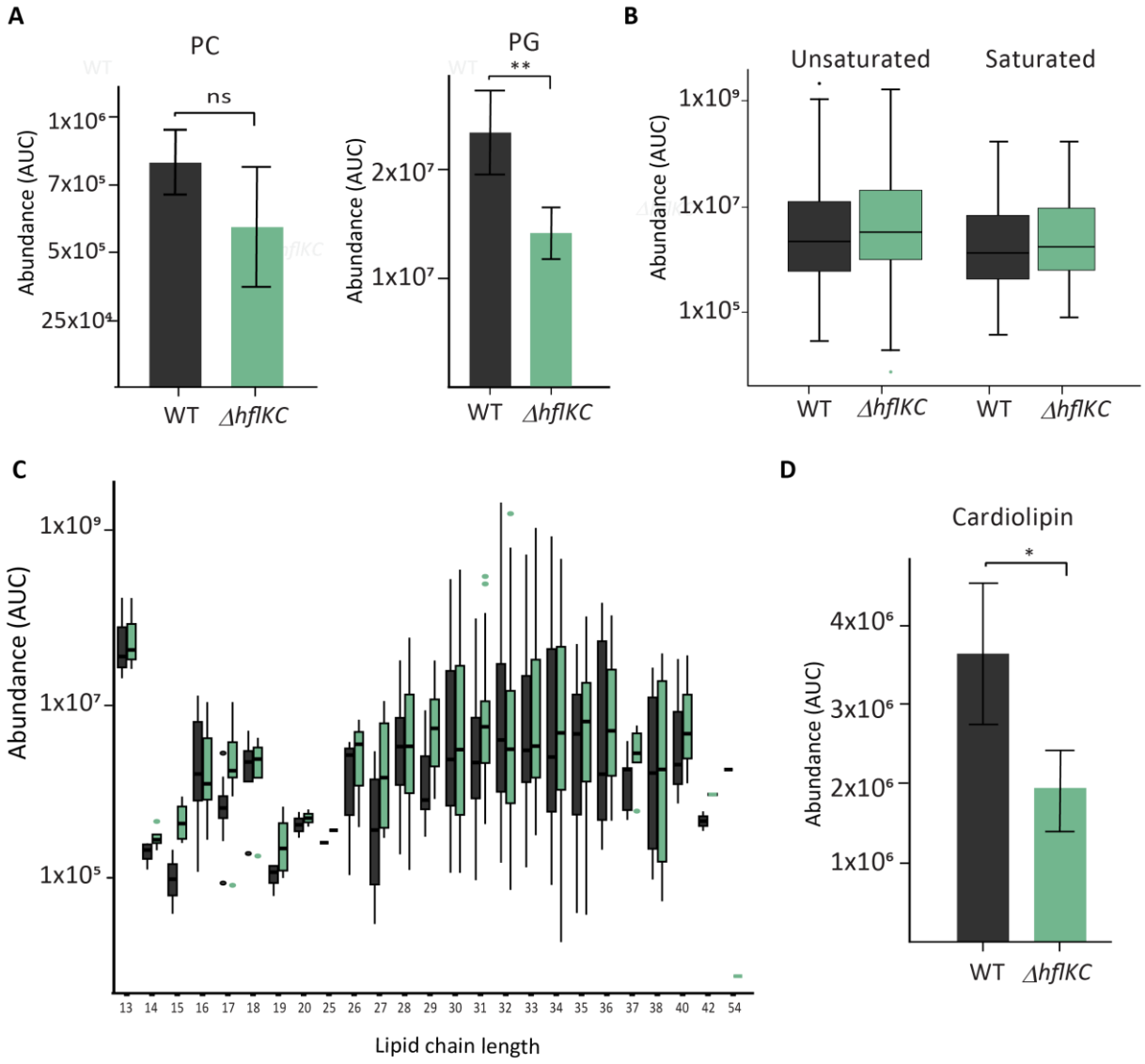

Figure 3.14 Lipid profile of ΔhflKC strain.

Gas chromatography results measuring fatty acid chain profiles for *ΔhflKC* and wildtype (WT) grown in TB at 37°C in an orbital shaker at 220rpm.

(A-D) Abundance of Phosphatidylcholine (PC) and phosphatidylglycerol (PG) (A). Abundance of unsaturated and saturated groups (B). Lipid chain length of *ΔhflKC* and wildtype (C). Cardiolipin levels (D). Data represent the mean value for three independent cultures grown in the same representative experiment. Significance of indicated differences between samples: * $p<0.05$, ** $p<0.01$, and ns = not significant according to an unpaired *t*-test.

3.2.5 Effect of *ΔhflKC* on motility

Considering the downregulation of motility proteins observed in LB and TB media, both under aerobic and anaerobic conditions, we further investigate this phenotype in the *ΔhflKC* strain. For our motility analysis, we used the well-established soft-agar technique to assess the bacteria's capacity to spread in semi-solid (0.27%) agar using motility. We compared the colony diameter of the wildtype strain to that of *ΔhflKC* to evaluate motility phenotype. However, our results show no significant difference between the strains, suggesting no drastic changes in motility behavior (**Figure 3.15 A**). Another parameter used to evaluate motility in liquid cultures is swimming velocity. In this regard, we noticed that the double mutant cells exhibited reduced swimming velocity compared to the wildtype (**Figure 3.15 B**), potentially consistent with their reduced expression of motility proteins.

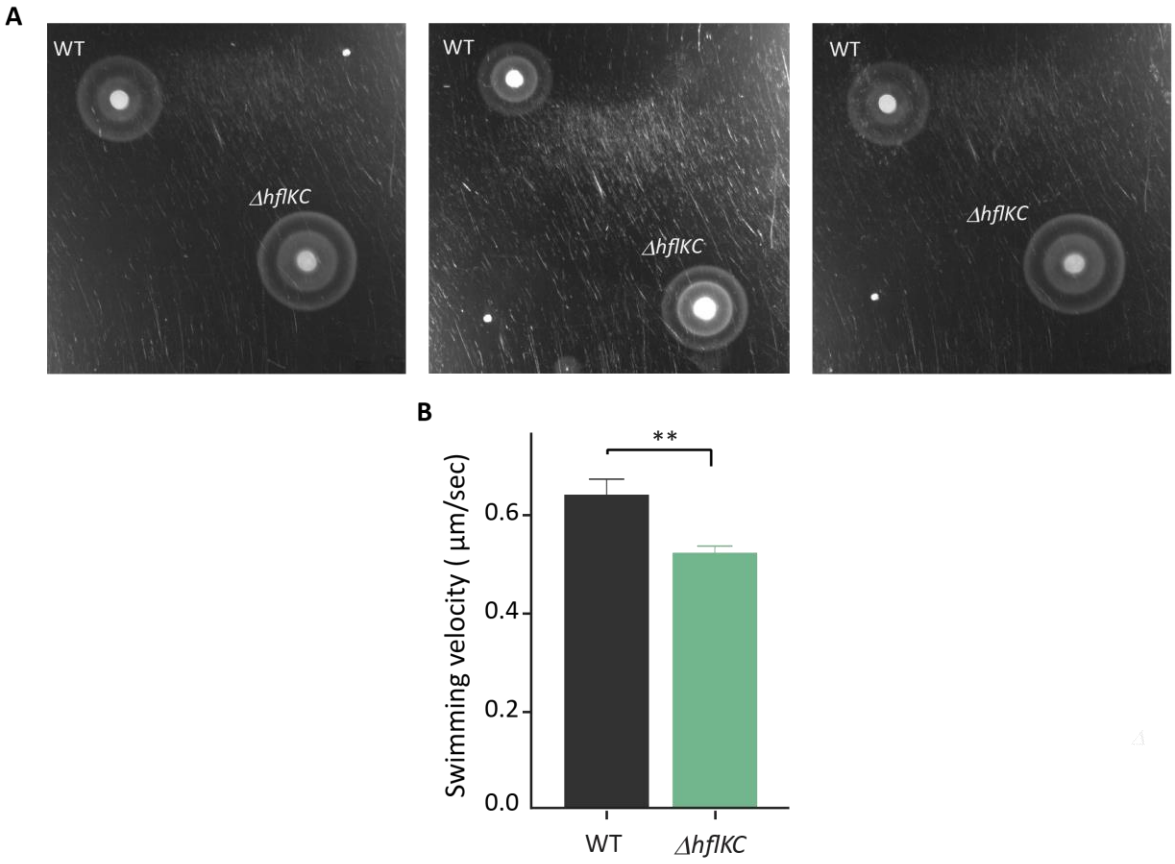

Figure 3.15 Motility behavior of *ΔhflKC* knockout.

(A, B) Images of motility in TB soft-agar medium (A). Motility in TB liquid medium (B). Data represent the mean value for three independent cultures grown in the same representative experiment. Significance of indicated differences between samples ** $p<0.01$.

3.2.6 Effect of *ΔhflKC* on MEP pathway

Given strongly reduced levels of IspG in the *ΔhflKC* strain, and the importance of MEP (methyl-D-erythritol phosphate) pathway for the biosynthesis of ubiquinone (**Figure 3.16 A**), we assessed the impact of the *ΔhflKC* deletion on the MEP pathway and ubiquinone levels. Consistent with low IspG activity, the level of IspG substrate, Me-cPP, was largely elevated in the *ΔhflKC* strain compared to the wildtype (**Figure 3.16 B**), whereas the levels of oxidized (ubiquinone-8) and particularly of the reduced (ubiquinol-8) forms of ubiquinone were strongly reduced (**Figure 3.16 C, D**). Thus, the downregulation of IspG, and possibly also of UbiE downstream in the pathway (**Figure 3.16 A**), apparently causes a disruption in the ubiquinone biosynthesis in absence of the HflKC complex.

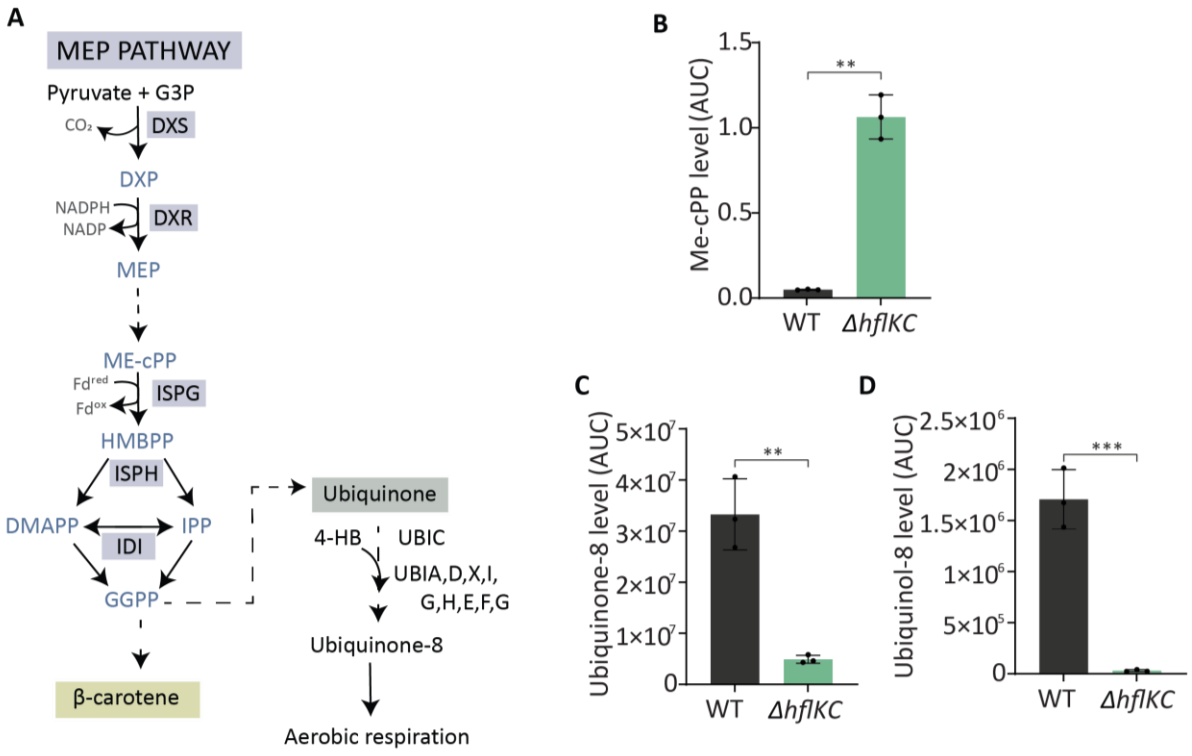

Figure 3.16 Reduction in ubiquinone levels in absence of the HflKC complex.

(A) Methyl-D-erythritol phosphate or non-mevalonate pathway (MEP pathway) in *E. coli.* Pathway metabolites (labeled with light blue color), including DXP: 1-deoxy-D-xylulose 5-phosphate; MEP: 2-C-methyl-D-erythritol 4-phosphate; ME-cPP: 2-C-methyl-D-erythritol 2,4-cyclic diphosphate; HMBPP: 1-hydroxy-2-methyl-2-(E)-butenyl 4-diphosphate; DMAPP: Dimethylallyl diphosphate; IPP: Isopentenyl

diphosphate; and GGPP: Geranylgeranyl diphosphate, are shown. In the ubiquinone biosynthesis branch, 4-HB: 4-hydroxybenzoate is highlighted.

(B-D) Levels of IspG substrate Me-cPP (B), ubiquinone-8 (C) and ubiquinol-8 (D) in wildtype (WT) and *ΔhflKC* cells grown at 220 rpm in M9 glucose minimal medium (B) or in TB (C, D). AUC is the area under the curve. Data represent the means and SD of three independent replicates.

Significance of indicated differences between samples: ** $p<0.01$, and *** $p<0.001$ according to an unpaired *t*-test.

3.2.7 Oxygen consumption by *ΔhflKC* cells

Since low levels of ubiquinone might cause the reduction of aerobic respiratory activity, we compared the consumption of dissolved oxygen by the cultures of *ΔhflKC* and wildtype cells. Indeed, oxygen consumption by the *ΔhflKC* cell culture was significantly reduced (**Figure 3.17 A**). Further consistent with reduced respiration, the level of reactive oxygen species (ROS) assessed using the dichlorodihydrofluorescein (DCF) probe (**Figure 3.17 B**), as well as membrane potential assessed using the 3,3'-diethyloxacarbocyanine iodide $DiOC_2(3)$ probe (**Figure 3.17 C**), were also reduced in *ΔhflKC* cells.

Such lower respiration, and resulting reduction in the membrane potential during aerobic growth, could lead to reduced production of ATP in *ΔhflKC* cells. This decrease was indeed evident when levels of ATP, ADP, and AMP were quantified in *ΔhflKC* and wildtype cultures using targeted metabolomics. We observed that the level of ATP was lower and the level of AMP was higher in *ΔhflKC* cells, whereas the level of ADP remained unchanged (**Figure 3.17 D**). Consequently, the *ΔhflKC* cells had lower energy charge, calculated as [(ATP) + ½(ADP)] / [(ATP) + (ADP) + (AMP)], compared to the wildtype cells (**Figure 3.17 E**).

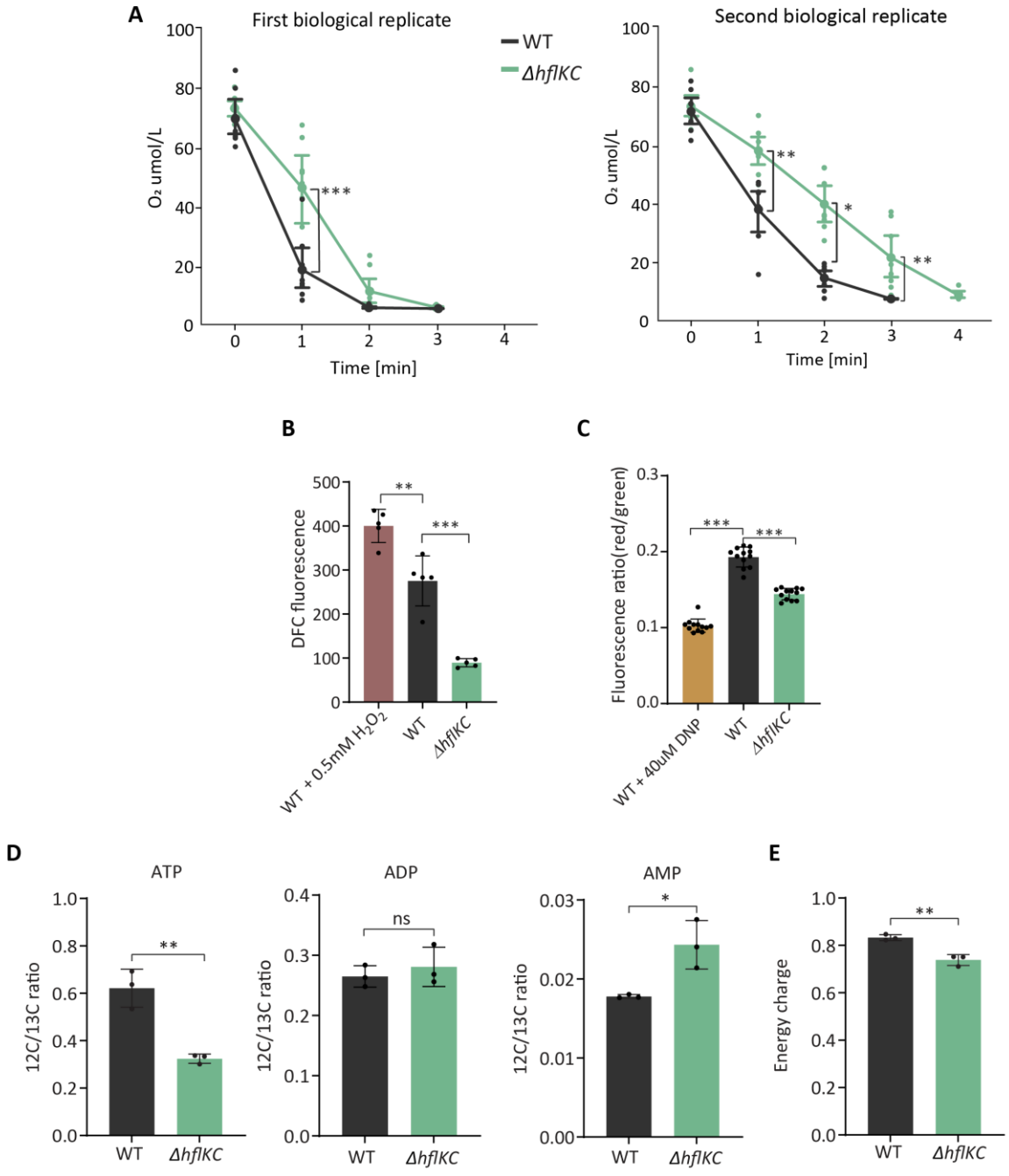

Figure 3.17 *ΔhflKC* strain shows reduced aerobic respiration.

(A) Oxygen consumption by wildtype and *ΔhflKC* cells. Cultures were grown in TB at 220 rpm, and resuspended in fresh TB, and changes in the levels of dissolved oxygen were quantified over time. Large symbols represent the means and SD of eight independent measurements (shown by small symbols) for cells from two independent cultures.

(B) Levels of ROS in wildtype and *ΔhflKC* cells grown in TB at 220 rpm, cells were incubated with the dye for 30 mins and fluorescence at 485nm was analyzed by flow cytometry. Treatment with hydrogen peroxide (H_2O_2) was used as a positive control for elevated ROS levels. Data correspond to one replicate with 5 measurements and 30.0000 events per data point. Error bars indicate SD.
(C) Membrane potential of wildtype and *ΔhflKC* cells grown in TB at 220 rpm, measured using the $DiOC_2(3)$ dye. Cells were incubated with the dye for 15 mins and fluorescence in red (670 nm) and green (510 nm) channels was analyzed by flow cytometry. The protonophore dinitrophenol (DNP) that dissipates the proton gradient across the cytoplasmic membrane was used as a control. Data correspond to two independent replicates with six measurements each and 30.0000 events per data point. Error bars indicate standard deviation.
(D and E) Levels of ATP, ADP, and AMP (H) and the corresponding energy charge (I) in cells grown in M9 glucose minimal medium at 220 rpm. Means of three biological replicates and SD are shown.
Significance of indicated differences between samples: * $p<0.05$, ** $p<0.01$, *** $p<0.001$ and ns = not significant according to an unpaired *t*-test.

3.2.8 *ΔhflKC* phenotype is restored with expression of IspG, an enzyme in the MEP pathway

Collectively, our data suggest that the lower ubiquinone levels, and consequently reduced aerobic respiration and poor growth at high aeration, might be due to low levels of IspG and/or UbiE in the *ΔhflKC* strain. Since the reduction in IspG abundance was more pronounced and consistent between all datasets, we hypothesized that it might be the primary cause of the observed respiratory phenotype. To verify this, we first expressed IspG in the *ΔhflKC* strain from a plasmid. Indeed, induced expression of IspG restored the levels of ubiquinone (**Figure 3.18 A**) and ubiquinol (**Figure 3.18 B**) in *ΔhflKC* cells, as well as their oxygen consumption (**Figure 3.18 C**), to the wildtype levels. Growth of the *ΔhflKC* strain at high aeration also increased upon induction of IspG expression, reaching even slightly higher values than that of the wildtype strain (**Figure 3.18 D, E**). Similarly, membrane potential in cells overexpressing IspG was restored even above the wildtype level (**Figure 3.18 F**). Thus, consistent with our hypothesis, all of the observed respiration-related phenotypes of the *ΔhflKC* strain could be complemented by overexpression of IspG.

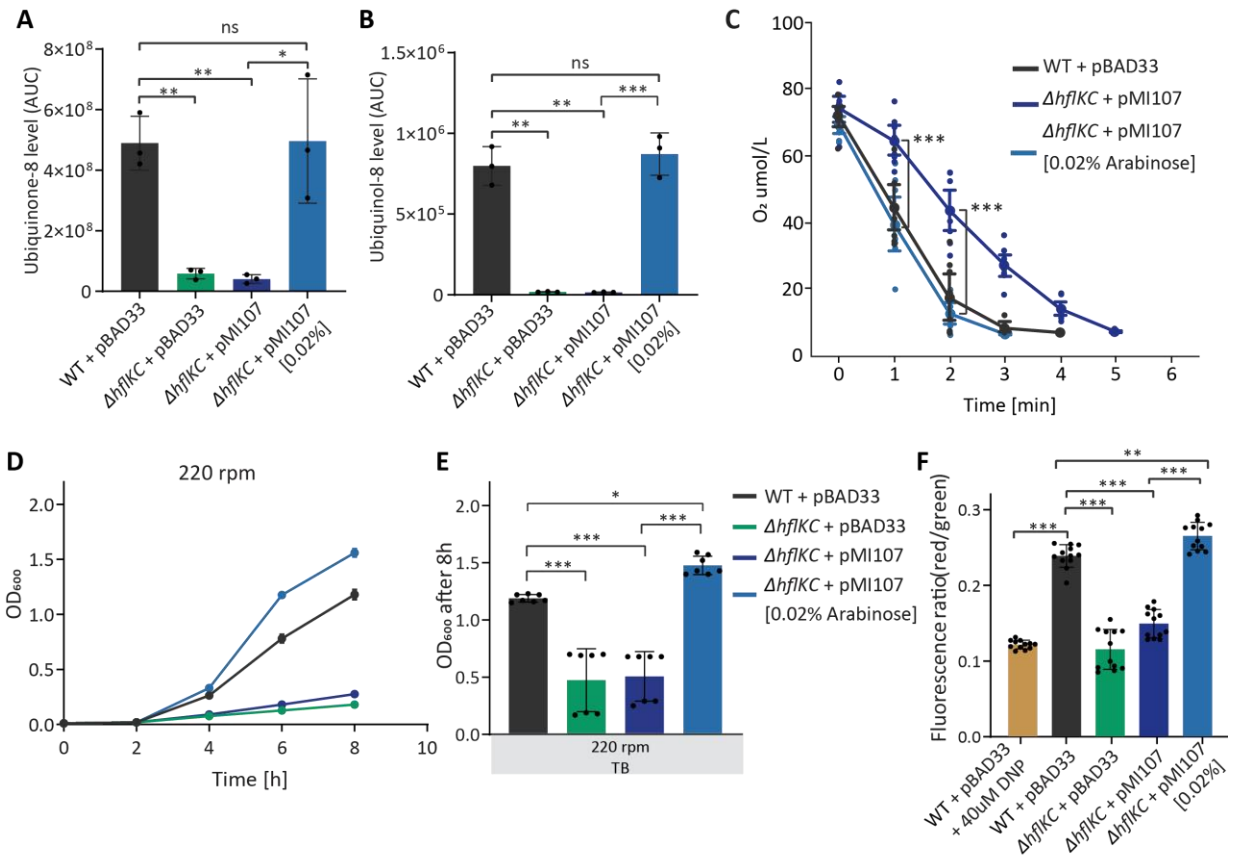

Figure 3.18 Impact of IspG levels on respiration and proteome composition.

(A, B) Levels of ubiquinone-8 (A) and ubiquinol-8 (B) are restored in the *ΔhflKC* strain by expression of IspG from inducible vector. Wildtype or mutant strains, transformed with either an empty vector pBAD33 or a pBAD33-derived plasmid pMI107 encoding *ispG* under pBAD promoter inducible by L-arabinose, were grown in TB at 220 rpm; 0.02% L-arabinose was added where indicated. Levels of ubiquinone-8 and ubiquinol-8 were quantified as in Figure 3.16 C and D, with AUC being the area under the curve. Data represent the mean and SD of three independent replicates.

(C) Oxygen consumption by the wildtype carrying pBAD33 vector and *ΔhflKC* strain carrying pMI107. Measurements were done as in Figure 3.17 A. Where indicated, 0.02% L-arabinose was added during culture growth to induce IspG expression. Large symbols represent means and SD of eight independent measurements (shown by small symbols) for cells from one culture.

(D, E) Growth of the wildtype or *ΔhflKC* strain carrying either pBAD33 vector or pMI107 in TB at 220 rpm. Where indicated, 0.02% L-arabinose was added during culture growth to induce IspG expression. For growth curves (D), data represent the mean value and SD for three independent cultures grown in the

same experiment. For final OD_{600} (E), data represent the mean and SD of seven independent replicates grown in three different experiments.

(F) Measurement of the membrane potential in the wildtype or *ΔhflKC* cells carrying pBAD33 vector or pMI107, as indicated. Measurements were performed using the $DiOC_2(3)$ dye as in Figure 3.17 C. Where indicated, 0.02% L-arabinose was added during culture growth to induce IspG expression. DNP-treated wildtype was used as a control. Data correspond to two independent replicates with six measurements each and 30.0000 events per data point. Error bars indicate SD.

3.2.9 *ispG* knockdown phenocopies *ΔhflKC* effects

Because *ispG* is essential in *E. coli*, we used the dCas9 *ispG* knockdown to assess the effect of reduced levels of IspG. This knockdown had no effect on *E. coli* growth at low aeration (**Figure 3.19 A**) but reduced growth at high aeration compared to the control (**Figure 3.19 B-D**), thus indeed phenocopying the effects of *ΔhflKC* deletion. Changes in abundance of some respiration-related proteins due to the *ispG* knockdown were similar to those in the *ΔhflKC* strain (**Figure 3.19 E, F** and **Table S 4**), with notably reduced levels of UbiE and of CyoAB and elevated levels of CydAB. This further confirms that both changes in the levels of respiratory proteins and growth phenotype of the *ΔhflKC* strain could be accounted for by the reduced level of IspG. In contrast, levels of motility-related and some other proteins were not affected by the *ispG* knockdown, suggesting that their changes are unrelated to the reduced IspG levels.

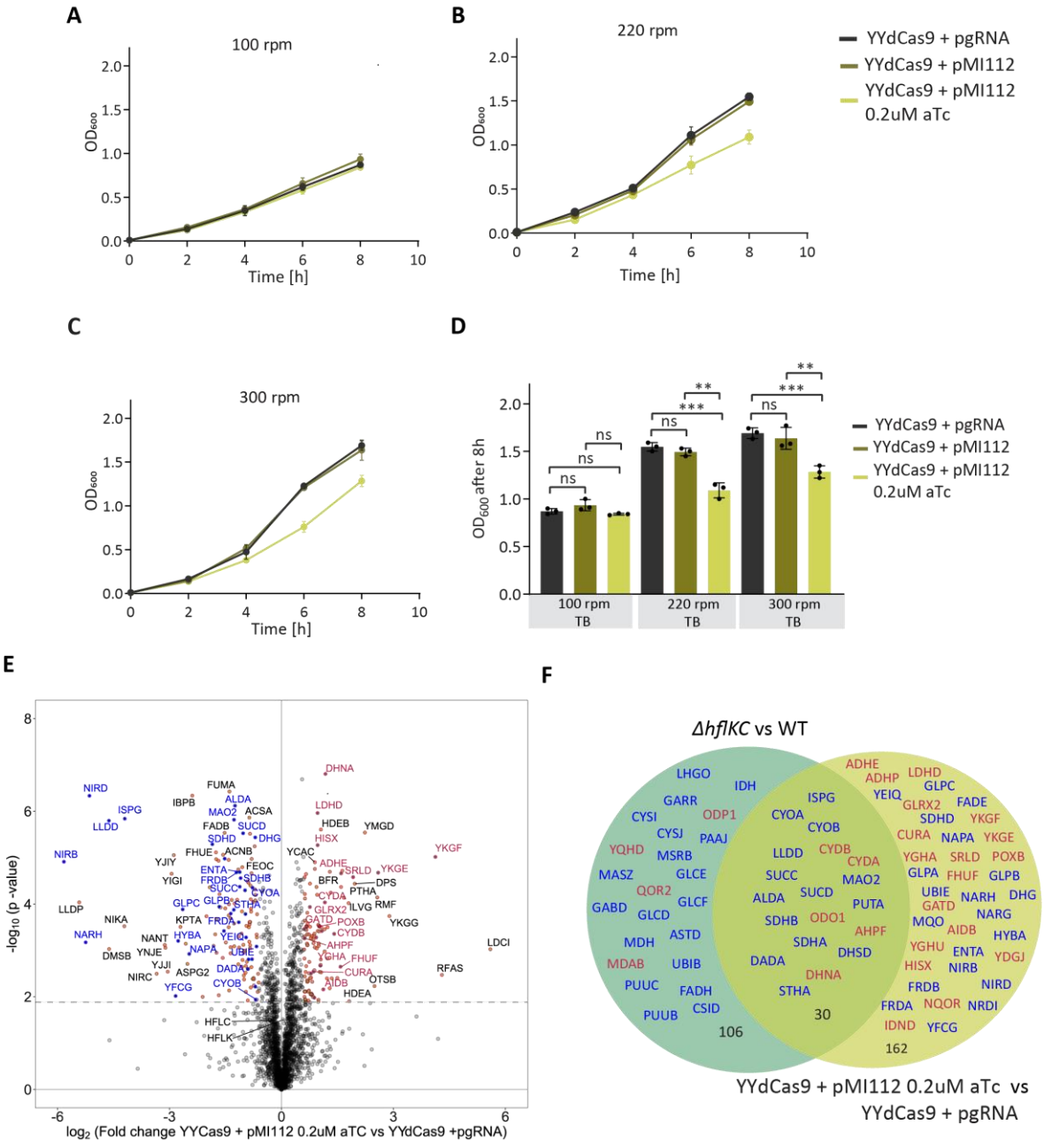

Figure 3.19 *ispG* knockdown phenocopying the effects of *ΔhflKC* deletion.

(A-D) Growth of *E. coli* YYdCas9 strain carrying either the empty pgRNA vector or pgRNA-derived pMI112 construct expressing guide RNA for *ispG* knockdown under a constitutive promoter. Where indicated, expression of dCas9 was induced with 0.02uM aTC. Cells were grown in TB at 100 rpm (A) 220 rpm (B) and 300 rpm (C). Data represent the mean value and SD for three independent cultures grown in the same experiment. For final OD_{600} comparisons (D), data represent the mean and SD of three independent

replicates grown in one experiment. Significance of indicated differences between samples: * p<0.05, ** p<0.01, *** p<0.001 and ns = not significant according to an unpaired *t*-test.
(E) Volcano plot showing the difference in protein levels between *E. coli* YYdCas9 carrying either pMI112 or pgRNA vector. Cells were grown in TB at 220 rpm for 4 h, with 0.2 uM aTc added to the pMI112-carrying strain. The data are for three independent replicates. Proteins with the p-value < 0.05 and fold change >1 were considered to be significantly different between the two strains and are labeled as in Figure 3.12 A.
(F) Venn diagram showing commonalities and differences between proteins that are significantly up- or downregulated upon *hlfKC* deletion and *ispG* knockdown. Labels are as in Figure 3.12 A.

3.2.10 Role of ArcAB system in *ΔhflKC* strain

Finally, we investigated the mechanism responsible for the observed global changes in abundance of respiratory proteins due to reduced levels of IspG. In *E. coli*, the levels of (oxidized) quinones are known to repress the two-component ArcAB system [61]. In turn, the system controls the expression of a large number of respiration-related genes to mediate transition from the aerobic to anaerobic growth [62]. We thus hypothesized that reduced biosynthesis of ubiquinone, observed in the *ΔhflKC* and *ispG* knockdown strains, might cause activation of the ArcAB system, leading to downregulation of the aerobic respiratory genes and induction of the microaerobic cytochrome oxidase *bd*-I.

Indeed, although the deletion of *arcB* gene encoding the sensory kinase of the ArcAB system itself negatively affected growth, we observed no additional impact of deleting *hflKC* genes in the *ΔarcB* background on aerobic growth in TB, regardless of the shaking rate (**Figure 3.20 A-D**). Further consistent with our hypothesis that most of the *ΔhflKC*-dependent changes in protein levels are mediated by ArcAB activation, changes in the proteome composition caused by the *arcB* deletion were largely opposite to those caused by the *hflKC* deletion (**Figure 3.20 E, F** and **Table S 5**). Moreover, no changes in the levels of CyoAB or CydAB proteins could be observed when comparing *ΔarcB* and *ΔhflKC ΔarcB* strains (**Figure 3.20 G,H** and **Table S 6**), further suggesting that these changes are dependent on the ArcAB system. In contrast to that, downregulation of IspG and UbiE, as well as of several other proteins, including those involved in motility, apparently happens independently of the ArcAB system.

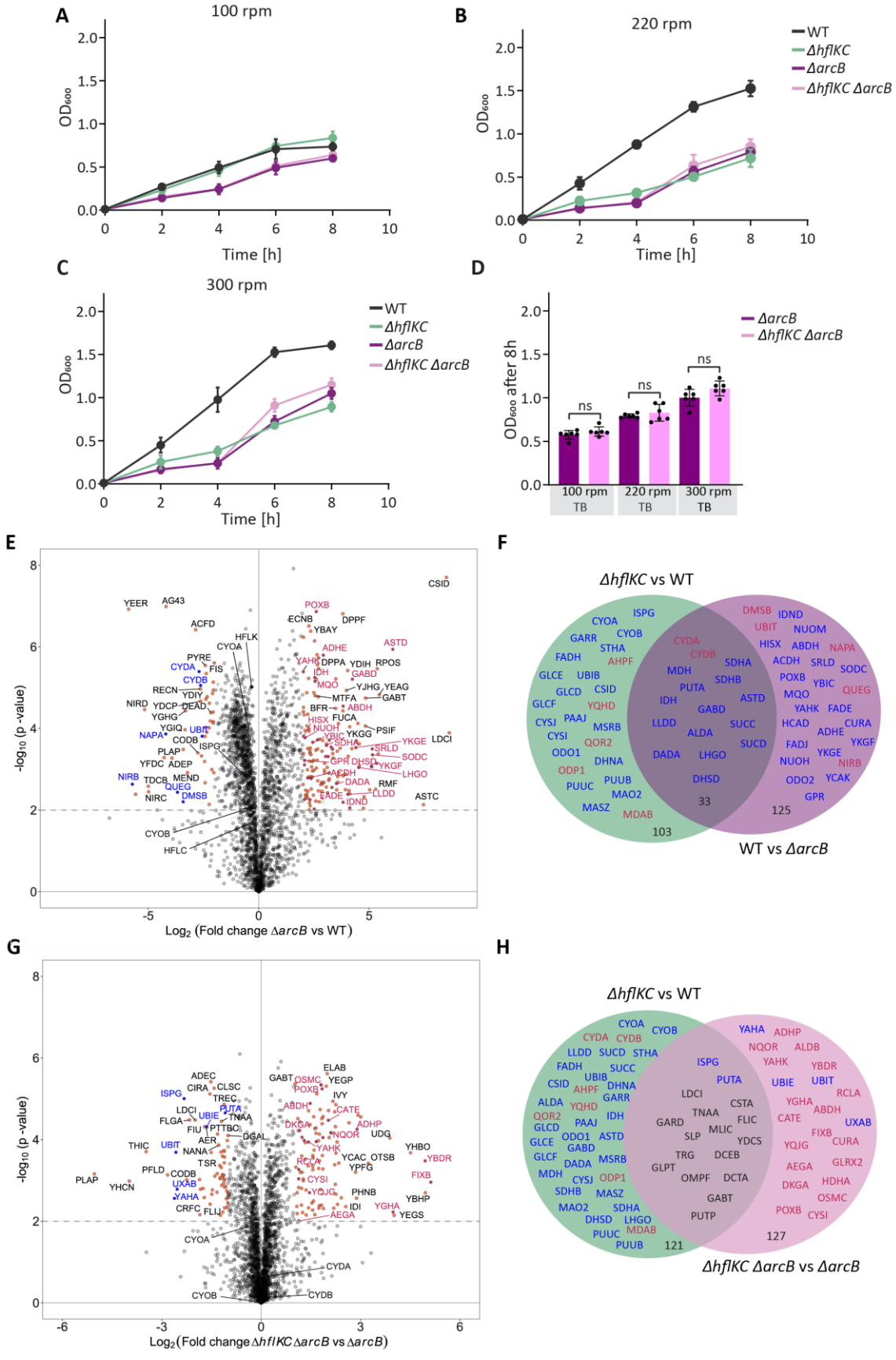
A
100 rpm
OD600
Time [h]
B
220 rpm
WT
ΔhflKC
ΔarcB
ΔhflKC ΔarcB
C
300 rpm
D
OD600 after 8h
ns
100 rpm TB
220 rpm TB
300 rpm TB
E
-log10 (p -value)
Log2 (Fold change ΔarcB vs WT)
F
ΔhflKC vs WT
103
33
125
WT vs ΔarcB
G
Log2 (Fold change ΔhflKC ΔarcB vs ΔarcB)
H
ΔhflKC vs WT
121
127
ΔhflKC ΔarcB vs ΔarcB

Figure 3.20 Growth phenotype and proteome changes in ΔhflKC strain are partly dependent on ArcAB system.

(A-D) Growth of the wildtype, *ΔhflKC, ΔarcB and ΔhflKC ΔarcB* strains in TB at 100 (A) 220 rpm (B), 300 (C) and final OD_{600} after 8 h at different shaking rates (D). For growth curves, data represent the mean value and SD for three independent cultures grown in the same experiment. For final OD_{600}, data represent the mean and SD of six independent replicates grown in three different experiments. ns = not significant according to an unpaired *t*-test.

(E) Volcano plot showing difference in protein levels between the wildtype (WT) and *ΔarcB* strains grown in TB at 220 rpm for 4 h. Labels are as in Figure 3.12 A.

(F) Venn diagram showing overlap between proteins that change significantly during growth in TB upon *hflKC* deletion and upon *arcB* deletion. Labels as in Figure 3.12 A, but the sign of changes upon *arcB* deletion is inverted.

(G) Volcano plot showing difference in protein levels between the *ΔhflKC ΔarcB* and *ΔarcB* strains strains grown in TB at 220 rpm for 4 h. The data are for three independent replicates. Labels are as in Figure 3.12 A.

(H) Venn diagram showing overlap between proteins that change significantly during growth in TB upon *hflKC* deletion in the wildtype or in *ΔarcB* strain. Labels are as in Figure 3.12 A.

4 Discussion

4.1 Phenotypes of SPFH proteins

4.1.1 SPFH fluorescent fusion proteins show similar localization patterns

In this study, we first investigated the expression and cellular localization of the SPFH proteins HflK, HflC, QmcA, and YqiK in *E. coli*. To accomplish this, we initially used a high-copy plasmid with the strong *trc* promoter to enhance protein expression and thereby facilitating the detection and visualization of these proteins under the microscope. Collectively, our results align with prior studies, supporting that SPFH proteins indeed localize within the cellular membrane. Previous reports for SPFH proteins have shown that flotillins in *B. subtilis* and prohibitins in eukaryotic cells form large complexes in membranes, resulting in a punctuate localization pattern *in vivo* [20], [63], [64].

Notably, HflK-sfGFP and HflC-sfGFP exhibited similar patterns, with bigger immobile spots localized on the poles and smaller mobile spots on the lateral border of the cell. Differences in spot size could be due to the fact that these two proteins form a complex of 24 proteins [41]. Thus, small spots might correspond to individual complexes, while large spots may denote the aggregation of several complexes. The localization of HflK and HflC proteins is expected to be similar since these two proteins interact to form a large complex that localizes in the membrane. Additionally, their expression levels are expected to be equivalent, as there are 12 copies of each protein involved in the complex's assembly [31]. Under the native promoter, QmcA-sfGFP displayed a high number of spots that are distributed along cell poles and lateral borders. Interestingly, HflKC and QmcA were found to co-localize in the detergent-resistant membrane (DRM) on *E. coli* membranes [21], which may suggest a possible co-localization of these three proteins in the membrane. YqiK-sfGFP displayed a discreet punctuate distribution with relatively dynamic spots along the cell. This pattern has been reported before by Jovanovic G. et. al., where they observed that overexpression of YqiK-GFP displayed membrane localizations with local movement of the spots located at the polar and lateral regions of the cell [65].

Overexpression of membrane proteins is crucial for enhancing visualization, but it can also lead to non-physiological outcomes within the cells. Thus, we took an additional step to investigate localization using

their own promoter from their native chromosomal location. Notably, the expression levels of SPFH proteins with native promoter exhibited a substantial decrease compared to the *trc* promoter expression. However, in overall localization pattern is similar. HflK and HflC also show small and big spots distributed along the lateral border and cell poles, primarily consisting of mobile spots. We consider the mobile spot to be the formation of a single complex, while the bigger spots could be the aggregation of several complexes making them less mobile. On the other hand, QmcA exhibited the higher expression level and mostly static spots distributed along the cell poles and lateral borders.

The expression of YqiK under its native promoter was drastically reduced. While under expression on *trc* promoter, it has a large number of spots distributed along cells; under native promoter, it could not be detected. This could suggest that, at least under this specific experimental growth condition, YqiK might not be required. YqiK belongs to the flotillin group of the SPFH family and proteins in this group have been reported to be expressed in a specific growth condition. For instance, in *B. subtilis* FloA is constitutively expressed, whereas FloT is expressed primarily during stationary growth, cell wall stress, and sporulation [66], [67].

Our observation regarding the localization of SPFH proteins under native expression partially aligns with a prior report by Wessel K. et al. in 2023. In their study, they also observed the formation of punctate foci for HflK and HflC, however, they report an exclusively localization of these proteins at the cell pole, while we also observe a lateral localization. Concerning QmcA and YqiK, their results were highly consistent with ours, as QmcA was found to be distributed throughout the entire cell, while YqiK was not detected [36]. Collectively, our results involved a group of different microscopy techniques that confirm SPFH localization but also offer new insights into their expression levels, distribution, and dynamics of these proteins in *E. coli.*

4.1.2 Challenges in membrane protein extraction for pull-down analysis of SPFH proteins

Knowledge about protein–protein interactions of SPFH proteins in bacteria is still limited. Therefore, we studied the protein interaction network of SPFH proteins in our model microorganism, *E. coli*. In our study, pull-down was used as a fundamental technique to elucidate the interacting partners of SPFH (HflK, HflC, QmcA, and YqiK) proteins.

A key aspect of the pull-down method involves the extraction and protein solubilization, which can be notably challenging, particularly when working with membrane proteins. These challenges come from the hydrophobic nature of membrane proteins and their integration within the lipid bilayer, which makes membrane proteins difficult to solubilize. In our efforts to address these difficulties, we used two different methods for membrane protein extraction.

We first used a traditional aqueous-based extraction method with Triton X-100 as detergent, along with various mechanical lysis techniques such as sonication, French press, and microfluidizer. To our surprise, none of these tested conditions resulted in highly effective protein solubilization. This unexpected outcome led us to consider the idea that SPFH proteins are integral components of FMMs, characterized by specific lipid compositions within the membrane. It is plausible that the challenges encountered in extracting SPFH proteins arise from the unique lipid environment, which creates a high-density packing around these proteins.

Despite these difficulties in achieving complete solubilization of the proteins, we decided to use the fraction of the samples that exhibited some degree of solubility for subsequent co-IP and mass spectrometry (MS) analyses. The results showed a high count of peptides for each of the tagged SPFH proteins. This outcome corroborates the successful extraction of the solubilized fraction of the samples. The large number of peptides identified by MS corresponds to the high copy number of *trc* operon used for the expression of SPFH proteins during these experiments. In our extraction condition, we were able to identify the interaction of HflK, HflC, and FtsH proteins, however, it is important to point out that the enrichment for other potential candidates was minimal. This may be attributed, in part, to the rigorous mechanical lysis employed for solubilization.

The second strategy we used to achieve better solubilization, was to use the polymer SMALP-300P, a styrene maleic acid co-polymer recently used for the extraction of membrane proteins [27]. This polymer demonstrates the capacity to encapsulate membrane proteins from native membranes, operating without the need for detergents. SMALP polymer achieves this action by enveloping a section of the lipid bilayer, forming a disc-like particle or nanodisc [68]. Our results show a remarkable efficiency in protein solubilization across all samples, reflected in the effective lysing and minimal membrane aggregation. However, the enrichment for possible candidates was barely detected, abundance of peptides was even lower compared to Triton X-100 results. Notably, the interaction between HflK-HflC and FtsH was absent in this tested condition. We hypothesize that the absence of detected protein interactions may be linked to the size of the nanodiscs produced by the polymer. According to previous research, these nanodiscs

typically range in diameter from 6 to 30nm [52]. Notably, the HflK-HflC complex is reported to have a diameter of approximately 20nm [31], which is close to the size range generated by the SMALP-300P polymer. This size discrepancy suggests that the smaller nanodiscs may have affected the interaction partners of the target proteins, potentially disturbing the protein-protein interactions.

The challenges in our pull-down results lead to thinking about the localization of SPFH proteins within the cell. SPFH proteins are hypothesized to be integral components of the DRM within FFM (functional membrane microdomains), which are characterized by high packing densities of specific lipids [21]. This unique localization pattern suggests that SPFH proteins may necessitate distinct strategies for extraction and solubilization. The challenges faced in this study underscore the complexity of working with membrane proteins and emphasize the need for adapted approaches to investigate their interactions within the context of functional membrane microdomains. In conclusion, our coIP experiments demonstrated the inherent difficulties in solubilizing membrane proteins like SPFH and highlighted the importance of considering their unique cellular localization when designing extraction and solubilization protocols. Further improvement of these techniques is necessary to find the complexities of SPFH protein interactions within functional membrane microdomains. We consider that techniques such as cross-linking could help to stabilize the interaction between proteins for future experiments.

4.1.3 Exploring the impact of SPFH proteins on growth, responses to temperature variations, and osmolality

SPFH proteins are known to form large homo-oligomeric complexes within cellular membranes, and some have even been found within DRMs, leading to speculation that SPFH proteins play a role as integral components of Functional Membrane Microdomains (FMMs) and may influence membrane structure and organization. These changes in membrane organization have the potential to impact growth responses to temperature variations. Therefore, we studied how different temperatures and osmolality could affect the growth of SPFH knockouts.

Our results yielded an important observation, the quadruple knockout significantly decreases its growth at lower temperatures (30°C and 25°C). Initially, we considered that this growth reduction might be linked to alterations in membrane fluidity. However, when we measured the generalized polarization at 25°C

using di-4-ANEPPDHQ, we did not detect substantial changes. It's important to note that none of the other single knockouts exhibited a growth defect at low temperatures, making it challenging to attribute this phenotype to a specific SPFH protein. The roles of SPFH proteins on lipid organization and fluidity are well-established; however, no reports have described their sensitivity to temperature changes.

One plausible explanation could be an imbalance of the PHB domain within the cell, but further investigation is required to determine the impact of this on SPFH proteins. On the other hand, we did not observe significant changes in high osmolality conditions, indicating that membrane integrity in the absence of SPFH proteins is not compromised.

4.1.4 Lack of SPFH protein reduces membrane fluidity at high temperature

SPFH proteins, particularly flotillin, have long been recognized as integral components of DRMs within FMMs in Gram-negative bacteria and are often considered markers for lipid rafts [4], [5], [70]. Their association with microdomains has raised speculations regarding their potential influence on lipid membrane dynamics and organization [7], [9], [71], [72]. While extensive research has explored the influence of flotillin on membrane organization in *B. subtilis,* our understanding of the impact of SPFH proteins in *E. coli* remains limited.

To bridge this gap and investigate the influence of SPFH proteins on membrane organization, we measured lipid organization using membrane fluidity as a parameter. We employed the fluorescent dye di-4-ANEPPDHQ to assess membrane fluidity within living *E. coli* cells. Notably, the quadruple SPFH knockout exhibited more sensitivity to a higher temperature, with a significant increase in fluidity observed at 42°C, whereas the impact at lower temperatures was less pronounced. It is well-established that high temperature leads to increased membrane fluidity in bacterial membranes [73]. From these findings, we can draw two significant conclusions: first, di-4-ANEPPDHQ is indeed a reliable indicator of membrane order, and second, the quadruple SPFH knockout strain is more fluid than the wildtype at elevated temperatures. On the other hand, at the standard growth temperature of 37°C, we observed a slight reduction in generalized polarization (GP) values for all single and multiple SPFH knockout strains compared to the wildtype. This reduction of GP suggests an increase in membrane fluidity. Even when the

effect described here is very small, this scale of magnitude could be significant for the disruption of biological processes.

The impact of SPFH proteins on membrane fluidity could be attributed to two primary factors. First, the formation of large protein complexes by SPFH proteins within the membrane may influence lipid organization, the absence of the complex could potentially increase the space between lipids and consequently enhance fluidity. Second, it is believed that SPFH proteins colocalize with cardiolipin, a critical component of membrane biophysical properties. The absence of SPFH proteins may disrupt the localization of cardiolipin, leading to alterations in membrane structure [74], [75].

Collectively, our data provide evidence of the effect of SPFH proteins on membrane fluidity. These findings offer fresh insights into the role of SPFH proteins in shaping the physical organization of membranes in *E. coli.* Interestingly, our observations closely align with prior studies that established a link between the absence of FloT and a decrease in membrane fluidity in *B. subtilis* [7], [74].

4.1.5 Biofilm formation defect of SPFH proteins in *E. coli*

Biofilms are communities of microorganisms that grow on surfaces, encased in self-produced extracellular matrices, displaying unique properties compared to free-floating cells [76]. Biofilms have been extensively studied using various experimental models; and over the years, different experimental models have been used to study the formation, structure, and protein expression of biofilms [77], [56], [78]. Flotillins within the SPFH protein family have been extensively studied for their role in biofilm formation in *B. subtilis* [6], [79][80]. However, the contributions of other SPFH family members to biofilm formation remain poorly understood.

To explore the broader role of SPFH proteins, we studied their role in *E. coli* biofilm formation. While our initial results showed reduced biofilm formation in single knockouts (*ΔhflK, ΔqmcA, and ΔyqiK*) and the quadruple mutant (*ΔhflKC ΔqmcA ΔyqiK*) when grown in LB medium, no significant differences were observed in TB medium. This discrepancy might be due to variations in growth factors and oxygen levels, as TB lacks yeast extract and our static incubation conditions in microplates limit oxygen supply.

Further investigation is needed to better understand our observations in LB. Biofilm assays in microplates have limitations, as they may lead to irregular biofilm distribution and thickness which introduce variability in the reproducibility of the data. Additionally, observations of colony morphology on agar plates did not reveal distinct differences among SPFH knockouts, highlighting the need for a more comprehensive understanding of their roles in various biofilm models.

4.1.6 Tolerance of SPFH quadruple knockout to antibiotics

In our experimental procedure, the SPFH quadruple mutant shows tolerance to Meropenem, a β-lactam antibiotic used for treating various bacterial infections. Meropenem's mechanism of action involves inhibiting the catalytic activity of bacterial transpeptidases, which disrupts cell wall synthesis [81]. Additionally, our mutant exhibited slight tolerance for two compounds that belong to the group of fluoroquinolone antibiotics, sarafloxacin and gatifloxacin. These antibiotics work by inhibiting bacterial DNA replication and transcription. They form complexes with DNA gyrase and topoisomerase IV enzymes, obstructing their ability to introduce negative supercoils into DNA and separate DNA strands. Consequently, vital processes such as DNA replication, transcription, and repair are disrupted [82].

A previous study has reported the increased sensitivity of the mutant lacking all SPFH genes in *E. coli* to aminoglycosides. They tested various aminoglycosides, including tobramycin, capreomycin, sisomicin, and paromomycin, and they found that the HflKC complex was exclusively responsible for the phenotypes [36]. In our tested library, which includes seven different aminoglycoside compounds, our results did not reveal any major effect on this group of antibiotics under our tested conditions.

In summary, further experiments, with more detailed evaluation and replicates are required to achieve an understanding of our data and the significance of the identified hits from our results.

4.2 Regulation of aerobic respiration by HflKC complex

4.2.1 Lack of HflKC complex is important for *E. coli* growth under high aeration

Although SPFH proteins are conserved between prokaryotes and eukaryotes, suggesting their fundamental importance in cellular function, the specific roles of these proteins appear to be diverse and remain poorly understood [4]. Particularly in prokaryotes, only a few examples of the functional importance of SPFH proteins have been reported [8], [74], [83], [84]. Studies of SPFH proteins in *E. coli* have so far identified only mild phenotypes that were not explained mechanistically [36]. This is particularly surprising for the HflKC complex, which is known to form a large oligomeric inner membrane cage that encloses an essential AAA-type protease FtsH, and is believed to regulate FtsH access to its substrates [41].

Here we provide strong evidence that the HflKC complex plays an important role during *E. coli* growth under conditions of high aeration. Whereas *ΔhflKC* strain grows similar to the wildtype *E. coli* under anaerobic conditions or at low aeration, its growth is severely reduced compared to the wildtype under high aeration. Our results, summarized in **Figure 4.2** suggest that this growth defect in absence of the HflKC complex could be explained by the reduction in the level of IspG, an enzyme in the methylerythritol phosphate (MEP) pathway for isoprenoid biosynthesis. MEP pathway provides essential precursors for several cellular processes, including biosynthesis of pigments and ubiquinone, an important molecule in aerobic respiration [85], [86], and level of ubiquinone-8 was indeed strongly reduced in *ΔhflKC* cells. Besides limiting precursor supply for ubiquinone biosynthesis, low levels of IspG further decrease the production of ubiquinone-8 indirectly, by affecting the level of UbiE, one of the downstream enzymes involved in this biosynthetic pathway.

The decrease in the ubiquinone-8 biosynthesis is consistent with the observed reduced aerobic respiration in *ΔhflKC* cells. This is likely to be a direct consequence of reduced activity of cytochrome ubiquinol oxidases, which could be further enhanced by perturbed expression of multiple respiration-related proteins, including downregulation of cytochrome ubiquinol oxidase bo_3 (CyoABCD) that operates under conditions of high O_2, and upregulation of less efficient cytochrome ubiquinol oxidase *bd* (CydAB) that is normally used by *E. coli* under microaerobic conditions [57].

In contrast to TB or minimal M9 medium, no growth defect was observed for *ΔhflKC* cells in LB that contains yeast extract, even at high aeration. Compared to TB, changes in the levels of respiration-related

proteins were also limited in LB to a smaller set of proteins, including IspG, UbiE and both cytochrome oxidases. Possible explanations for this difference could be the presence of isoprenoids or quinones in the yeast extract that partly complement the effect of the IspG and UbiE downregulation on the ubiquinone biosynthesis and thus on respiratory activity, or lesser importance of respiration for *E. coli* growth in LB.

4.2.2 Reduced levels of IspG account for the respiratory phenotype of *ΔhflKC* strains

Collectively, our data suggest that the lower ubiquinone levels, decrease in aerobic respiration, and growth defect under high aeration, are caused by the low levels of IspG and/or UbiE in the *ΔhflKC* strain. Since the reduction in IspG abundance was more pronounced and consistent between all datasets, we hypothesized that it is the primary cause of the observed respiratory phenotype. Indeed, induction of IspG in *ΔhflKC* cells restored the levels of ubiquinone-8 and ubiquinol-8, as well as oxygen consumption and growth. On the other hand, when levels of IspG are reduced by dCas9, this strain phenocopy the *ΔhflKC* growth effects at high aeration conditions.

Our data also shows that levels of IspG substrate (Me-cPP) accumulate in the *ΔhflKC* strain, this suggests a disruption of the MEP pathway that might limit the precursor supply to the production of ubiquinone. This notion comes from the fact that IspG enzyme is involved in the second to last step of the MEP pathway and catalyzes the conversion of the substrate ME-cPP (2C-methyl-D-erythritol 2,4-cyclodiphosphate) into HMBPP (hydroxym-ethylbutenyl 4-diphosphate) [85]. Then, IspH converts HMBPP into IPP (isopentenyl diphosphate) and DMAPP (dimethylallyl diphosphate) in a 5:1 mixture respectively [85]. These two molecules can be formed from each other by an isomerase encoded by the *idi* gene. IPP and DMAPP are the final products of the MEP pathway and they are the precursors for the side chain of ubiquinone [87], [88]. IPP and DMAPP are converted by IspA (4-hydroxybenzoate octaprenyltransferase) into Farnesyl diphosphate (FPP), which has three isoprenol units. Then, FPP is extended with the sequential addition of IPP molecules, which generate the different lengths of the tail in ubiquinone molecules. It is important to mention, that IPP and DMAPP are also the precursors for other groups of natural products such as sterols, carotenoids, and chlorophylls [89].

Ubiquinone molecule is also composed of a conserved aromatic ring called 4-hydroxybenzoate (4-HB) which is synthesized from chorismate in *E. coli* cells [88]. Ubiquinone-8 biosynthesis follows a highly

conserved pathway involving a group of genes known as *ubi* genes and most of these genes encode enzymes that decorate the aromatic ring of the universal precursor 4-HB [90]. The initial step involves the condensation of the side-chain FPP with the head 4-HB, which is catalyzed by UbiA (polyprenyl-4-hydroxybenzoate transferase) (

Figure 4.1) [91]. Thus, the isoprenoid chain provides lipid solubility and anchors the molecule in the membrane lipid bilayers, while the hydrophilic head group enables interaction with hydrophilic parts of proteins [92]**.**

Ubiquinone has been extensively study due to its roles in aerobic respiration for both eukaryotes and prokaryotes[88]. This molecule is part of a group of quinones that includes menaquinone (MK) and demethylmenaquinone (DMK), which participate in anaerobic respiration. Ubiquinone, also known as coenzyme Q (Q), carries electrons and protons through various cytochrome complexes in the aerobic respiratory chain [86]. The number of isoprenyl units in the ubiquinone tail varies among species: eight in *E. coli* (Q8), six in *S. cerevisiae*, and ten in humans [86], [91], [93]. In this study, we did not check levels of MK_8 or MK since in our condition they are not predominantly important.

Several studies have shown that reduction of *ubi* genes leads to accumulation of their substrates and thus, a decrease of ubiquinone-8 levels yields strains unable to grow aerobically on non-fermentable substrates [94], [95] [96]. For instance, the *ubiA* mutant is unable to grow aerobically on non-fermentable substrates but can grow anaerobically on glycerol with alternative electron acceptors, such as fumarate [94]. Similarly, it has been shown that *ispB* gene of the MEP pathway is also involved in the production of ubiquinone [97]. Additionally, Bentiger et al. postulated that 4-hydroxybenzoate (4-HB), which is synthesized from tyrosine in eukaryotic cells, is generally present in excess so that the rate of ubiquinone reaction is determined by the availability of the isoprenoid chain [91].

Recent evidence suggests that the *ubiE* gene is required for the C-methyl-transferase step of ubiquinone-8 synthesis, converting 2-polyprenyl-6-methoxy-1,4-benzoquinol ($DDMQ_8$) to 2-polyprenyl-3-methyl-6-methoxy-1,4-benzoquinol (DMQ_8) [98]. It's important to mention that *ubiE* is also required in the synthesis of menaquinone (MK). However, MK and Q8 biosynthesis are independent pathways except for the step that involves UbiE [99]. Previous studies have shown that changes in UbiE lead to a decrease in MK_8 and Q_8 levels [98].

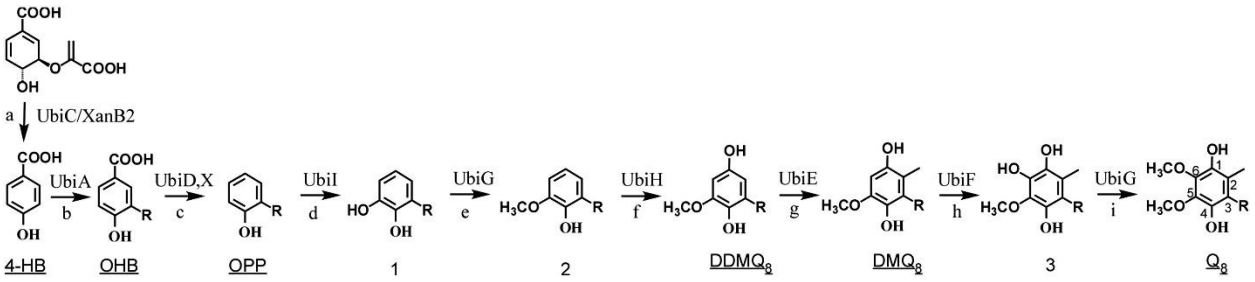

Figure 4.1 Biosynthetic pathway of ubiquinone in *E coli*.

The isoprenoil tail is represented by R on C-3 of the different biosynthetic intermediates. Abbreviations used for 4-hydroxybenzoate (4-HB), 3-octaprenyl-4-hydroxybenzoate (OHB), 3-octaprenylphenol (OPP), coenzyme Q_8 (Q_8), C1-demethyl-C6-demethoxy-Q8 (DDMQ8), and C6-demethoxy-Q8 (DMQ8) are underlined. The XanB2 protein, present in some prokaryotes but not in E. coli, catalyzes the production of 4-HB from chorismate Illustration taken from Ausssel L., et al [58].

4.2.3 Functional asymmetry of HflK and HflC in the regulation of FtsH activity

Interestingly, although the FtsH-regulatory membrane complex formed by HflK and HflC normally contains an equal number of HflK and HflC subunits [31], we observed a striking asymmetry in the effects of individual deletions of *hflK* and *hflC* genes. Whereas loss of *hflK* causes similar phenotypes as the lack of the entire HflKC complex, the deletion of *hflC* gene in the wildtype cells results in no apparent effect on growth and little if any changes in protein levels. The effect of *hflC* deletion on growth only becomes visible in the *ΔhflK* background, where it slightly enhances the phenotype of the latter. This observation is even more surprising given that deletion of either, *hflK* or *hflC*, causes a decrease in the level of its respective partner protein, as commonly occurs for the unassembled components of the heterooligomeric complexes [34], [39]. It means that HflK alone, even at reduced protein levels, can largely execute the function of the HflKC complex. This difference in the functionality between HflK and HflC might be related to their structural features. Although the overall structures of HflK and HflC are similar, and their monomers alternate in the HflKC complex: HflK possesses an additional C-terminal extension that resides inside the HflKC complex and interacts with FtsH, indicating that HflK might play a unique role in the assembly of the HflKC-FtsH complex and/or in FtsH regulation[41]. Although it remains to be proven, our data indicate that HflK can alone regulate FtsH activity, and probably assemble into a homooligomer, albeit less efficiently than in a complex with HflC.

4.2.4 Cardiolipin and phosphatidylglycerol levels decrease in *ΔhflKC* strain

Given that SPFH proteins are known to localize within and facilitate the recruitment of other proteins into Functional Membrane Microdomains (FMM), which are regions characterized by a high content of cardiolipin (CL) and phosphatidylglycerol (PG) [20], the absence of SPFH proteins could potentially impact the levels of these specific lipids. Therefore, we conducted a study to investigate changes in lipid composition in the *ΔhflKC* strain, and our results revealed a significant decrease in the abundance of CL and PG compared to the wildtype.

Interestingly, CL is predominantly located at the cell poles, where we found HflK and HflC to localize. Several studies have demonstrated that proteins homologous to the HFLKC complex in eukaryotes preferentially bind to CL. This has been observed through pull-down assays with liposomes containing various phospholipid compositions, although the exact specificity of this interaction remains to be fully elucidated [100].

Furthermore, studies on prohibitins in yeast have shown that their absence leads to a decrease in cardiolipin levels and, consequently, membrane disorganization. Prohibitins in yeast are proposed to act as membrane organizers by serving as protein and lipid scaffolds [63], highlighting a functional connection between lipid synthesis and prohibitin activity.

4.2.5 Lack of the HflKC complex affects the abundance of motility proteins

Besides establishing the function of the HflKC complex in bacterial respiration, we observed that the absence of this complex leads to changes in the levels of a few other proteins, independently of the IspG regulation or activation of the ArcAB two-component system. Although none of these proteins have been so far established as substrates of FtsH, this might be due to the reduced activity of this protease in presence of the HflKC complex in wildtype cells. Most prominent group among these proteins are those involved in *E. coli* motility, whereby levels of all classes of motility proteins were reduced in *ΔhflKC* strain, indicating increased degradation of an upstream regulator as an underlying mechanism.

On the other hand, when we checked motility behavior in soft agar we did not observe any significant difference. In contracts, in liquid media, there was a significant reduction in swimming velocity, which is another parameter of motility. These results need further investigation, perhaps using one of the more

advanced microfluidics techniques to test the reduction of motility in *ΔhflKC* strain and its effect on chemotaxis.

4.2.6 ArcAB system is active in *ΔhflKC* strain

ArcAB system (aerobic respiration control) is a sensor of oxygen consumption and its primary modulator is the quinone pool [101]. It is composed of sensor kinase ArcB and response regulator ArcA, which control a wide list of proteins involved in aerobic respiration and fermentation [102]. Our data suggests that the ArcB kinase repression might be relieved in *ΔhflKC* cells due to the reduction in the ubiquinone levels, causing an aberrant activation of the ArcAB system even at high O_2 levels. Indeed, we observed a large overlap in the profile of affected proteins between *ΔhflKC* and *ΔarcB* knockouts, and in the *ΔarcB* background, the levels of cytochrome ubiquinol oxidases were no longer affected by the *ΔhflKC* deletion. Moreover, no additional growth phenotype was observed upon *ΔhflKC* deletion in the *ΔarcB* strain, although the *ΔarcB* strain is already highly affected in its growth under aerobic conditions, likely due to the misregulation of respiratory proteins. In contrast, the levels of IspG and UbiE were affected by the *ΔhflKC* deletion independently of ArcB, confirming that the ArcAB system is downstream in the regulatory cascade. Consistent with that, reduced levels of IspG and UbiE were also observed in anaerobically grown *ΔhflKC* cells, where the ArcAB system should be similarly active in the wildtype cells.

Our hypothesis is consistent with the proposed regulatory mechanism for the ArcAB system described in the literature. Oxidized ubiquinone works as a negative signal and prevents ArcB kinase activity under aerobic conditions [103]. Georgellis and colleagues showed that when oxygen is present, the ubiquinone is oxidized as electrons are shuttled through to terminal oxidoreductases, ultimately reducing oxygen to water [104]. They demonstrated that Q_8 induced the formation of two intermolecular cysteine disulfide bonds within the cytosolic domains of an ArcB dimer, leading to the inactivation of ArcB kinase activity [105]. Now inactive, ArcB cannot transphosphorylates the response regulator ArcA. In turn, ArcA does not multimerizes and cannot serve as a global transcription factor suppressing aerobic metabolic pathways and promoting fermentation among other processes.

4.2.7 What is the cause of the strong reduction of the IspG levels in *ΔhflKC* cells?

The most likely explanation of low levels of IspG would be its increased degradation by FtsH in absence of the HflKC complex, which controls the activity of this protease in wildtype cells. Notably, while IspG is a cytoplasmic protein, it has not yet been identified as one of the substrates for FtsH [40]. Nevertheless, genetic interaction maps, a powerful technique for systematically revealing functional relationships between genes and often also indicate physical interactions, have indicated a possible interaction between IspG and FtsH [106]. It's important to highlight that this result needs to be validated using complementary techniques such as Bacterial Two-Hybrid among others.

Our hypothesis is supported by the structural model described by Qiao Z. et al. and Chengying Ma et al. in 2022, which suggests that the membrane and periplasmic regions of FtsH are protected by HflKC complex to prevent FtsH degradation of normal functional membrane proteins. Therefore, they suggested that the absence of HflKC might affect the degradation of both membrane and cytoplasmic proteins, as under this condition, FtsH is more exposed to substrates [31].

In our efforts to identify the molecular mechanisms of IspG degradation by FtsH, we conducted mRNA extraction from both the wildtype and *ΔhflKC* strains for subsequent qPCR analysis. Unfortunately, our preliminary data was inconclusive, and we are not able to identify at which level the degradation occurs. Importantly, HflKC protein is believed to have a proteolytic activity against λ cII protein, however, some reports have shown that null mutation of HflKC accelerated the degradation of SecY and YccA [39]. This shows the pleiotropic function of HflKC complex in the regulation of FtsH.

On the other hand, it is believed that FtsH protease activity is tightly controlled, as the degradation of one substrate does not impact others. Our observations align with this phenomenon, as the abundance of well-known FtsH substrates remains unchanged under all tested conditions (LB and TB media). This confirms that the *ΔhflKC* deletion does not lead to a general alteration in FtsH activity. For instance, the specific regulation of cellular LPS levels by FtsH protease activity towards LpxC, without affecting the degradation of other FtsH substrates, both membrane and cytoplasmic proteins [107].

4.2.8 SPFH proteins and aerobic respiration in more complex organisms

The HflKC complex and the prohibitin complex (PHB1 and PHB2) both belong to the SPFH family, as they all have the PHB domain or SPFH domain. While the HflKC complex is exclusively found in bacteria, the prohibitin complex is present in humans, yeast, and plants [4], [108]. Despite the phylogenetic distance between HflK and HflC and the prohibitins, they share structurally similar features. The prohibitin complex forms a multimeric, ∼1.2 MDa ring complex in the inner mitochondrial membrane (IMM) [64] that interacts with the human m-AAA protease AFG3L2 to regulate its activity. Expression levels of PHB1 and PHB2 are interdependent [109], which aligns with our observation in proteomic results, where the absence of HflK results in the degradation of HflC and vice-versa.

Prohibitins are multifunctional proteins since they are implicated in different cellular processes such as signaling, apoptosis, and transcriptional regulation [110]–[112]. Absence of this complex causes a change in mitochondrial morphology and a decrease in cardiolipin levels [109]. Interestingly, previous studies have shown that these proteins are also involved in aerobic respiration, given that the absence of prohibitin 1 reduces the complex I activity in the respiratory chain in human cells [113]. Notably, respiration and the assembly of respiratory super complexes were not reduced in absence of Phb2 [114]. Moreover, PHBs are associated with complex IV subunits in yeast [115] and with complex I subunits in mammalian cells [116], hinting at the possibility that PHBs might participate in the assembly of mitochondrial electron transport chain (ETC) complexes [117] [109], [118]. However, the relation between PHBs complex, its associated protease, and these respiratory phenotypes remained uncertain.

Our results demonstrate the regulation of respiratory activity by SPFH proteins at a different level, specifically through the control of ubiquinone biosynthesis. Although the relevance of this mechanism for eukaryotes requires further investigation, the structural and functional similarities between the HflKC and PHB1-PHB2 complexes suggest that a similar mechanism may operate in mitochondria.

Remarkably, recent research in 2022 by Qiao Z and collaborators using nuclear magnetic resonance (NMR) and Alphafold2 revealed a significant similarity between the PHB domain of HflK and PHB1 and the periplasmic domain of FtsH and AFG3L2. This finding has allowed them to propose a model demonstrating how AFG3L2 and prohibitin likely assemble into a functional complex [31]. This is particularly relevant to our study, as in our proteomic we observed a dominant role of HflK which could suggest its potential role in the phenotype.

4.2.9 Concluding remarks

E. coli HflK, HflC, QmcA, and YqiK belong to a highly conserved family of SPFH proteins that are found in all domains of life. Despite the similarity of these proteins with their eukaryotic homologs, their exact physiological function remains unclear. The only unambiguously established function of the HflK-HflC complex is the regulation of the FtsH metalloprotease, but the physiological importance of this regulation, and other possible functions are not known.

The main goal of this project was therefore a comprehensive study of the role of SPFH proteins in *E. coli*, with a particular focus on HflK-HflC complex. We addressed this goal using different approaches, including several microscopy techniques, protein-protein interaction studies, analysis of biophysical properties of the membrane, different microbiology assays, and omics techniques such as proteomics, lipidomics, and metabolomics.

In summary, our study provides valuable insights into the characteristics of SPFH proteins within *E. coli*. Through different microscopy analyses, we established their predominant localization within the cellular membrane, characterized by similar patterns of mobile and non-mobile spots. We highlighted the challenge of extracting these proteins due to their hydrophobic nature, emphasizing the need for different techniques such as crosslinking to enhance the stability of protein interactions during extraction for pull-down assay. Additionally, our study explored the biophysical aspects of membrane dynamics influenced by SPFH proteins. Notably, the SPFH quadruple knockout strain exhibited higher membrane fluidity at elevated temperatures, a phenomenon that underlines the critical role these proteins play in maintaining membrane integrity under varying environmental conditions. Additionally, our findings also revealed that this strain has a growth defect at lower temperatures. However, this particular growth effect needs further investigation to better understand the phenotype.

Moreover, our study provided a novel observation regarding the function of the HflK-HflC complex in *E. coli*. We elucidated the crucial role of HflKC complex in aerobic respiration, displaying a direct link to the abundance of IspG, a vital enzyme in the isoprenoid biosynthesis pathway. We showed that the defect in aerobic growth in absence of HflKC is due to the dramatically decreased abundance of IspG, which leads to reduced levels of ubiquinone. As a consequence, the *hflKC* deletion strain of *E. coli* exhibits reduced respiration, lower ATP levels, and changes in the expression of respiratory proteins (**Figure 4.2**). We hypothesis that lack of IspG proteins is due to FtsH protease activity, that in the absence of the protective

cage provided by HflKC complex, IspG is more accessible, and thus degradation occurs faster. We also propose that this regulation of aerobic respiration via isoprenoid biosynthesis and ubiquinone levels might also be conserved in eukaryotic prohibitin proteins, explaining previously reported lack of respiration of prohibitin mutations in mammalian and yeast cells.

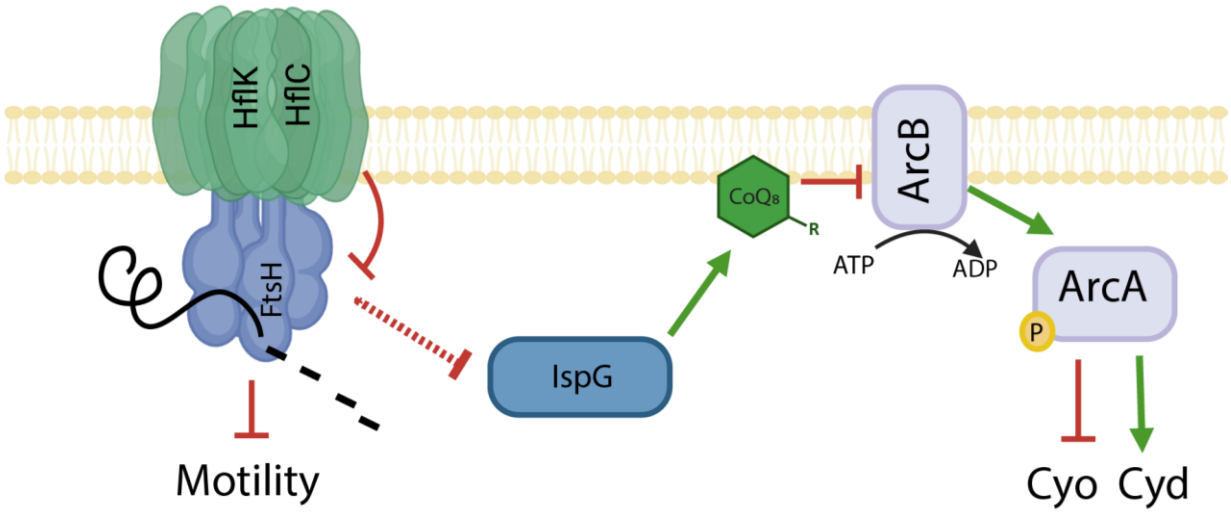

Figure 4.2 Model of the HflKC function in respiration control.

In absence of HflKC complex, FtsH degrades IspG. Lack of IspG results in lower levels of ubiquinone and thus, there is no negative regulation of ArcAB system and thus a downregulation of cytochrome ubiquinol oxidase *bo*$_3$ (Cyo) and upregulation of cytochrome ubiquinol oxidase *bd* (Cyd).

5 Materials and methods

5.1 Reagents and kits used

List of reagents used in this study

Chemical	Company
Yeast extract	Applichem
NaCl	Carl Roth
D-glucose	Applichem
$MgSO_4$	Carl Roth
$CaCl_2$	Carl Roth
Ampicillin	Applichem
Chloramphenicol	Applichem
Kanamycin	Sigma-Aldrich
L(+)-Arabinose	Carl Roth
Isopropyl β-D-1-thiogalactopyranoside (ISPG)	Carl Roth
Tris-base	Sigma-Aldrich
Tween 20	Carl Roth
Dimethyl sulphoxide (DMSO)	Carl Roth
Dinitrophenol (DNP)	Sigma-Aldrich
Benzyl alcohol (BnOH)	Sigma-Aldrich
Triton X-100	Sigma-Aldrich
KCl	Carl Roth
KH_2PO_4	Carl Roth
Na_2HPO_4	Carl Roth
Tris base	Carl Roth
PEG800	Sigma-Aldrich
$MgCl_2$	Carl Roth
Chloroform	Sigma-Aldrich
Methanol	Sigma-Aldrich

KCl	Sigma-Aldrich
Anhydrotetracycline	Sigma-Aldrich

All enzymes were purchased from New England Biosciences.

All primers were purchased from Eurofins Scientific

Kits used in this study

The kits were used according to the instructions of the guidelines given by the manufacturers.

Kit	Manufacturer
Q5 High-Fidelity DNA Polymerase	NEB
DreamTaq Green PCR Master Mix (2x)	NEB
Gibson assembly Master Mix	NEB
BacLight Bacterial Membrane Potential Kit	Molecular Probes
Cellular ROS Assay Kit	Abcam
Di-4-ANEPPDHQ	Invitrogen
SMALP-300P	Orbiscope
GFP-Trap magnetic beads	Chromotek

Multi-well plate

96-well plates transparent bottom, company Greiner Bio-one.

5.2 Media and buffer solutions

Media

Lysogeny broth (LB)

10 g/l Tryptone

5 g/l Yeast extract

5 g/l NaCl

Adjusted to pH 7. For preparing LB agar plates, 15 g of agar were added to 1 l of LB liquid medium.

Terrific Broth (TB)

10 g/l Tryptone

5 g/l NaCl

Adjusted to pH 7. For preparing LB agar plates, 15 g of agar were added to 1 l of LB liquid medium.

M9 glucose minimal medium

42.2 mM Na_2HPO_4

22 mM KH_2PO_4

11.3 mM $(NH_4)_2SO_4$

8.56 mM NaCl

1 mM $MgSO_4 \cdot 7H_2O$

100 µM $CaCl_2 \cdot 2H_2O$

60 µM $FeCl_3$

7.6 µM $CoCl_2 \cdot 6H_2O$

7.1 µM $MnSO_4 \cdot 2H_2O$

7 µM $CuCl_2 \cdot 2H_2O$

6.3 µM $ZnSO_4 \cdot 7H2O$

0.4% Glucose

0.2% casamino acids

The salts were prepared as 5x, diluted and sterile filtered. Nutrients were mixed with the 1x M9 salts prior to culture inoculation.

Buffers

Phosphate-buffered saline (PBS)

137 mM NaCl

2.7 mM KCl

8 mM Na_2HPO_4

1.8 mM KH_2PO_4

Buffered to pH 7.4

***TAE* buffer (Tris-Acetate-EDTA - 50 x)**

242 g Tris base

57.1 g Glacial acetic acid

100 ml 0.5 M EDTA, pH 8

ddH_2O was added up to a total volume of 1 l.

SDS-PAGE sample buffer (Laemmli), 4x

0.25 M Tris base, pH 6.8

8% SDS

40% glycerol

20% β-mercaptoethanol

0.02% w/v Bromophenol blue

SDS-PAGE running buffer, 10x

30.3 g Tris base

144 g glycine

10 g SDS

Dissolve in 1000 ml ddH_2O

Western blot transfer buffer, 10x

30 g Tris base

144 g glycine

Dissolve in 1000 ml ddH_2O.

To make 1x transfer buffer, 100 ml of 10x transfer buffer are mixed with 200 ml of methanol and 700 ml of ddH2O.

Tris buffered saline (TBS), 10x

24 g Tris base

88 g NaCl

Dissolve in 1000 ml ddH_2O

Buffered to pH 7.6 with HCl. To make 1x TBS-T, mix 100 ml 10x TBS with 900 ml ddH2O and 1 ml of Tween20 (0.1%).

5.3 Antibiotics and inducers

Ampicillin 100 mg/ml in ddH_2O

Kanamycin 50 mg/ml in ddH_2O

Chloramphenicol 34 mg/ml in ethanol

IPTG 0.1 M in ddH_2O

L-arabinose 10% in ddH_2O

Anhydrotetracycline 1mM

5.4 Molecular biology methods

5.4.1 Polymerase chain reaction (PCR)

PCR was used to either amplify genes and plasmids for cloning (Q5 polymerase) or to verify positive plasmid assembly or genomic knockout (single-colony PCR). The PCR reactions were run in peqSTAR thermocyclers (PEQLAB). Amplified DNA fragments were analyzed using gel electrophoresis in 1% TAE-agarose gels and purified using the GeneJET PCR purification kit. Amplified plasmids were treated with DpnI for plasmid template degradation.

Single-colony PCR reaction mix

25 µl DreamTaq Green PCR Master Mix (2x)

1 µl forward primer (10 pmol/ µl)

1 µl reverse primer (10 pmol/ µl)

Colony picked from plate.

up to 50 µl ddH_2O

Thermocycler settings

Step	Temperature [°C]	Time [min]
1	95	10
2	95	1
3	60-72	0.5
4	72	1/kb
	Repeat 2-4 35x	
5	72	15

PCR with Q5 polymerase reaction mix

10 µl Q5 reaction buffer (5x)

2.5 µl forward primer (25 pmol/ µL)

2.5 µl reverse primer (25 pmol/ µL)

1 µl dNTPs (0.8 mM)

0.5 µl Q5 high fidelity DNA polymerase

1 µl template DNA (~25 ng for plasmid, ~1 mg/ml for genomic DNA)

up to 50 µl ddH_2O

Thermocycler settings

Step	Temperature [°C]	Time [min]
1	98	10
2	98	1
3	50-72	0.5
4	72	1/kb
	Repeat 2-4 35x	
5	72	2

5.4.2 DpnI treatment

In order to remove the methylated template DNA from a PCR reaction and prevent false positive *E. coli* colonies, PCRs were incubated with DpnI prior to any subsequent step. DpnI is a restriction enzyme that cleaves methylated recognition sites on template plasmid DNA while leaving intact PCR amplicon. After DpnI treatment, PCR products were purified using the GeneJET PCR Purification kit.

DpnI reaction mix

5 µl CutSmart 10x

1 µl DpnI

44 µl purified PCR product

5.4.3 Agarose gel electrophoresis

The size of amplified gene fragments or plasmids was verified by agarose gel electrophoresis. Agarose gel electrophoresis separates DNA fragments according to their size when an electric field is applied. PCR products amplified for downstream cloning were verified by loading 5 µl with 6x loading dye on a 1% agarose TAE gel supplemented with peqGREEN (Peqlab) for visualization of the DNA bands under UV light.

For Colony PCR products, 15 µl was loaded on the gel. The gels were run at 135 V in a chamber with TAE buffer for 10-20 min.

5.4.4 Gibson assembly

Gibson Assembly is a DNA assembly method, that allows to assemble 2-6 linear DNA fragments with overlapping ends in a one-pot and one-step reaction [119]. Overlapping regions were designed to be at least 25 bp long. DNA fragments and the receiver plasmid were amplified by PCR using Q5 polymerase, verified by gel electrophoresis and the plasmid was additionally treated with DpnI. To prepare the Gibson assembly, parts were combined in a 1:3 molar ratio of backbone to insert, with 100 ng backbone.

Gibson assembly reaction mix

10 µl Gibson Assembly Mastermix 2x

100 ng backbone

3:1 molar amount of inserts

ddH_2O to 20 µl

Thermocycler settings

Step	Temperature [°C]	Time [min]
1	50	30min

5.5 List of bacterial strains

All strains used in this study are listed in **Table 7**

Table 7 List of strains used in this study

Code	Relevant genotype	Reference or source
MI22	*E. coli MG1655*	[120]
MI23	*Keio collection JW 4132* (*ΔhflK::kan*)	[121]
MI24	*Keio collection JW4133* (*ΔhflC*::kan)	[121]
MI25	*Keio collection JW0478* (*ΔqmcA*::kan)	[121]
MI26	*Keio collection JW3023* (*ΔyqiK*::kan)	[121]
MI36	*ΔhflK* in *E. coli* MG1655	This study
MI37	*ΔhflC* in *E. coli* MG1655	This study

MI38	*ΔqmcA* in *E. coli* MG1655	This study
MI39	*ΔyqiK* in *E. coli* MG1655	This study
MI59	*ΔhflKC* in *E. coli* MG1655	This study
MI60	*ΔhflKC ΔqmcA* in *E. coli* MG1655	This study
MI61	*ΔhflKC ΔqmcA ΔyqiK* in *E. coli* MG1655	This study
MI66	*ΔtaR* in *E. coli* MG1655	This study
MI76	*hflK-sfGFP* in *E. coli* MG1655	This study
MI77	*hflC-sfGFP* in *E. coli* MG1655	This study
MI78	*qmcA-sfGFP* in *E. coli* MG1655	This study
MI79	*yqiK-sfGFP* in *E. coli* MG1655	This study
MI94	*E. coli YYdCas9* Δ(araD-araB)567 λrph-1 Δ(rhaD-rhaB)568 hsdR514 dCas9 specR chlR	[122]
MI120	*ΔhflKC ΔarcB* in *E. coli* MG1655	This study
MI122	*ΔarcB* in *E. coli* MG1655	This study

5.5.1 Keio collection and P1 transduction

The kanamycin-resistant *ΔhflK*::kan, *Δhfl*C::kan, *ΔqmcA*::kan and *Δyqik*::kan deletion strain of the Keio collection [121] was used as donor strain for P1 phage transduction [123], into the wildtype (WT) *E. coli* MG1655 background. The resulting transduced strains were tested for correct insertion of the FRT-site flanked kanamycin cassette into the genome, using gene and kanamycin cassette specific primers. The kanamycin cassette was removed from the deletion strain using the temperature sensitive pCP20 plasmid encoding a FLP recombinase [124] and tested for the loss of antibiotic resistance after several rounds of growth on LB plates at 42°C.

5.5.2 Lambda red

For the double or triple knockouts, pkD46 was transformed into the corresponding donor strain. Then, the donor strain carrying pKD46 was transformed with a DNA fragment with the flanked region corresponding to the gene to knockout. After recovery, lambda red recombinase expression was induced by heat-shocking of the cells. This triggers homologous recombination between the Lambda Red-encoded DNA and the target region. Recombinant clones were selected using appropriate antibiotic resistance markers. Finally, PCR was used to confirm the successful recombination event. The kanamycin cassette was removed from the deletion strain using the temperature sensitive pCP20 plasmid encoding a FLP

recombinase [124] and tested for the loss of antibiotic resistance after several rounds of growth on LB plates at 42°C.

5.5.3 IspG knockdown

The *E. coli* YYdCas9 with the follow genome Δ(*araD-araB*)567 λ- rph-1 Δ(*rhaD-rhaB*)568 hsdR514 dCas9 $spec^R$ chl^R was used for the knock-down. Different protospacers were used for IspG knock-down, and each of them was transformed into the plasmid pgRNA *Amp resistance*, however, the one with the stronger inhibition was in the sequence AATTCCTGACGCGAACAGGT. 2uM of aTc (anhydrotetracycline) was used for induction.

5.6 List of plasmids

To obtain plasmid from *E. coli*, overnight cultures grown in LB or TB supplemented with the appropriate antibiotic were used and the plasmid was purified using the GeneJET Plasmid Miniprep Kit. DNA was eluted in ddH_2O. The concentration of the purified DNA, as well as its purity, were determined using spectrophotometric estimation (NanoDrop 2000). Newly constructed plasmids were sent for Sanger sequencing (Microsynth) to verify the correct assembly.

The plasmids used in this study are listed in **Table 8**

Table 8 Plasmids used in this study

Code	Relevant genotype	Reference or source
pTrc99A	Amp^r; expression vector; pBR ori; trc promoter, IPTG inducible	[125]
pMI05	Amp^r; *hflK-sfGFP* in pTrc99A	This study
	Amp^r*; sfGFP-hflK* in pTrc99A	This study
pMI06	Amp^r; *hflC-sfGFP* in pTrc99A	This study
pMI07	Amp^r*; yqiK-sfGFP* in pTrc99A	This study

pMI08	Amp^r; *sfGFP-qmcA* in pTrc99A	This study
pMI09	Amp^r; sfGFP-yqiK in pTrc99A	This study
pNB1	Amp^r; *sfGFP* in pTrc99A	[126]
pMI32	Amp^r; *qmcA-sfGFP* in pTrc99A	This study
pCP20	Amp^r; Cam^r; *flp*	[124]
pMI62	Amp^r; *taR-sfGFP* in pTrc99A	This study
pMI93	Cm^r; *hflk_hflC* in pBAD33	This study
pBAD33	Cm^r; expression vector; araC promoter, Arabinose inducible	[127]
pMI107	Cm^r; *ispG* in pBAD33	This study
pMI109	pgRNA	[128]
pMI112	*ispG* in pgRNA with protospacer AATTCCTGACGCGAACAGGT	Hannes Link's lab University of Tübingen, Germany

5.6.1 Chemical competent cells with calcium chloride

An LB overnight culture was diluted to final OD_{600} = 0.035 in 100 ml fresh LB media and grown at 37 °C to an OD_{600} = 0.6. Cells were harvested by centrifugation for 5 min at 4000 rpm at 4°C and the pellet was resuspended in 50 ml of ice-cold 0.1 M CaCl2 and incubated on ice for 20 min. Cells were centrifuged for 5 min at 4000 rpm and the pellet was resuspended in 50 ml ice-cold 0.1 M CaCl2, and incubated once more on ice for 20 min. Cells were centrifuged once more as previously and resuspended in 5 ml 0.1 M CaCl2 with 20% glycerol and aliquoted. The aliquots were snap-frozen in liquid nitrogen and stored at - 80 °C.

5.6.2 Transformation

0.5-1 µl of purified plasmid DNA (~100 ng) or 10 µl Gibson assembly reaction was mixed gently with 100 µl competent cells in a 1.5 ml Eppendorf tube and incubated on ice for 30 min. For heat shock, the sample was placed at 42°C for 45 s in a heating block. After the heat shock, the tube was immediately placed on

ice for 5 min. 900 µl of LB medium were added and the cells were incubated at 37 °C for 30- 45 min. Cells were then plated on LB agar plates with selective antibiotics. Plates were incubated over night at 37 °C.

5.6.3 sfGFP-constructs: *trc* and native promoter

The stability of *E. coli* SPFH proteins and sfGFP fusion were verified by polyacrylamide gel electrophoresis and western blot (immunoblotting). The same protocol was used for expression under *trc* promoter expression and native promoter expression.

E. coli SPFH cultures expressing all plasmid-encoded sfGFP and sfGFP integrated into the genome were grown as described in paragraph 5.7.1. 10 ml culture was spun 4000g for 10 min and washed in 5 ml 1X PBS. Cells were then resuspended in 350 µl 1x SDS-PAGE (Laemmli) sample buffer and samples were heated at 95°C for 10 min, briefly vortexed (~10 s) and stored at -20°C overnight.

5.6.4 Sodium dodecyl sulfate-polyacrylamide gel electrophoresis (SDS-PAGE)

The method of SDS-PAGE allows the separation of proteins depending on their mass. SDS is an anionic detergent that binds proteins in a constant stoichiometry. Proteins bound to SDS are linearized and charged negatively, thus allowing their separation by size depending on the electrophoretic mobility in a polyacrylamide gel. Gels were cast in two steps, starting with the preparation of the 10% resolving gel. Components were used in the amounts indicated below and mixed by inversion before and after the addition of TEMED which initiated the polymerization of the gel. The mixture was applied to a gel caster system and isopropanol was added on top of the gel in order to flatten the surface and prevent the formation of bubbles. In the second step, the 5% stacking gel was prepared under the same conditions and poured on top of the resolving gel after the isopropanol had been discarded. The wells for sample loading were formed by the insertion of a comb in the gel caster system. Hardened gels were either stored in moist paper at 4°C or immediately used for gel electrophoresis.

Resolving 10% gel

2 ml ddH2O

1.3 ml 1.5 M Tris-HCl, pH 8.8

1.6 ml 30% Acrylamide

100 µl 10 % SDS

50 µl 10% Ammonium Persulfate

5 µl TEMED

Stacking 5% gel

ddH2O 1.95 ml

315 µl 1 M Tris-HCl, pH 6.8

165 µl 30% Acrylamide Stock

12.5 µl 10 % SDS

6.25 µl 10% Ammonium Persulfate

1.25 µl TEMED

When loading the gel, 5 µl of protein molecular weight markers (PageRuler Plus Prestained Protein Ladder, 10 to 180 kDa, ThermoScientific) were applied to one of the wells to serve as size standard. 8 – 15 µl of samples were applied to the remaining gel wells. The stacking gel was run at 100 V for 30 min, the resolving gel was run at 120V for ~90 min. The run was performed in the running buffer. The progress of the gel electrophoresis could be monitored by observation of the tracking dye bromophenol blue which was included in the Laemmli buffer and due to its low molecular weight moved ahead of most of the negatively charged proteins towards the positively charged anode.

5.6.5 Western blot

By using the Western blotting technique, proteins that have been separated by gel electrophoresis are transferred to a nitrocellulose membrane and afterward detected by incubation with specific antibodies. Proteins were transferred from the respective SDS gel to nitrocellulose membranes by wet blotting procedure. For every gel to be blotted two blotting papers were cut to approximate gel size and two blotting sponges were soaked in transfer buffer. A nitrocellulose membrane was cut to gel size and shortly soaked in transfer buffer. The SDS gel was equally incubated in blotting buffer before being assembled into the transfer “sandwich” of blotting papers, sponges, and nitrocellulose membrane and placed in the transfer tank. Electroblotting was performed at 100 V for 1 h, or overnight at 30 V. During transfer the negatively charged proteins are pulled from the SDS gel onto the nitrocellulose membrane towards the positively charged electrode of the blotting tank. To prevent overheat, the transfer was performed in the cold room and a cooling pack was placed in the tank. In order to prevent unspecific antibody binding

during the following incubation steps, membranes were first blocked in 5 % skimmed dry milk dissolved in TBS-Tween (TBS-T milk). Incubation was carried out under gentle agitation for 60 min at RT. For specific labeling of sfGFP-tagged proteins, an anti-GFP primary antibody (JL-8 monoclonal, mouse, Takara) was diluted 1:10000 in 5 % TBS-T milk and applied to the blocked membrane. Samples were then incubated at RT for 1 h or at 4°C overnight under gentle shaking. Thereafter, membranes were washed three times in TBS-T to eliminate unbound antibody residues and subsequently incubated with anti-mouse secondary antibody (IRDye® 800CW Rabbit anti-mouse IgG) equally 1:10000 diluted in 5 % TBS-T milk. After incubation at RT for 1 h, membranes were again rinsed three times in TBS-T for residual antibody removal. Gel was revealed using an Odyssey CLx equipment.

5.6.6 Protein solubilization with Triton X-100

E. coli SPFH-sfGFP fusions were grown in LB with 2µM IPTG induction until OD_{600} of 0.4-0.6. We used the lysis buffer described in **Table 9**. Samples were incubated with the lysis buffer for 3h in a rotating shake at 4°C. After that, sonication steps were used with 0.5 cycles and 80% Amplitude. After the disruption, samples were centrifuged at 10,000 rpm and supernatants were used for the SDS-page and pull-down test using magnetic beads for GFP. We include negative control *E. coli* pTrc99A-sfGFP empty plasmid and positive control *E. coli* pTrc99A-taR-sfGFP.

Table 9 Lysis buffer

Lysis buffer	Concentration used	Reference of concentrations	Description
Tris-HCl pH 7.5	20mM	20mM – 50mM	Buffer
NaCl	100mM	50mM-150mM	Maintain ionic strength of medium
Glycerol	5%	5%-10%	Stabilization of proteins
Triton X-100	2%	0.1% - 1%	Break protein-lipid and lipid-lipid associations
Lysozyme	2mg/ml	1mg/ml	Cleaving the peptidoglycan
Protease inhibitors			Prevent the degradation of proteins by proteases
Water			

5.6.7 Protein solubilization with SMALP-30010P

The polymer styrene maleic acid lipid particle (SMALP) which efficiently solubilizes membranes into native nanodiscs was used. *E. coli* SPFH sfGFP fusions were grown in LB with 2uM IPTG induction up to OD_{600} of 0.4-0.6. We used the protocol described by Lee C.S. and collaborators with some modifications [52]. Cell pellets were suspended in 50ml of buffer mentioned above (without the detergent). Cells were disrupted by passage microfluidizer 16.000 psi. Unbroken cells were removed by centrifugation at 4,000rpm (4˚C, 10 min). The polymer was added to the supernatant to a final concentration of 5uM. Samples were incubated overnight at 4^{o}C with gentle shaking. As the SMALP solubilizes the membrane, the suspension should become less opaque. Samples were ultracentrifuged at 100,000g, 4^{o}C for 50 min. The supernatant, which represents solubilized membranes was used for SDS-page and pull-down test using magnetic beads for GFP.

5.6.8 Pull-down

The beads were added to the sample and incubated for 1h. Then, beads were collected by centrifugation at 5000 ×g for 1 min and suspended in 700 µl of 100 mM ammoniumbicabonate (ABC). Using a magnetic separator, beads were washed 3 times in 100 mM ABC and then incubated in 100 µl E1 buffer (1.6 M urea, 100 mM ABC, 5 µg/ml trypsin) at 1200 rpm, 27 °C for 30 min. The supernatant was collected in a new tube and beads were washed twice in 40 µl E2 buffer (1.6 M urea, 100 mM ABC, 1 mM tris(2-carboxyethyl)phosphine (TCEP)). The elutions were left for trypsin digestion overnight. On the following day, the peptides were first alkylated by the addition of 40 µl lodoacetamid (5 mg/ml in 100 mM ABC) in the dark for 30 min. Subsequently, the samples were acidified with 150 µl trifluoroacetic acid (TFA), pH < 2. C18-columns were conditioned twice with 150 µl acetonitrile and equilibrated three times with 150 µl buffer A (0.1% TFA). Afterward, the supernatants were loaded onto the columns, which then were washed three times with 150 µl buffer C (5% acetonitrile, 95% water, 0.1 % TFA). To elute bond peptides, the columns were washed three times with 100 µl buffer B (50% acetonitrile, 50 % water, 0.1% TFA). Collected peptides were concentrated by vacuum drying. The subsequent analyses by LC-MS/MS were carried out by Dr. Timo Glatter (Max Plank Institute for Terrestrial Microbiology, Marburg, Germany).

5.7 Microbiology culture methods

5.7.1 Growth curve

Plate-reader: Measurements of bacterial growth were performed using 96-well plates. Overnight cultures were inoculated at an initial OD_{600} of 0.01 in the same medium as used for growth in other experiments. Each well contained 150 µl of culture and the plate was covered with the plastic cover provided by the producer and further sealed with parafilm that prevents evaporation but allows air exchange. Plates were incubated at 37°C, 42°C, 30°C and 25°C with continuous shaking, alternating between 150 s orbital and 150 s linear, in a Tecan Infinite® 200 PRO plate reader. Same protocol was used for growth under osmotic stress by sodium chloride (NaCl) and sucrose (concentrations ranging from 0.25 to 1 M).

Glass flask: Overnight cultures of the strains were diluted 1:100 in fresh media and grown at 37°C in a glass flask and orbital shaker under different shaking rates (100 rpm, 200 rpm, and 300 rpm). Optical density at 600 nm (OD_{600}) was acquired every 1 or 2 hours. Special flasks were used for anaerobic TB cultures where oxygen was removed with nitrogen. When needed 0.05% L-arabinose, 2uM of IPTG, or 0.2 uM aTc was added as inducer of expression.

5.7.2 Membrane fluidity with Di-4-ANEPPDHQ

All the corresponding strains were labeled with Di-4-ANEPPDHQ. Cells were grown in LB medium until reached cell density between 0.4 and 0.6 OD. 1ml of the cell cultures were incubated with 5 µM di-4-ANEPPDHQ final concentration. Wildtype strain with 25 mM ethanol (Eth) at 0.75% concentration was used as positive control. Samples were incubated for 30 minutes at 25°C, 37°C or 42°C. 3ul of the sample was mounted in the agarose pads and TIRF microscopy was used for image acquisition. The dye was excited at 488 nm, it has an emission wavelength of ~ 560 nm (ordered phase), and ~ 620 nm (disordered phase). Image analysis was performed as described by Owen D. in 2006 [53].

Generalized polarization (GP) was calculated as follows:

$$GP = \frac{I_{500-580} - GI_{620-750}}{I_{500-580} + GI_{620-750}}$$

Where *I* represent the intensity in each pixel in the image acquired in the indicated spectral channel.

5.7.3 Chemical library screening

The Prestwick Chemical Library (1200 drugs) was purchased from Specs.net and preformatted in master plates so that all compounds were solubilized in 100% DMSO at a final concentration of 10 mM. A fully automated Hamilton Star workstation was used for all liquid handling protocols. The final drug concentration of 20 µM in 200 ul of LB medium was loaded into 96-well plates. SPFH quadruple knockout and wildtype were used for the screening. Wells containing only cells or only LB medium were used as positive and negative controls, respectively. Assay plates were cultured at 37°C in an orbital shaking at 220 rpm. Every 1 h, 2 h, or 3 hours measurements of OD_{600} in a Tecan Infinite® 200 PRO plate reader were done, and results were processed using Rstudio.

5.7.4 Biofilm assay

Biofilm formation in microtiter plates was measured using crystal violet assay as described previously by O'Toole [56]. Overnight cultures of the SPFH knockouts were diluted 1:100 into fresh LB and TB media and incubated in an orbital shaking at 37°C 220rpm. When cultures reached OD_{600} between 0.3 and 0.4, the samples were diluted to an OD_{600} of 0.04 in the corresponding media, and 300ul of the dilution was added per well in a 96 plate. We used 12 replicates well for each strain. The plate was incubated at 37°C for a period of 24 hours without shaking. After this time crystal violated staining was performed. Unattached cells were removed by turning the plate over and shaking out the liquid and two washed steps were done with 1X PBS. The biofilms were fixed by adding 300ul of 96 % ethanol into the wells. After the ethanol is removed and evaporated, 200ul of 0.5% solution of crystal violet was added and the plate was incubated at room temperature for 15 min. Then, the plate was rinsed two times with water and let it dry at room temperature. 125ul of 30% acetic acid in water were added to each well to solubilize the crystal violet dye. Biofilm biomass was quantified by measuring the absorbance at 595 nm using a Tecan Infinite® 200 PRO plate reader, with acetic acid diluted in LB and TB medium as blanks. The *E. coli ΔfliC* was used as a negative control.

5.7.5 Motility assay

3ul of overnight cultures of both wildtype and double SPFH knockout strains were used for inoculation in soft TB agar plates (0.3% agar). These plates were subsequently incubated at 37°C, and after 3 hours of incubation, images were captured utilizing a PeqLab transilluminator. ImageJ was used to measure the diameter of the spread colony.

5.7.6 Complemented phenotype of *ΔhflK*C

ispG gene was amplified to obtain linear fragments by PCR using Q5 High-Fidelity DNA Polymerase. The DNA product was cleaned and ligand to pBAD33 by Gibson assembly and the insertion was verified by DNA sequencing. Consequently, the constructs were transformed into *ΔhflKC*. Empty pBAD33 was transformed into WT and *ΔhflKC* strains to be used as negative controls. Induction of IspG was given by adding 0.02% of L-arabinose, and growth curves were performed in TB medium at 220rpm.

5.7.7 Measurements of Oxygen consumption

Cultures were grown in a glass flask with TB at 37^{o}C and 220rpm. Cultures grow until OD_{600} is equal to 0.5. Suspension of cells was adjusted to have an OD_{600} equal to 1. Cultures were centrifuged and fresh TB medium was added. Samples were transferred to a glass tube that contained an oxygen sensor spot PSt3-YAU-D5-YOP (PresSens, precision sensing). Sample tubes were in constant shaking for 10 mins, then shaking was stopped and oxygen consumption was measured via the oxygen spot with a fiber optic transmitter. Measurements correspond to one biological replicate with 8 technical replicates. The same procedure applies for WT transformed with the empty vector pBAD33 and *ΔhflKC* transformed with the IspG expression construct pBAD33 without induction or induced by 0.02% L-arabinose.

5.7.8 Measurement of reactive oxygen species (ROS)

Reactive oxygen species (ROS) were assessed using the dichlorodihydrofluorescein (DCF) probe (ab113851 Kit from abcam). Strains were grown in TB at 220 rpm, and then incubated with 20 uM of the dye for 30 mins and fluorescence at 485nm was analyzed by flow cytometry. Treatment with hydrogen peroxide

(H_2O_2) was used as a positive control for elevated ROS levels. Data correspond to one replicate with 5 measurements and 30.0000 events per data point. Error bars indicate SD.

5.7.9 Determination of membrane potential (MP)

BacLight Bacterial Membrane Potential kit (B34950 Molecular Probes) was used to terminate the MP. Cultures were grown in TB at 37°C and 220rpm. All samples were diluted in 1X PBS and biomass was adjusted to have OD_{600} equal to 0.4 in 1ml. Samples were transferred to a 1.5ml Eppendorf tube where $DiOC_2(3)$ was added to have a final concentration of 0.03mM. Samples were gently mixed by inversion, followed by dark incubation for 15 mins at 37°C. WT with 40uM of dinitrophenol (DNP) was used as a negative control. Flow cytometry was used to measure the fluorescence of red (670 nm) and green (510 nm) channels of $DiOC_2(3)$. Excited at 488 nm was used and fluorescence was measured through a 530-nm-bandpass filter. MP was estimated from the ratio of the red and green fluorescence as described in the protocol. For IspG expression, 0.02% L-arabinose was used. Data correspond to six independent measurements with 30.0000 events each.

5.8 Microscopy

5.8.1 Epifluorescence

Strains were grown in TB medium at 37ºC under shaking conditions until exponential growth. 3 µl of bacterial cells were spread on a small 1% agarose pad prepared in PBS. Conventional light microscopy was performed using a Zeiss Observer Z1 (Carl Zeiss) with an oil immersion objective (100 x magnification, 1.45 numerical aperture, Carl Zeiss). Data were processed using ImageJ.

5.8.2 Structured Illumination Microscopy (SIM)

Strains were grown in TB at 37ºC under shaking conditions until exponential growth. 3 µl of bacterial cells were spread on a small 1% agarose pad prepared in PBS. For localization experiments, image Z-stacks (~100 nm steps) were acquired using brightfield (BF) image acquisition (transmitted light) or structured illumination microscopy (SIM) with a ZEISS ELYRA PS.1 setup (Andor EMCCD camera, 160 nm pixel size; 3× rotations and 5× phases per z-slice; grating period: 42 µm; 100 mW laser line (between 80 and 200 W/cm^2) at excitation laser wavelength 488 nm; ZEISS alpha Plan-Apochromat 100x/NA 1.46 Oil DIC M27 objective).

SIM reconstructions were processed using ZEN-Black software by ZEISS. ImageJ2/Fiji version 1.52p was used for visualization and image processing. Region(s) of interest (ROI) were defined by cell borders using the brush-selection tool to maintain good contrast levels of cellular areas. SIM reconstructions were manually cropped in axial and lateral dimensions, depending on plausibility of cellular positions, using "Duplicate"-function. Signal located outside cell borders was background and was therefore eliminated. Resulting image z-stacks were projected using Fiji implemented "Z-project"-function (e.g., "Average Intensity"), false-coloured and colour-balance adjusted to generate tomographic representations. 3D SIM image z-stacks movies were visualized using Fiji implemented 3D-Project function (with interpolation) for 360° visualization and z-stacks for a tomographic walk-through. Resulting 3D-visualizations were generated with merged channels, processed, and transformed as.avi movies, and finally combined in a sequential manner using Fiji.

5.8.3 Total internal reflection fluorescence (TIRF) Microscopy

Cells were spotted on coverslips (25 mm, Menzel) and covered using 1% agarose pads prepared before with ddH_2O. All coverslips were cleaned before use by sonication in Hellmanex II solution (1% v/v) for 15 min followed by rinsing in distilled water and a second round of sonication in double distilled water. The excitation laser beam was directed to underfill the back aperture of the objective lens, generating a concentrated parallel light source, which leads to a strong excitation followed by rapid bleaching of the fluorophores. Only unbleached molecules as well as newly synthesized and folded fluorophores can be tracked. When an observed molecule is bleached in a single step during imaging, it is assumed to be a single molecule [206]. Images were acquired with an Olympus IX71 microscope (Olympus, Japan) equipped with a UAPON 100×OTIRF objective (Olympus, Japan) and an electronmultiplying CCD (EMCCD) camera iXon Ultra (Andor Technology, Belfast, UK). A 514-nm laser diode was used as the excitation light source, and the band corresponding to the fluorophore was filtered out. A total of 2500 frames were taken per movie with an exposure time of 20 ms (23 fps). The acquired streams were loaded into Fiji [129] for analysis and the automated tracking of single molecules was performed by the MATLAB-based software u-track 2.2.0 [130], [131].

5.9 Proteomics, metabolomics, and lipidomics

5.9.1 Abundance of proteins

Cultures were grown in LB and TB at 37°C and 220rpm until OD_{600} was equal to 0.5. Cultures were grown anaerobically in TB at 220rpm and cells were collected at OD_{600} equal to 0.15. Cultures were centrifuged and pellets were washed three times with ice-cold phosphate-buffered saline (PBS). All samples have three independent cultures where biomass was adjusted to OD_{600} equal to 3. Pellets were frozen with liquid nitrogen and stored at -80°C. For protein extraction, cell pellets were dissolved in 2% Sodium-lauroyl sarcosinate (SLS) in 100mM Ammonium bicarbonate. Cells were lysated by incubation at 90°C for 15 mins and sonication (Vial Tweeter, Hielscher). Cell lysates were then reduced by adding 5 mM Tris(2-caboxyethyl)phosphine and incubating at 95°C for 15 minutes followed by alkylation (10 mM iodoacetamide, 30min at 25°C). Cell lysates were cleared by centrifugation and the total protein was estimated for each sample with Pierce™ BCA Protein Assay Kit (ThermoFisher Scientific). After adjusting the protein concentration a solid phase extraction using C18 purification columns was performed in order to purify peptide. The final peptide concentration for all samples is around 0.5ug/ul. The eluted peptides were dried and resuspended in 0.1% TFA for analysis of peptides. Analysis of peptides was performed by a Q-Exactive Plus mass spectrometer connected to an Ultimate 3000 RSLC nano with a Prowflow upgrade and a nanospray flex ion source (Thermo Scientific) as previously described. Briefly, peptides were separated by a reverse-phase HPLC column (75 µm × 42 cm) packed with 2.4 µm C18 resin (Dr. Maisch GmbH, Germany) at a flow rate of 300 nl/min by gradient model which is from 98% solvent A (0.15% formic acid) and 2% solvent B (99.85% acetonitrile, 0.15% formic acid) to 35% solvent B over 84 min. The data acquisition was set to obtain one high-resolution MS scan at a resolution of 70,000 full widths at half maximum (at m/z 200) followed by MS/MS scans of the 10 most intense ions. To increase the efficiency of MS/MS attempts, the charged state screening modus was enabled to exclude unassigned and singly charged ions. The dynamic exclusion duration was set to 30 seconds. The ion accumulation time was set to 50 ms for MS and 50 ms at 17,500 resolution for MS/MS. Data was processed using Pereus and Rstudio software.

5.9.2 Abundance of isoprenol substrate, Me-cPP

WT and *ΔhflKC* knockout were grown in glass flask on M9 glucose minimal medium at 37°C and 220 rpm. For steady-state metabolomics, cells were grown to an OD_{600} of 0.5, and 2 ml culture aliquots were vacuum-filtered. For time-course metabolomics, volumes of samples were adjusted based on the OD_{600} of the culture to obtain in 1 ml an OD_{600} of 1. Culture aliquots were immediately filtered on a 0.45 µm pore size filter (HVLP02500, Merck Millipore) and filters were transferred into an extraction solution consisting of acetonitrile/methanol/water (40:40:20 (v/v)). Extracts were centrifuged for 20 min at −9 °C at 17,000 × g to remove the cell debris. Centrifuged extracts were mixed with 13C-labeled internal standard and analyzed by LC–MS/MS, with an Agilent 6495 triple quadrupole mass spectrometer (Agilent Technologies). An Agilent 1290 Infinity II UHPLC system (Agilent Technologies) was used for liquid chromatography and controlled by the Agilent MassHunter Acquisition software (Version B.07.01).
The temperature of the column oven was 30 °C, and the injection volume was 3 µl. LC solvents A were water with 10 mM ammonium formate and 0.1% formic acid (v/v) (for acidic conditions); and water with 10 mM ammonium carbonate and 0.2% ammonium hydroxide (for basic conditions). LC solvents B were acetonitrile with 0.1% formic acid (v/v) for acidic conditions and acetonitrile without additive for basic conditions. LC columns were an Acquity BEH Amide (30 × 2.1 mm, 1.7 µm) for acidic conditions, and an iHILIC-Fusion(P) (50 × 2.1 mm, 5 µm) for basic conditions. The gradient for basic and acidic conditions was: 0 min 90% B; 1.3 min 40% B; 1.5 min 40% B; 1.7 min 90% B; 2 min 90% B. Quantification of intracellular metabolite concentrations was based on the ratio of 12C and 13C peak heights.

5.9.3 ATP measurements and energy change calculation

WT and *ΔhflKC* strains were grown out of glycerol stocks in LB medium for 6h. Dilution of 1:5000 was then preculture in M9 glucose minimal medium (as described above) at 37°C and 220rpm. For steady-state metabolomics, cells were grown to an OD_{600} of 0.5. The next day, each preculture was used to inoculate three glass flasks with a final volume of 10 ml M9 glucose minimal medium and starting OD_{600} of 0.05 until 0.5. Three individual replicas per sample were used. A Standard Operating Procedure (SOP) for stream metabolites was implemented. Biomass of OD_{600} 0.8 was used to put on filter disc (PVDF Membranes: 0.45µ pore size) and immediately transferred into 1ml acetonitrile: methanol: water (40:40:20) kept at -20°C. Samples were incubated for 30min at -20°C. After that time, 500ul of the samples were transferred into a 1.5ml tube at -20oC and centrifuged at -9°C and >13.000 rpm for 15min. 350ul of supernatant were transferred to new Eppendorf tubes and stored at-80°C. used to run LCMS analysis. To proceed with the analysis, 15 µl of each sample was mixed with 15 µl of 13C standard. An Agilent 6495 triple quadrupole

mass spectrometer (Agilent Technologies) was used for mass spectrometry. An Agilent 1290 Infinity II UHPLC system (Agilent Technologies) was used for liquid chromatography. The methodology for measurement is described Guder J.C et al. [132].

5.9.4 Lipid extraction and annotation

WT and *ΔhflKC* knockout were grown in TB until reached OD_{600} of 0.5. For all the samples biomass was adjusted to OD_{600} of 5. Cells were collected by centrifugation and washed twice with 1X PBS. Pellet samples were dissolved in a mixture of 150ul of chloroform, 300ul of methanol, and 120ul of water, then shaken for 10min at 4^{c}C. After that time, 150 ul of chloroform and 150 ul of 0.85% KCL were added. Samples were centrifuged for 10min at max g and 4^{o}C. The lipid phase was transferred to a new tube and dried with nitrogen. All samples have three independent cultures. The relative quantification and annotation of lipids were performed by using HRES-LC-MS/MS.

Lipid annotation was done employing Compound Discoverer 3.3 (CD) using a customized CD workflow and matching the metabolic features against three different data libraries. Most lipids were matched against the MS-Dial LipidBlast library (version68). In addition, two customized in-house libraries were used. The "IS-List.massList" contained the names of the 8 lipids that were used as internal standards (LPE 13:0, PE 40:8, PG 40:8, CL 56:4, Cer 22:1;2, HexCer 26:1;2 and SM 24:1;2) and the "targetedCompounds.massList" contained the ammonium adduct of the ubiquinol-8 and ubiquinone-8 (CoQ8). The library focus for the targeted analytes was created by the in-house MS/MS measured spectra from previous runs and the library focus on the internal standards was created based the theoretical mass calculated by the elemental formula.

The CD workflow consisted of different nodes, where each node represents one step of the data analysis and annotation. The workflow is depicted in supplemental figure SI1. It consisted of the following nodes: "Input Files", "Select Spectra", "Align Retention Time", "Detect Compounds" (Min. Peak: 5000), "Group Compounds", "Fill Gaps", "Normalize Areas" (Normalization: Constant Sum), and "Mark Background Compounds". The "Search mzVault" (mzVault Library: \MSDIAL-LipidBlast_VS68-Neg.db, \MSDIAL-LipidBlast_VS68-Pos.db, Match Ionization Method: FALSE, Search Algorithm: NIST, Use Retention Time: FALSE) node and "Search Mass Lists" (Mass Lists: \IS-Lipids.massList\targetCompounds.massList, Use Retention Time: FALSE) for the features annotation and finally the node "Assign Compound Annotations". If not stated otherwise, default settings were used for each node.

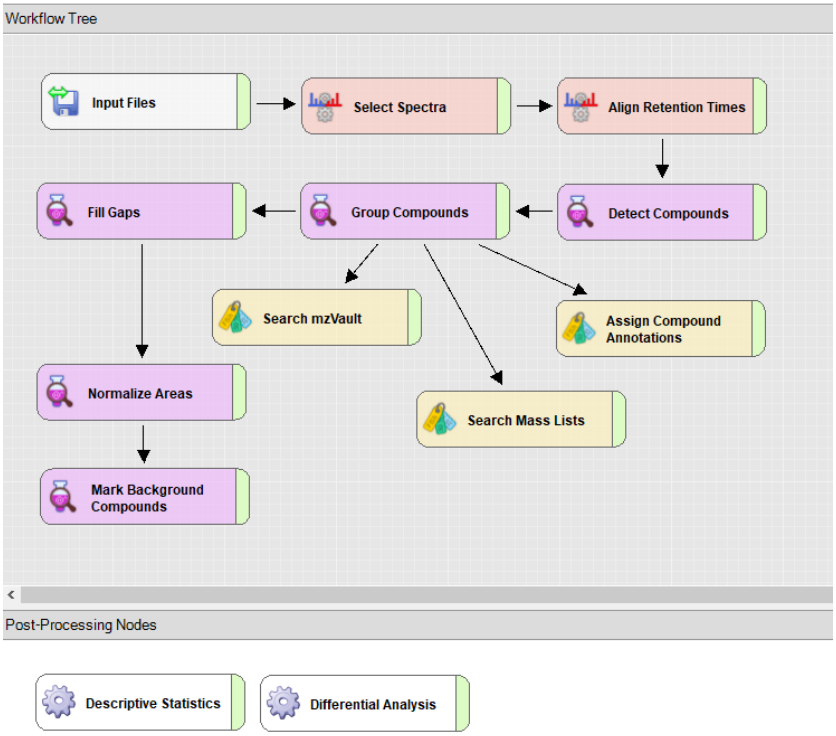

The Post-Processing Nodes “Descriptive Statistics” and “Differential Analysis” were used as quality control and the main statistical tests. The results of the workflow were further filtered according to the following criteria: 1) Metabolic features were only considered if an MS2 spectra had been determined for the corresponding ion. 2) Metabolic features were only considered if they could be matched against an entry in the LipidBlast database, the list of internal standard lipids or targeted compounds based on accurate mass (Delta = ± 5) and MS2 spectrum. 3) Metabolic features were only considered if the signal quality, quantified in the parameter “peak rating” (indicating among others the peak shape, signal-to-noise ratio, and signal intensity) by the CD software was 6 or higher in all samples of the same biological condition.

5.9.5 Abundance of ubiquinone-8 and uniquinol-8

WT and *ΔhflKC* knockout were grown in TB until reached OD_{600} of 0.5. For all the samples biomass was adjusted to OD_{600} of 5. Cells were collected by centrifugation and washed twice with 1X PBS. Pellet samples were dissolved in a mixture of 150 ul of chloroform, 300 ul of methanol, and 120ul of water, then shaken for 10min at $4^{O}C$. After that time, 150 ul of chloroform and 150 ul of 0.85% KCL were added. Samples were centrifuged for 10 min at max g and $4^{o}C$. The lipid phase was transferred to a new tube and dried with nitrogen. All samples have three independent cultures. The relative quantification and annotation of lipids were performed by using HRES-LC-MS/MS. The chromatographic separation was performed using an Acquity Premier CSH C18 column (2.1 × 100 mm, 1.7 µm particle size, VanGuard) a constant flow rate of 0.3 ml/min with mobile phase A being 10mm Ammonium Formate in 6:4 Acetonitrile:water and phase B being 9:1 Isopropanol:Acetonitrile (Honeywell, Morristown, New Jersey, USA) at 40° C. The injection volume was 5 µl. The mobile phase profile consisted of the following steps and linear gradients: 0 – 1.5 min constant at 37 % B; 1.5 – 4 min from 37 to 45 % B; 4 – 5 min from 45 to 52 % B; 5 – 8 min from 52 to 58 % B; 8 - 11 min from 58 to 66 % B; 11 - 14 min from 66 to 70 % B; 11 - 14 min from 66 - 70 % B; 14 - 18 min from 70 to 75 % B; 18 - 20 min from 75 to 98 % B; 20 - 25 min constant at 98 % B; 25 – 25.1 min from 98 to 37 % B; 25.1 – 30 min constant at 37 % B.

For the measurement, a Thermo Scientific ID-X Orbitrap mass spectrometer was used. Ionization was performed using a high temperature electro-spray ion source at a static spray voltage of 3500 V (positive) and a static spray voltage of 2800 V (negative), Sheath gas at 50 (Arb), Auxiliary Gas at 10 (Arb), and Ion transfer tube and Vaporizer at 325 and 300°C. HCD was performed on the ten most abundant ions per scan with a relative collision energy of 25 %. Fragments were detected using the orbitrap mass analyzer at a predefined mass resolution of 15,000. Dynamic exclusion with an exclusion duration of 5 seconds after 1 scan with a mass tolerance of 10 ppm was used to increase coverage.

Compound Discoverer 3.3 (Thermo-Fisher Scientific) was used for lipid annotation by matching accurate mass and MS2 spectra against the MS/MS library MS-DIAL LipidBlast (version 68). In addition, two customized in-house libraries were used for the annotation of the target analytes Ubiquinone-8 and Ubiquinol-8, and a set of eight lipids that served as internal standards. For the semi-quantitative comparison of lipid abundance, annotated peaks were integrated using Compound Discoverer 3.3 (Thermo Scientific) and normalization by the default method provided by Compound Discoverer 3.3 and further processed by the statistical tools described elsewhere.

References

[1] N. Tavernarakis, M. Driscoll, and N. C. Kyrpides, “The SPFH domain: Implicated in regulating targeted protein turnover in stomatins and other membrane-associated proteins,” *Trends Biochem. Sci.*, vol. 24, no. 11, pp. 425–427, 1999, doi: 10.1016/S0968-0004(99)01467-X.

[2] D. T. Browman, M. B. Hoegg, and S. M. Robbins, “The SPFH domain-containing proteins: more than lipid raft markers,” *Trends Cell Biol.*, vol. 17, no. 8, pp. 394–402, 2007, doi: 10.1016/j.tcb.2007.06.005.

[3] M. Hinderhofer, C. A. Walker, A. Friemel, C. A. Sturmer, H. M. Moller, and A. Reuter, “Evolution of prokaryotic SPFH proteins,” *BMC Evol. Biol.*, vol. 9, no. 1, p. 10, 2009, doi: 10.1186/1471-2148-9-10.

[4] E. Rivera-Milla, C. A. O. Stuermer, and E. Málaga-Trillo, “Ancient origin of reggie (flotillin), reggie-like, and other lipid-raft proteins: Convergent evolution of the SPFH domain,” *Cell. Mol. Life Sci.*, vol. 63, no. 3, pp. 343–357, 2006, doi: 10.1007/s00018-005-5434-3.

[5] I. C. Morrow and R. G. Parton, “Flotillins and the PHB domain protein family: Rafts worms and anaesthetics,” *Traffic*, vol. 6, no. 9, pp. 725–740, 2005, doi: 10.1111/j.1600-0854.2005.00318.x.

[6] A. Yepes *et al.*, “The biofilm formation defect of a Bacillus subtilis flotillin-defective mutant involves the protease FtsH,” *Mol. Microbiol.*, vol. 86, no. 2, pp. 457–471, 2012, doi: 10.1111/j.1365-2958.2012.08205.x.

[7] A. Zielińska *et al.*, “Flotillin mediated membrane fluidity controls peptidoglycan synthesis and MreB movement.,” *bioRxiv*, p. 736819, 2020, doi: 10.1101/736819.

[8] E. García-Fernández *et al.*, “Membrane Microdomain Disassembly Inhibits MRSA Antibiotic Resistance,” *Cell*, vol. 171, no. 6, pp. 1354-1367.e20, 2017, doi: 10.1016/j.cell.2017.10.012.

[9] M. F. Langhorst, A. Reuter, and C. A. O. Stuermer, “Scaffolding microdomains and beyond: The function of reggie/flotillin proteins,” *Cell. Mol. Life Sci.*, vol. 62, no. 19–20, pp. 2228–2240, 2005, doi: 10.1007/s00018-005-5166-4.

[10] L. J. Pike, “Rafts defined: a report on the Keystone symposium on lipid rafts and cell function,” *J. Lipid Res.*, vol. 47, no. 7, pp. 1597–1598, 2006, doi: https://doi.org/10.1194/jlr.E600002-JLR200.

[11] K. Simons and D. Toomre, “Lipid rafts and signal transduction,” *Nat. Rev. Mol. Cell Biol.*, vol. 1, no. 1, pp. 31–39, 2000, doi: 10.1038/35036052.

[12] E. Sezgin, I. Levental, S. Mayor, and C. Eggeling, “The mystery of membrane organization: Composition, regulation and roles of lipid rafts,” *Nat. Rev. Mol. Cell Biol.*, vol. 18, no. 6, pp. 361–374, 2017, doi: 10.1038/nrm.2017.16.

[13] L. D. Zajchowski and S. M. Robbins, “Lipid rafts and little caves. Compartmentalized signalling in membrane microdomains.,” *Eur. J. Biochem.*, vol. 269, no. 3, pp. 737–752, Feb. 2002, doi: 10.1046/j.0014-2956.2001.02715.x.

[14] D. T. Browman, M. E. Resek, L. D. Zajchowski, and S. M. Robbins, “Erlin-1 and erlin-2 are novel members of the prohibitin family of proteins that define lipid-raft-like domains of the ER,” *J. Cell Sci.*, vol. 119, no. 15, pp. 3149–3160,

2006, doi: 10.1242/jcs.03060.

[15] S. Mishra, L. C. Murphy, B. L. G. Nyomba, and L. J. Murphy, “Prohibitin: A potential target for new therapeutics,” *Trends Mol. Med.*, vol. 11, no. 4, pp. 192–197, 2005, doi: 10.1016/j.molmed.2005.02.004.

[16] D. López, M. A. Fischbach, F. Chu, R. Losick, and R. Kolter, “Structurally diverse natural products that cause potassium leakage trigger multicellularity in *Bacillus subtilis*,” *Proc. Natl. Acad. Sci.*, vol. 106, no. 1, pp. 280–285, 2009, doi: 10.1073/pnas.0810940106.

[17] D. Lopez and R. Kolter, “Functional microdomains in bacterial membranes,” *Genes Dev.*, vol. 24, no. 17, pp. 1893–1902, 2010, doi: 10.1101/gad.1945010.

[18] X. Feng *et al.*, “Structural and functional analysis of Bacillus subtilis YisP reveals a role of its product in biofilm production.,” *Chem. Biol.*, vol. 21, no. 11, pp. 1557–1563, Nov. 2014, doi: 10.1016/j.chembiol.2014.08.018.

[19] R. M. Wagner, L. Kricks, and D. Lopez, “Functional Membrane Microdomains Organize Signaling Networks in Bacteria,” *J. Membr. Biol.*, vol. 250, no. 4, pp. 367–378, 2017, doi: 10.1007/s00232-016-9923-0.

[20] C. Donovan and M. Bramkamp, “Characterization and subcellular localization of a bacterial flotillin homologue,” *Microbiology*, vol. 155, no. 6, pp. 1786–1799, 2009, doi: 10.1099/mic.0.025312-0.

[21] J. E. Guzmán-Flores *et al.*, “Proteomic analysis of *Escherichia coli* detergent-resistant membranes (DRM),” *PLoS One*, vol. 14, no. 10, p. e0223794, 2019, doi: 10.1371/journal.pone.0223794.

[22] H. M. Zhang, Z. Li, M. Tsudome, S. Ito, H. Takami, and K. Horikoshi, “An alkali-inducible flotillin-like protein from Bacillus halodurans C-125,” *Protein J.*, vol. 24, no. 2, pp. 125–131, 2005, doi: 10.1007/s10930-004-1519-3.

[23] F. Dempwolff, H. M. Möller, and P. L. Graumanna, “Synthetic motility and cell shape defects associated with deletions of flotillin/reggie paralogs in Bacillus subtilis and interplay of these proteins with NfeD proteins,” *J. Bacteriol.*, vol. 194, no. 17, pp. 4652–4661, 2012, doi: 10.1128/JB.00910-12.

[24] D. Lopez, “Molecular composition of functional microdomains in bacterial membranes,” *Chem. Phys. Lipids*, vol. 192, pp. 3–11, 2015, doi: 10.1016/j.chemphyslip.2015.08.015.

[25] E. Kannenberg and K. Poralla, “The influence of hopanoids on growth of Mycoplasma mycoides,” *Arch. Microbiol.*, vol. 133, no. 2, pp. 100 – 102, 1982, doi: 10.1007/BF00413519.

[26] R. A. Moreau, J. Agnew, K. B. Hicks, and M. J. Powell, “Modulation of lipoxygenase activity by bacterial hopanoids,” *J. Nat. Prod.*, vol. 60, no. 4, pp. 397 – 398, 1997, doi: 10.1021/np960611y.

[27] R. F. Taylor, “Bacterial triterpenoids.,” *Microbiol. Rev.*, vol. 48, no. 3, pp. 181–198, Sep. 1984, doi: 10.1128/mr.48.3.181-198.1984.

[28] W. K. Subczynski, A. Wisniewska-Becker, and J. Widomska, “Can macular xanthophylls replace cholesterol in formation of the liquid-ordered phase in lipid-bilayer membranes?,” *Acta Biochim. Pol.*, vol. 59, no. 1, pp. 109 – 114, 2012, doi: 10.18388/abp.2012_2183.

[29] M. Bramkamp and D. Lopez, “Exploring the Existence of Lipid Rafts in Bacteria,” *Microbiol. Mol. Biol. Rev.*, vol. 79, no. 1, pp. 81–100, 2015, doi: 10.1128/mmbr.00036-14.

[30] D. Lopez and G. Koch, “Exploring functional membrane microdomains in bacteria: an overview,” *Curr. Opin. Microbiol.*, vol. 36, pp. 76–84, 2017, doi: 10.1016/j.mib.2017.02.001.

[31] Z. Qiao *et al.*, “Cryo-EM structure of the entire FtsH-HflKC AAA protease complex,” *Cell Rep.*, vol. 39, no. 9, p. 110890, 2022, doi: 10.1016/j.celrep.2022.110890.

[32] B. Mielich-Süss *et al.*, “Flotillin scaffold activity contributes to type VII secretion system assembly in Staphylococcus aureus,” *PLoS Pathog.*, vol. 13, no. 11, p. e1006728, 2017, doi: 10.1371/journal.ppat.1006728.

[33] S. Chiba, K. Ito, and Y. Akiyama, “The Escherichia coli plasma membrane contains two PHB (prohibitin homology) domain protein complexes of opposite orientations,” *Mol. Microbiol.*, vol. 60, no. 2, pp. 448–457, 2006, doi: 10.1111/j.1365-2958.2006.05104.x.

[34] A. Kihara, Y. Akiyama, and K. Ito, “Host regulation of lysogenic decision in bacteriophage λ: Transmembrane modulation of FtsH (HflB), the cII degrading protease, by HflKC (HflA),” *Proc. Natl. Acad. Sci. U. S. A.*, vol. 94, no. 11, pp. 5544–5549, 1997, doi: 10.1073/pnas.94.11.5544.

[35] Y. Akiyama, “Quality control of cytoplasmic membrane proteins in escherichia coli,” *J. Biochem.*, vol. 146, no. 4, pp. 449–454, 2009, doi: 10.1093/jb/mvp071.

[36] A. K. Wessel *et al.*, “Escherichia coli SPFH Membrane Microdomain Proteins HflKC Contribute to Aminoglycoside and Oxidative Stress Tolerance,” *Microbiol. Spectr.*, pp. 1–27, 2023, doi: 10.1128/spectrum.01767-23.

[37] F. Padilla-Vaca *et al.*, “Flotillin homologue is involved in the swimming behavior of Escherichia coli,” *Arch. Microbiol.*, vol. 201, no. 7, pp. 999–1008, 2019, doi: 10.1007/s00203-019-01670-8.

[38] O. Kobiler, A. Rokney, and A. B. Oppenheim, “Phage lambda CIII: A protease inhibitor regulating the lysis-lysogeny decision,” *PLoS One*, vol. 2, no. 4, 2007, doi: 10.1371/journal.pone.0000363.

[39] A. Kihara, Y. Akiyama, and K. Ito, “A protease complex in the Escherichia coli plasma membrane: HflKC (HflA) forms a complex with FtsH (HflB), regulating its proteolytic activity against SecY.,” *EMBO J.*, vol. 15, no. 22, pp. 6122–6131, 1996, doi: 10.1002/j.1460-2075.1996.tb01000.x.

[40] J. Arends, N. Thomanek, K. Kuhlmann, K. Marcus, and F. Narberhaus, “In vivo trapping of FtsH substrates by label-free quantitative proteomics,” *Proteomics*, vol. 16, no. 24, pp. 3161–3172, 2016, doi: 10.1002/pmic.201600316.

[41] C. Ma *et al.*, “Structural insights into the membrane microdomain organization by SPFH family proteins.,” *Cell Res.*, no. November, 2022, doi: 10.1038/s41422-021-00598-3.

[42] J. Brand *et al.*, “A stomatin dimer modulates the activity of acid-sensing ion channels.,” *EMBO J.*, vol. 31, no. 17, pp. 3635–3646, Aug. 2012, doi: 10.1038/emboj.2012.203.

[43] G. Steglich, W. Neupert, and T. Langer, “Prohibitins regulate membrane protein degradation by the m-AAA protease in

mitochondria.," *Mol. Cell. Biol.*, vol. 19, no. 5, pp. 3435–3442, May 1999, doi: 10.1128/MCB.19.5.3435.

[44] S. Langklotz, U. Baumann, and F. Narberhaus, "Structure and function of the bacterial AAA protease FtsH," *Biochim. Biophys. Acta - Mol. Cell Res.*, vol. 1823, no. 1, pp. 40–48, 2012, doi: 10.1016/j.bbamcr.2011.08.015.

[45] K. Ito and Y. Akiyama, "Cellular Functions, Mechanism of Action, and Regulation of Ftsh Protease," *Annu. Rev. Microbiol.*, vol. 59, no. 1, pp. 211–231, 2005, doi: 10.1146/annurev.micro.59.030804.121316.

[46] K. Leonhard, J. M. Herrmann, R. A. Stuart, G. Mannhaupt, W. Neupert, and T. Langer, "AAA proteases with catalytic sites on opposite membrane surfaces comprise a proteolytic system for the ATP-dependent degradation of inner membrane proteins in mitochondria," *EMBO J.*, vol. 15, no. 16, p. 4218—4229, Aug. 1996, doi: 10.1002/j.1460-2075.1996.tb00796.x.

[47] M. Graef, G. Seewald, and T. Langer, "Substrate recognition by AAA+ ATPases: distinct substrate binding modes in ATP-dependent protease Yme1 of the mitochondrial intermembrane space.," *Mol. Cell. Biol.*, vol. 27, no. 7, pp. 2476–2485, Apr. 2007, doi: 10.1128/MCB.01721-06.

[48] S. Chiba, Y. Akiyama, and K. Ito, "Membrane protein degradation by FtsH can be initiated from either end.," *J. Bacteriol.*, vol. 184, no. 17, pp. 4775–4782, Sep. 2002, doi: 10.1128/JB.184.17.4775-4782.2002.

[49] Y. Shotland, D. Teff, S. Koby, O. Kobiler, and A. B. Oppenheim, "Characterization of a conserved alpha-helical, coiled-coil motif at the C-terminal domain of the ATP-dependent FtsH (HflB) protease of Escherichia coli.," *J. Mol. Biol.*, vol. 299, no. 4, pp. 953–964, Jun. 2000, doi: 10.1006/jmbi.2000.3767.

[50] J. D. Pédelacq, S. Cabantous, T. Tran, T. C. Terwilliger, and G. S. Waldo, "Engineering and characterization of a superfolder green fluorescent protein," *Nat. Biotechnol.*, vol. 24, no. 1, pp. 79–88, 2006, doi: 10.1038/nbt1172.

[51] L. M. Oviedo-Bocanegra, R. Hinrichs, D. A. O. Rotter, S. Dersch, and P. L. Graumann, "Single molecule/particle tracking analysis program SMTracker 2.0 reveals different dynamics of proteins within the RNA degradosome complex in Bacillus subtilis," *Nucleic Acids Res.*, vol. 49, no. 19, pp. e112–e112, 2021, doi: 10.1093/nar/gkab696.

[52] S. C. Lee *et al.*, "A method for detergent-free isolation of membrane proteins in their local lipid environment," *Nat. Protoc.*, vol. 11, no. 7, pp. 1149–1162, 2016, doi: 10.1038/nprot.2016.070.

[53] D. M. Owen, C. Rentero, A. Magenau, A. Abu-Siniyeh, and K. Gaus, "Quantitative imaging of membrane lipid order in cells and organisms," *Nat. Protoc.*, vol. 7, no. 1, pp. 24–35, 2012, doi: 10.1038/nprot.2011.419.

[54] M. C. Mansilla and D. de Mendoza, "The Bacillus subtilis desaturase: a model to understand phospholipid modification and temperature sensing.," *Arch. Microbiol.*, vol. 183, no. 4, pp. 229–35, May 2005, doi: 10.1007/s00203-005-0759-8.

[55] O. Besharova, V. M. Suchanek, R. Hartmann, K. Drescher, and V. Sourjik, "Diversification of gene expression during formation of static submerged biofilms by Escherichia coli," *Front. Microbiol.*, vol. 7, no. OCT, pp. 1–17, 2016, doi: 10.3389/fmicb.2016.01568.

[56] G. A. O'Toole, "Microtiter dish Biofilm formation assay," *J. Vis. Exp.*, no. 47, pp. 10–11, 2010, doi: 10.3791/2437.

[57] G. Unden, P. A. Steinmetz, and P. Degreif-Dünnwald, " The Aerobic and Anaerobic Respiratory Chain of Escherichia coli and Salmonella enterica : Enzymes and Energetics ," *EcoSal Plus*, vol. 6, no. 1, 2014, doi: 10.1128/ecosalplus.esp-0005-2013.

[58] L. Aussel, F. Pierrel, L. Loiseau, M. Lombard, M. Fontecave, and F. Barras, "Biosynthesis and physiology of coenzyme Q in bacteria," *Biochim. Biophys. Acta - Bioenerg.*, vol. 1837, no. 7, pp. 1004–1011, 2014, doi: 10.1016/j.bbabio.2014.01.015.

[59] M. Lee *et al.*, "Biosynthesis of Isoprenoids: Crystal Structure of the [4Fe-4S] Cluster Protein IspG," *J. Mol. Biol.*, vol. 404, no. 4, pp. 600–610, 2010, doi: 10.1016/j.jmb.2010.09.050.

[60] L. M. Bittner, J. Arends, and F. Narberhaus, "When, how and why? Regulated proteolysis by the essential FtsH protease in Escherichia coli," *Biol. Chem.*, vol. 398, no. 5–6, pp. 625–635, 2017, doi: 10.1515/hsz-2016-0302.

[61] A. N. Brown, M. T. Anderson, M. A. Bachman, and H. L. T. Mobley, "The ArcAB Two-Component System: Function in Metabolism, Redox Control, and Infection," *Microbiol. Mol. Biol. Rev.*, vol. 86, no. 2, 2022, doi: 10.1128/mmbr.00110-21.

[62] S. Iuchi and E. C. Lin, "Mutational analysis of signal transduction by ArcB, a membrane sensor protein responsible for anaerobic repression of operons involved in the central aerobic pathways in Escherichia coli.," *J. Bacteriol.*, vol. 174, no. 12, pp. 3972–3980, Jun. 1992, doi: 10.1128/jb.174.12.3972-3980.1992.

[63] S. Solomon, M. Masilamani, L. Rajendran, M. Bastmeyer, C. A. O. Stuermer, and H. Illges, "The Lipid Raft Microdomain-Associated Protein Reggie-1/ Flotillin-2 is Expressed in Human B Cells and Localized at the Plasma Membrane and Centrosome in PBMCs," *Immunobiology*, vol. 205, no. 1, pp. 108–119, 2002, doi: https://doi.org/10.1078/0171-2985-00114.

[64] T. Takashi, A. Kirstin, Model, and L. Thomas, "Formation of Membrane-bound Ring Complexes by Prohibitins in Mitochondria," *Mol Biol Cell*, vol. 15, no. January, pp. 248–259, 2005, doi: 10.1091/mbc.E04-09-0807.

[65] G. Jovanovic, P. Mehta, L. Ying, and M. Buck, "Anionic lipids and the cytoskeletal proteins MreB and RodZ define the spatio-temporal distribution and function of membrane stress controller PspA in Escherichia coli," *Microbiol. (United Kingdom)*, vol. 160, pp. 2374–2386, 2014, doi: 10.1099/mic.0.078527-0.

[66] J. Schneider *et al.*, "Spatio-temporal remodeling of functional membrane microdomains organizes the signaling networks of a bacterium," *PLoS genetics*, vol. 11, no. 4. Research Center for Infectious Diseases ZINF, University of Würzburg, Würzburg, Germany., p. e1005140, 2015. doi: 10.1371/journal.pgen.1005140.

[67] P. Nicolas *et al.*, "Condition-dependent transcriptome reveals high-level regulatory architecture in Bacillus subtilis.," *Science*, vol. 335, no. 6072, pp. 1103–1106, Mar. 2012, doi: 10.1126/science.1206848.

[68] S. J. Hesketh *et al.*, "Styrene maleic-acid lipid particles (SMALPs) into detergent or amphipols: An exchange protocol for membrane protein characterisation," *Biochim. Biophys. Acta - Biomembr.*, vol. 1862, no. 5, p. 183192, 2020, doi: https://doi.org/10.1016/j.bbamem.2020.183192.

[69] P. Angelisová *et al.*, "The use of styrene-maleic acid copolymer (SMA) for studies on T cell membrane rafts," *Biochim. Biophys. Acta - Biomembr.*, vol. 1861, no. 1, pp. 130–141, 2019, doi: 10.1016/j.bbamem.2018.08.006.

[70] N. Slaughter *et al.*, "The flotillins are integral membrane proteins in lipid rafts that contain TCR-associated signaling components: implications for T-cell activation.," *Clin. Immunol.*, vol. 108, no. 2, pp. 138–151, Aug. 2003, doi: 10.1016/s1521-6616(03)00097-4.

[71] H. Strahl and J. Errington, "Bacterial Membranes: Structure, Domains, and Function," *Annu. Rev. Microbiol.*, vol. 71, no. 1, pp. 519–538, 2017, doi: 10.1146/annurev-micro-102215-095630.

[72] A. S. Scholz, S. S. M. Baur, D. Wolf, and M. Bramkamp, "An Stomatin, Prohibitin, Flotillin, and HflK/C-Domain Protein Required to Link the Phage-Shock Protein to the Membrane in Bacillus subtilis," *Front. Microbiol.*, vol. 12, no. October, pp. 1–17, 2021, doi: 10.3389/fmicb.2021.754924.

[73] L. Cybulski and D. Mendoza, "Bilayer Hydrophobic Thickness and Integral Membrane Protein Function," *Curr. Protein Pept. Sci.*, vol. 12, pp. 760–766, 2011, doi: 10.2174/138920311798841681.

[74] J. N. Bach and M. Bramkamp, "Flotillins functionally organize the bacterial membrane," *Mol. Microbiol.*, vol. 88, no. 6, pp. 1205–1217, 2013, doi: 10.1111/mmi.12252.

[75] E. Mileykovskaya and W. Dowhan, "Cardiolipin membrane domains in prokaryotes and eukaryotes.," *Biochim. Biophys. Acta*, vol. 1788, no. 10, pp. 2084–2091, Oct. 2009, doi: 10.1016/j.bbamem.2009.04.003.

[76] G. O'Toole, H. B. Kaplan, and R. Kolter, "Biofilm formation as microbial development.," *Annu. Rev. Microbiol.*, vol. 54, pp. 49–79, 2000, doi: 10.1146/annurev.micro.54.1.49.

[77] D. O. Serra and R. Hengge, "Stress responses go three dimensional - the spatial order of physiological differentiation in bacterial macrocolony biofilms.," *Environ. Microbiol.*, vol. 16, no. 6, pp. 1455–1471, Jun. 2014, doi: 10.1111/1462-2920.12483.

[78] L. A. Pratt and R. Kolter, "Genetic analysis of Escherichia coli biofilm formation: roles of flagella, motility, chemotaxis and type I pili.," *Mol. Microbiol.*, vol. 30, no. 2, pp. 285–293, Oct. 1998, doi: 10.1046/j.1365-2958.1998.01061.x.

[79] J. N. Bach and M. Bramkamp, "Dissecting the molecular properties of prokaryotic flotillins," *PLoS One*, vol. 10, no. 1, pp. 11–15, 2015, doi: 10.1371/journal.pone.0116750.

[80] J. Schneider, B. Mielichsüss, R. Böhme, and D. Lopez, "In vivo characterization of the scaffold activity of flotillin on the membrane kinase KinC of Bacillus subtilis," *Microbiol. (United Kingdom)*, vol. 161, no. 9, pp. 1871–1888, 2015, doi: 10.1099/mic.0.000137.

[81] L. M. Lima, B. N. M. da Silva, G. Barbosa, and E. J. Barreiro, "β-lactam antibiotics: An overview from a medicinal chemistry perspective," *Eur. J. Med. Chem.*, vol. 208, p. 112829, 2020, doi: 10.1016/j.ejmech.2020.112829.

[82] L. S. Redgrave, S. B. Sutton, M. A. Webber, and L. J. V Piddock, "Fluoroquinolone resistance: mechanisms, impact on bacteria, and role in evolutionary success," *Trends Microbiol.*, vol. 22, no. 8, pp. 438–445, 2014, doi: https://doi.org/10.1016/j.tim.2014.04.007.

[83] G. Koch *et al.*, "Attenuating Staphylococcus aureus Virulence by Targeting Flotillin Protein Scaffold Activity," *Cell Chem. Biol.*, vol. 24, no. 7, pp. 845-857.e6, 2017, doi: 10.1016/j.chembiol.2017.05.027.

[84] B. Mielich-Süss, J. Schneider, and D. Lopez, "Overproduction of Flotillin Influences Cell Differentiation and Shape in Bacillus subtilis," *MBio*, vol. 4, no. 6, pp. e00719-13, Dec. 2013, doi: 10.1128/mBio.00719-13.

[85] S. Sauret-Güeto, A. Ramos-Valdivia, E. Ibáñez, A. Boronat, and M. Rodríguez-Concepción, "Identification of lethal mutations in Escherichia coli genes encoding enzymes of the methylerythritol phosphate pathway," *Biochem. Biophys. Res. Commun.*, vol. 307, no. 2, pp. 408–415, 2003, doi: 10.1016/S0006-291X(03)01211-7.

[86] B. Nowicka and J. Kruk, "Occurrence, biosynthesis and function of isoprenoid quinones," *Biochim. Biophys. Acta - Bioenerg.*, vol. 1797, no. 9, pp. 1587–1605, 2010, doi: 10.1016/j.bbabio.2010.06.007.

[87] M. Rodríguez-Concepción *et al.*, "Genetic evidence of branching in the isoprenoid pathway for the production of isopentenyl diphosphate and dimethylallyl diphosphate in Escherichia coli.," *FEBS Lett.*, vol. 473, no. 3, pp. 328–332, May 2000, doi: 10.1016/s0014-5793(00)01552-0.

[88] F. Pierrel, A. Burgardt, J. H. Lee, L. Pelosi, and V. F. Wendisch, "Recent advances in the metabolic pathways and microbial production of coenzyme Q," *World J. Microbiol. Biotechnol.*, vol. 38, no. 4, pp. 1–13, 2022, doi: 10.1007/s11274-022-03242-3.

[89] A. Banerjee and T. D. Sharkey, "Methylerythritol 4-phosphate (MEP) pathway metabolic regulation," *Nat. Prod. Rep.*, vol. 31, no. 8, pp. 1043–1055, 2014, doi: 10.1039/c3np70124g.

[90] G. B. Cox and F. Gibson, "Biosynthesis of vitamin K and ubiquinone relation to the shikimic acid pathway in Escherichia coli," *Biochim. Biophys. Acta - Gen. Subj.*, vol. 93, no. 1, pp. 204–206, 1964, doi: https://doi.org/10.1016/0304-4165(64)90285-5.

[91] M. Bentinger, M. Tekle, and G. Dallner, "Coenzyme Q - Biosynthesis and functions," *Biochem. Biophys. Res. Commun.*, vol. 396, no. 1, pp. 74–79, 2010, doi: 10.1016/j.bbrc.2010.02.147.

[92] G. Lenaz, R. Fato, G. Formiggini, and M. L. Genova, "The role of Coenzyme Q in mitochondrial electron transport.," *Mitochondrion*, vol. 7 Suppl, pp. S8-33, Jun. 2007, doi: 10.1016/j.mito.2007.03.009.

[93] M. Turunen, J. Olsson, and G. Dallner, "Metabolism and function of coenzyme Q," *Biochim. Biophys. Acta - Biomembr.*, vol. 1660, no. 1–2, pp. 171–199, 2004, doi: 10.1016/j.bbamem.2003.11.012.

[94] G. Wu, H. D. Williams, F. Gibson, and R. K. Poole, "Mutants of Escherichia coli affected in respiration: the cloning and nucleotide sequence of ubiA, encoding the membrane-bound p-hydroxybenzoate:octaprenyltransferase.," *J. Gen. Microbiol.*, vol. 139, no. 8, pp. 1795–1805, Aug. 1993, doi: 10.1099/00221287-139-8-1795.

[95] G. Wu, H. D. Williams, M. Zamanian, F. Gibson, and R. K. Poole, "Isolation and characterization of Escherichia coli mutants affected in aerobic respiration: the cloning and nucleotide sequence of ubiG," *Microbiology*, vol. 138, no. 10, pp. 2101–2112, 1992, doi: https://doi.org/10.1099/00221287-138-10-2101.

[96] M. Gulmezian, K. R. Hyman, B. N. Marbois, C. F. Clarke, and G. T. Javor, "The role of UbiX in Escherichia coli coenzyme

Q biosynthesis," *Arch. Biochem. Biophys.*, vol. 467, no. 2, pp. 144–153, 2007, doi: https://doi.org/10.1016/j.abb.2007.08.009.

[97] K. Okada *et al.*, "The ispB gene encoding octaprenyl diphosphate synthase is essential for growth of Escherichia coli," *J. Bacteriol.*, vol. 179, no. 9, pp. 3058–3060, 1997, doi: 10.1128/jb.179.9.3058-3060.1997.

[98] P. T. Lee, A. Y. Hsu, H. T. Ha, and C. F. Clarke, "A C-methyltransferase involved in both ubiquinone and menaquinone biosynthesis: Isolation and identification of the Escherichia coli ubiE gene," *J. Bacteriol.*, vol. 179, no. 5, pp. 1748–1754, 1997, doi: 10.1128/jb.179.5.1748-1754.1997.

[99] R. Meganathan and O. Kwon, "Biosynthesis of Menaquinone (Vitamin K2) and Ubiquinone (Coenzyme Q).," *EcoSal Plus*, vol. 3, no. 2, Aug. 2009, doi: 10.1128/ecosalplus.3.6.3.3.

[100] D. A. Christie *et al.*, "Stomatin-like protein 2 binds cardiolipin and regulates mitochondrial biogenesis and function.," *Mol. Cell. Biol.*, vol. 31, no. 18, pp. 3845–3856, Sep. 2011, doi: 10.1128/MCB.05393-11.

[101] E. C. Lin and S. Iuchi, "Regulation of gene expression in fermentative and respiratory systems in Escherichia coli and related bacteria.," *Annu. Rev. Genet.*, vol. 25, pp. 361–387, 1991, doi: 10.1146/annurev.ge.25.120191.002045.

[102] S. Iuchi, D. C. Cameron, and E. C. Lin, "A second global regulator gene (arcB) mediating repression of enzymes in aerobic pathways of Escherichia coli.," *J. Bacteriol.*, vol. 171, no. 2, pp. 868–873, 1989, doi: 10.1128/jb.171.2.868-873.1989.

[103] D. Georgellis, O. Kwon, and E. C. C. Lin, "Quinones as the redox signal for the Arc two-component system of bacteria," *Science (80-.).*, vol. 292, no. 5525, pp. 2314 – 2316, 2001, doi: 10.1126/science.1059361.

[104] V. B. Borisov and M. I. Verkhovsky, "Oxygen as Acceptor," *EcoSal Plus*, vol. 6, no. 2, pp. 10.1128/ecosalplus.ESP-0012–2015, 2015, doi: 10.1128/ecosalplus.esp-0012-2015.

[105] R. Malpica, B. Franco, C. Rodriguez, O. Kwon, and D. Georgellis, "Identification of a quinone-sensitive redox switch in the ArcB sensor kinase," *Proc. Natl. Acad. Sci. U. S. A.*, vol. 101, no. 36, pp. 13318 – 13323, 2004, doi: 10.1073/pnas.0403064101.

[106] M. Babu *et al.*, "Genetic interaction maps in Escherichia coli reveal functional crosstalk among cell envelope biogenesis pathways.," *PLoS Genet.*, vol. 7, no. 11, p. e1002377, Nov. 2011, doi: 10.1371/journal.pgen.1002377.

[107] R. L. Guest, S. T. Rutherford, and T. J. Silhavy, "Border Control: Regulating LPS Biogenesis," *Trends Microbiol.*, vol. 29, no. 4, pp. 334–345, 2021, doi: https://doi.org/10.1016/j.tim.2020.09.008.

[108] C. Merkwirth and T. Langer, "Prohibitin function within mitochondria: Essential roles for cell proliferation and cristae morphogenesis," *Biochim. Biophys. Acta - Mol. Cell Res.*, vol. 1793, no. 1, pp. 27–32, 2009, doi: 10.1016/j.bbamcr.2008.05.013.

[109] C. Osman, C. Merkwirth, and T. Langer, "Prohibitins and the functional compartmentalization of mitochondrial membranes," *J. Cell Sci.*, vol. 122, no. 21, pp. 3823–3830, 2009, doi: 10.1242/jcs.037655.

[110] K. Rajalingam *et al.*, “Prohibitin is required for Ras-induced Raf–MEK–ERK activation and epithelial cell migration,” *Nat. Cell Biol.*, vol. 7, no. 8, pp. 837–843, 2005, doi: 10.1038/ncb1283.

[111] G. Fusaro, P. Dasgupta, S. Rastogi, B. Joshi, and S. Chellappan, “Prohibitin induces the transcriptional activity of p53 and is exported from the nucleus upon apoptotic signaling,” *J. Biol. Chem.*, vol. 278, no. 48, p. 47853—47861, Nov. 2003, doi: 10.1074/jbc.m305171200.

[112] V. Kurtev, R. Margueron, K. Kroboth, E. Ogris, V. Cavailles, and C. Seiser, “Transcriptional regulation by the repressor of estrogen receptor activity via recruitment of histone deacetylases.,” *J. Biol. Chem.*, vol. 279, no. 23, pp. 24834–24843, Jun. 2004, doi: 10.1074/jbc.M312300200.

[113] M. Schleicher *et al.*, “Prohibitin-1 maintains the angiogenic capacity of endothelial cells by regulating mitochondrial function and senescence,” *J. Cell Biol.*, vol. 180, no. 1, pp. 101–112, 2008, doi: 10.1083/jcb.200706072.

[114] C. Merkwirth *et al.*, “Prohibitins control cell proliferation and apoptosis by regulating OPA1-dependent cristae morphogenesis in mitochondria.,” *Genes Dev.*, vol. 22, no. 4, pp. 476–488, Feb. 2008, doi: 10.1101/gad.460708.

[115] G. M. Strub *et al.*, “Sphingosine-1-phosphate produced by sphingosine kinase 2 in mitochondria interacts with prohibitin 2 to regulate complex IV assembly and respiration,” *FASEB J.*, vol. 25, no. 2, pp. 600–612, 2011, doi: 10.1096/fj.10-167502.

[116] I. Bourges *et al.*, “Structural organization of mitochondrial human complex I: Role of the ND4 and ND5 mitochondria-encoded subunits and interaction with prohibitin,” *Biochem. J.*, vol. 383, no. 3, pp. 491–499, 2004, doi: 10.1042/BJ20040256.

[117] C. Jian *et al.*, “Deficiency of PHB complex impairs respiratory supercomplex formation and activates mitochondrial flashes,” *J. Cell Sci.*, vol. 130, no. 15, pp. 2620–2630, 2017, doi: 10.1242/jcs.198523.

[118] B. Gehl and L. J. Sweetlove, “Mitochondrial Band-7 family proteins: Scaffolds for respiratory chain assembly?,” *Front. Plant Sci.*, vol. 5, no. APR, pp. 1–6, 2014, doi: 10.3389/fpls.2014.00141.

[119] D. G. Gibson, L. Young, R.-Y. Chuang, J. C. Venter, C. A. 3rd Hutchison, and H. O. Smith, “Enzymatic assembly of DNA molecules up to several hundred kilobases.,” *Nat. Methods*, vol. 6, no. 5, pp. 343–345, May 2009, doi: 10.1038/nmeth.1318.

[120] F. R. Blattner *et al.*, “The complete genome sequence of Escherichia coli K-12.,” *Science*, vol. 277, no. 5331, pp. 1453–1462, Sep. 1997, doi: 10.1126/science.277.5331.1453.

[121] T. Baba *et al.*, “Construction of Escherichia coli K-12 in-frame, single-gene knockout mutants: the Keio collection.,” *Mol. Syst. Biol.*, vol. 2, p. 2006.0008, 2006, doi: 10.1038/msb4100050.

[122] M. J. Lawson, D. Camsund, J. Larsson, Ö. Baltekin, D. Fange, and J. Elf, “In situ genotyping of a pooled strain library after characterizing complex phenotypes.,” *Mol. Syst. Biol.*, vol. 13, no. 10, p. 947, Oct. 2017, doi: 10.15252/msb.20177951.

[123] L. C. Thomason, N. Costantino, and D. L. Court, “E. coli genome manipulation by P1 transduction.,” *Curr. Protoc. Mol. Biol.*, vol. Chapter 1, pp. 1.17.1-1.17.8, Jul. 2007, doi: 10.1002/0471142727.mb0117s79.

[124] P. P. Cherepanov and W. Wackernagel, “Gene disruption in Escherichia coli: TcR and KmR cassettes with the option of Flp-catalyzed excision of the antibiotic-resistance determinant,” *Gene*, vol. 158, no. 1, pp. 9–14, 1995, doi: https://doi.org/10.1016/0378-1119(95)00193-A.

[125] E. Amann, B. Ochs, and K. J. Abel, “Tightly regulated tac promoter vectors useful for the expression of unfused and fused proteins in Escherichia coli,” *Gene*, vol. 69, no. 2, p. 301—315, Sep. 1988, doi: 10.1016/0378-1119(88)90440-4.

[126] N. Bellotto, J. Agudo-Canalejo, R. Colin, R. Golestanian, G. Malengo, and V. Sourjik, “Dependence of diffusion in Escherichia coli cytoplasm on protein size, environmental conditions, and cell growth.,” *Elife*, vol. 11, Dec. 2022, doi: 10.7554/eLife.82654.

[127] L. M. Guzman, D. Belin, M. J. Carson, and J. Beckwith, “Tight regulation, modulation, and high-level expression by vectors containing the arabinose PBAD promoter.,” *J. Bacteriol.*, vol. 177, no. 14, pp. 4121–4130, Jul. 1995, doi: 10.1128/jb.177.14.4121-4130.1995.

[128] L. S. Qi *et al.*, “Repurposing CRISPR as an RNA-guided platform for sequence-specific control of gene expression.,” *Cell*, vol. 152, no. 5, pp. 1173–1183, Feb. 2013, doi: 10.1016/j.cell.2013.02.022.

[129] J. Schindelin *et al.*, “Fiji: an open-source platform for biological-image analysis.,” *Nat. Methods*, vol. 9, no. 7, pp. 676–682, Jun. 2012, doi: 10.1038/nmeth.2019.

[130] J.-Y. Tinevez *et al.*, “TrackMate: An open and extensible platform for single-particle tracking.,” *Methods*, vol. 115, pp. 80–90, Feb. 2017, doi: 10.1016/j.ymeth.2016.09.016.

[131] K. Jaqaman *et al.*, “Robust single-particle tracking in live-cell time-lapse sequences.,” *Nat. Methods*, vol. 5, no. 8, pp. 695–702, Aug. 2008, doi: 10.1038/nmeth.1237.

[132] J. C. Guder, T. Schramm, T. Sander, and H. Link, “Time-Optimized Isotope Ratio LC-MS/MS for High-Throughput Quantification of Primary Metabolites,” *Anal. Chem.*, vol. 89, no. 3, pp. 1624–1631, 2017, doi: 10.1021/acs.analchem.6b03731.

Supplementary tables

Table S 1 Proteins showing significant differences between *ΔhflKC*, *ΔhflK* or *ΔhflC* and wildtype strains during growth in TB

Protein	**Function**	**Log2 (Fold change)[a]**		
Respiratory proteins		*ΔhflKC* vs WT	*ΔhflK* vs WT	*ΔhflC* vs WT
PAAJ	Acetyl-CoA C-didehydroadipoyltransferase	-5.57	-2.50	-0.45
PUTA	Oxidoreductase, proline dehydrogenase	-4.30	-2.73	-0.10
CSID	Oxidoreductase, glutarate hydroxylase	-4.29	-1.43	-0.05
PUUC	NADP/NAD-dependent aldehyde dehydrogenase	-4.02	-2.97	-0.39
ASTD	Aldehyde dehydrogenase	-3.43	-2.27	-0.06
MASZ	Transferases, glyoxylate transacetylase	-3.33	-2.89	0.13
GLCE	Glycolate dehydrogenase, putative FAD-binding subunit	-3.16	-2.46	0.30
GLCF	Glycolate dehydrogenase	-3.14	-1.63	0.31
GABD	Succinate-semialdehyde dehydrogenase	-2.76	-1.11	-0.02
ISPG	Oxidoreductase involved in isoprenol biosynthesis	-2.71	-1.64	-0.01
CYSI	Sulfite reductase, hemoprotein subunit	-2.67	0.07	-0.10
ALDA	Lactaldehyde dehydrogenase	-2.60	-2.42	-0.11
DHSD	Oxidoreductase, succinate dehydrogenase cytochrome b	-2.48	-2.22	-0.02
GARR	Oxidoreductase, tartronate semialdehyde reductase	-2.37	-1.43	0.21
FADH	Oxidoreductase, 2,4-dienoyl-CoA reductase	-2.36	-1.25	0.00
LHGO	L-2-hydroxyglutarate dehydrogenase	-2.33	-1.82	-0.14
STHA	Oxidoreductase, NAD(P)+ transhydrogenase	-2.21	-1.89	-0.07
SUCC	Succinyl-CoA synthetase subunit β	-2.09	-1.78	-0.08
SUCD	Succinyl-CoA synthetase subunit α	-2.08	-2.08	-0.11
SDHB	Succinate dehydrogenase iron-sulfur subunit	-1.98	-1.88	-0.08
SDHA	Succinate dehydrogenase flavoprotein subunit	-1.97	-1.86	-0.06
PUUB	Gamma-glutamylputrescine oxidase	-1.96	ND	ND
CYSJ	Sulfite reductase, flavoprotein subunit	-1.95	1.20	0.14
LLDD	L-lactate dehydrogenase	-1.92	-1.30	0.11
MAO2	Malate dehydrogenase	-1.92	-1.67	-0.05
GLCD	Glycolate dehydrogenase, putative FAD-linked subunit	-1.68	-0.51	0.10
ODO1	Oxidoreductase, 2-oxoglutarate dehydrogenase	-1.67	-1.31	-0.04
DADA	D-amino acid dehydrogenase	-1.64	-1.21	-0.06
UBIB	Ubiquinone biosynthesis protein	-1.61	0.21	0.38
MSRB	Oxidoreductases, methionine sulfoxide reductase	-1.54	-1.27	-0.10

IDH	Oxidoreductase, isocitrate dehydrogenase	-1.47	-1.48	-0.07
CYOA	Cytochrome bo(3) ubiquinol oxidase subunit 2	-1.42	-1.42	-0.02
MDH	Malate dehydrogenase	-1.35	-1.37	-0.11
CYOB	Cytochrome bo(3) ubiquinol oxidase subunit 1	-1.20	-1.61	0.11
MDAB	NADPH:quinone oxidoreductase	2.17	1.45	-0.08
DHNA	Type II NADH:quinone oxidoreductase	1.92	2.16	-0.02
CYDB	Cytochrome bd-I ubiquinol oxidase subunit 2	1.62	2.13	0.08
CYDA	Cytochrome bd-I ubiquinol oxidase subunit 1	1.53	2.10	-0.07
QOR2	Quinone reductase 2	1.31	1.31	-0.21
ODP1	Oxidoreductase, pyruvate dehydrogenase	1.30	1.28	0.09
YQHD	NADPH-dependent aldehyde reductase	1.29	1.02	-0.18
AHPF	Oxidoreductase, alkyl hydroperoxide reductase	1.12	1.55	0.13
Other proteins				
XYLF	Xylose ABC transporter periplasmic binding protein	-5.88	-0.34	-0.22
ASTC	Succinylornithine aminotransferase	-5.11	-2.82	-0.11
LSRR	DNA-binding transcriptional repressor	-4.89	-0.96	0.02
UGPB	Transport of sn-glycerol 3-phosphate	-4.64	-2.12	-0.16
ACTP	Acetate transpor	-4.54	-6.15	-0.51
POTF	Putrescine ABC transporter periplasmic binding protein	-4.50	-0.82	0.11
GARD	Galactarate dehydratase	-4.39	-1.47	0.19
PAAK	Phenylacetate-CoA ligase	-4.11	-1.70	-0.63
DPPC	Dipeptide ABC transporter membrane subunit	-4.05	-5.72	-0.08
GLCC	Glc operon transcriptional activator	-4.04	-1.93	-0.20
FADI	Acetyl-CoA acyltransferase	-4.03	-2.22	-0.22
ACSA	Acetyl-coenzyme A synthetase	-4.01	-3.33	-0.23
LSRB	Autoinducer-2 ABC transporter periplasmic binding	-3.99	-2.14	-0.44
YDCI	DNA-binding transcriptional dual regulator	-3.92	-1.89	-0.19
GLCG	Unknown function	-3.84	-2.83	0.19
YDCS	Putative ABC transporter periplasmic binding	-3.7	-1.77	-0.16
FADJ	Unsaturated acyl-CoA hydratase	-3.46	-1.97	0.12
DPPF	Dipeptide ABC transporter ATP binding subunit	-3.36	-2.39	-0.07
LSRF	Acyltransferase, 3-hydroxy-2,4-pentadione 5-phosphate thiolase	-3.33	-2.49	-0.30
FUMC	Fumarase C	-3.30	-2.12	-0.07
TNAB	Tryptophan:H+ symporter, transporter of tryptophan	-3.29	-2.14	-0.09
YHHZ	Putative endonuclease YhhZ	-3.16	ND	ND
PAAX	DNA-binding transcriptional repressor	-3.11	-1.30	-0.43
PAAY	Phenylacetic acid degradation protein	-3.07	-0.27	0.35
GUDD	D-glucarate dehydratase	-3.06	-1.43	0.20

CSTA	Pyruvate transporter	-2.99	-2.88	-0.22
ASPG2	L-asparagine 2	-2.97	1.87	0.41
TRPGD	Anthranilate synthase subunit	-2.93	ND	ND
GARL	5-keto-4-deoxy-D-glucarate aldolase	-2.91	-2.14	0.12
TRPC	Indole-3-glycerol phosphate synthase	-2.91	-1.85	-0.31
GLXK1	Glycerate 2-kinase	-2.9	-1.17	-0.23
PUTP	Sodium/proline transporter	-2.83	-3.14	-0.24
ARGT	lysine, arginine and ornithine transport	-2.81	-2.94	-0.11
PUUR	DNA-binding transcriptional repressor	-2.74	-2.11	-0.15
TRPB	Tryptophan synthase subunit beta	-2.73	-0.47	0.03
PAAE	Phenylacetyl-CoA 1,2-epoxidase, reductase subunit	-2.68	ND	ND
TRG	Methyl-accepting chemotaxis protein	-2.68	-2.04	-0.18
ASTB	N-succinylarginine dihydrolase	-2.67	-1.76	-0.39
DPPA	Dipeptide ABC transporter periplasmic binding protein	-2.57	-3.08	-0.10
PUUD	Amine and polyamine degradation	-2.54	-2.89	-0.43
PAAC	Phenylacetyl-CoA 1,2-epoxidase, structural subunit	-2.54	ND	ND
PUUE	4-aminobutyrate aminotransferase	-2.51	-1.1	-0.28
ARAF	Arabinose ABC transporter periplasmic	-2.51	-1.19	-0.27
GABT	4-aminobutyrate aminotransferase	-2.48	-1.90	-0.08
CYCA	D-serine/D-alanine/glycine transporter	-2.46	-3.97	-0.15
ASTA	Arginine N-succinyltransferase	-2.38	-0.34	-0.13
OMPF	Outer membrane porin F	-2.27	-2.1	-0.10
GLNH	L-glutamine ABC transporter periplasmic binding protein	-2.25	-1.95	-0.12
TRPA	Tryptophan synthase subunit alpha	-2.24	-0.64	-0.02
FUMA	Fumarate hydratase class I	-2.23	-1.65	-0.13
NDK	Nucleoside diphosphate kinase	-2.2	-2.04	-0.31
MASY	Malate synthase A	-2.19	-2.96	-0.16
LSRK	Autoinducer-2 kinase	-2.17	-3.45	-0.40
TNAA	Tryptophanase	-2.16	-2.21	-0.17
DCTA	Aerobic C4-dicarboxylate transport protein	-2.15	-1.35	0.01
CISY	Citrate synthase	-2.11	-1.98	-0.08
ACEA	Isocitrate lyase	-2.07	-2.73	-0.21
PAAG	1,2-epoxyphenylacetyl-CoA isomerase	-1.91	ND	ND
ALR2	Alanine racemase 2	-1.88	-1.23	0.06
GLPF	Glycerol uptake facilitator protein	-1.88	-1.64	0.01
ACNB	Aconitate hydratase	-1.87	-1.63	-0.06
GLTI	Glutamate/aspartate ABC transporter periplasmic binding	-1.87	-1.42	-0.11
YQEF	Putative acyltransferase	-1.82	-1.55	-0.14
PAAZ	Oxepin-CoA hydrolase	-1.81	ND	ND

OPPA	Oligopeptide ABC transporter periplasmic binding protein	-1.74	-1.64	-0.14
LCFA	Long-chain-fatty-acid--CoA ligase	-1.73	-2.63	-0.05
NAPA	Periplasmic nitrate reductase subunit	-1.73	-0.31	0.31
RPPH	RNA pyrophosphohydrolase	-1.70	ND	ND
ODO2	Succinyltransferase	-1.70	-1.47	-0.04
ENTC	Isochorismate synthase	-1.61	ND	1.11
XYLA	Xylose isomerase	-1.60	-0.21	-0.09
GLPK	Glycerol kinase	-1.58	-1.39	-0.06
GLNQ	L-glutamine ABC transporter ATP binding subunit	-1.58	-1.41	-0.06
YEGW	Putative DNA-binding transcriptional regulator	-1.57	-0.75	0.05
FADL	Long-chain fatty acid transport	-1.56	-1.39	0.05
HISP	lysine/arginine/ornithine ABC transporter	-1.52	-2.74	-0.14
YTFJ	Unknown function	-1.46	-0.87	-0.18
PAAH	3-hydroxyadipyl-CoA dehydrogenase	-1.46	ND	ND
YEDF	Putative sulfurtransferase	-1.43	-0.91	-0.21
FLIC	Flagellar filament structural protein	-1.40	-0.60	-0.08
DPPB	Dipeptide ABC transporter membrane subunit	-1.33	ND	ND
GLPT	Sn-glycerol 3-phosphate:phosphate antiporter	-1.32	-0.88	0.04
RIBB	3,4-dihydroxy-2-butanone-4-phosphate synthase	-1.30	-0.65	-0.20
ASNA	Asparagine synthetase A	-1.28	-2.35	0.06
YNJH	Unknown function	-1.24	-1.57	-0.18
MALM	Maltose regulon periplasmic protein	-1.21	-1.11	-0.11
GLPQ	Glycerophosphoryl diester phosphodiesterase	-1.17	-0.67	-0.06
MTFA	Mlc titration factor	-1.17	-1.02	-0.18
RIHC	Ribonucleoside hydrolase	-1.16	-1.11	-0.36
FLIY	L-cystine-binding protein	-1.16	-0.76	-0.18
GSIB	Glutathione ABC transporter periplasmic binding protein	-1.16	-0.21	ND
OPPF	Oligopeptide transport ATP-binding protein	-1.15	-0.51	-0.06
RBSB	Ribose ABC transporter periplasmic binding protein	-1.15	-1.07	-0.13
CHEB	Vhemotaxis protein	-1.07	-0.93	-0.03
YIDQ	Unknown function	-1.07	-1.54	0.32
CSPD	DNA replication inhibitor	-1.06	-0.95	0.09
PSPE	Tthiosulfate sulfurtransferase	-1.04	-0.50	-0.25
TAR	Methyl-accepting chemotaxis protein II	-1.00	-0.72	-0.11
NUDL	Unknown function	6.29	ND	ND
SLP	Starvation lipoprotein, involved in acid resistance	6.16	6.01	-0.22
HDEA	Acid stress chaperone	6.02	5.59	0.16
DCEB	Glutamate decarboxylase B	5.5	6.91	0.27

LDCI	lysine decarboxylase 1	4.79	5.38	0.49
YMGD	Unknown function	3.7	4.95	-0.04
OSMB	Osmotically-inducible lipoprotein	2.9	4.18	0.26
SFGH1	S-formylglutathione hydrolase	2.48	ND	ND
YHAM	Putative L-cysteine desulfidase	2.45	1.28	0.75
MLTB	Membrane-bound lytic murein transglycosylase B	2.38	0.47	0.06
MLIC	Membrane-bound lysozyme inhibitor	2.27	2.73	0.09
EPTA	Phosphoethanolamine transferase	2.27	2.20	0.20
MSCS	Small conductance mechanosensitive channel	2.11	0.99	0.11
CFA	Cyclopropane fatty acyl phospholipid synthase	2.10	0.98	0.03
NUPC	Nucleoside: H + symporter	2.00	0.90	0.34
HSLJ	Lipoprotein implicated in Novobiocin resistance	1.91	2.28	0.31
YECN	Unknown function	1.83	ND	ND
APBE	FAD:protein FMN transferase	1.71	-0.53	-0.08
DEOC	Deoxyribose-phosphate aldolase	1.71	1.78	0.06
CDD	Cytidine/deoxycytidine deaminase	1.63	1.76	-0.05
TYPH	Thymidine phosphorylase	1.6	1.59	-0.04
DEOB	Phosphopentomutase	1.57	1.56	0.05
HHA	Hemolysin expression-modulating protein	1.47	ND	ND
SUFD	Fe-S cluster scaffold complex subunit	1.39	ND	ND
UDP	UDP-glucose	1.38	2.01	-0.05
USPD	Universal stress protein D	1.35	1.52	0.24
G6PI	Lucose-6-phosphate isomerase	1.29	1.56	-0.02
KPYK1	Pyruvate kinase I	1.28	1.57	0.12
EDD	Phosphogluconate dehydratase	1.27	0.67	0.07
MLTA	Membrane-bound lytic murein transglycosylase A	1.24	0.48	0.23
OMPX	Outer membrane protein X	1.24	1.19	0.26
ODP2	Dihydrolipoamide acetyltransferase	1.23	1.43	0.04
GPMI	2,3-bisphosphoglyerate-dependent	1.13	1.35	0.12
YIAD	Family lipoprotein	1.09	1.06	0.17
TESB	Acyl-CoA thioesterase II	1.04	0.71	-0.05
FRSA	Fermentation-respiration switch protein	1.04	1.34	0.08
RNPH	RNA pyrophosphohydrolase	1.03	1.16	-0.22
GSP	Glutathionylspermidine synthetase	1.01	1.19	-0.04

[a]Values in grey indicate no significant change; ND: no detected.

Table S 2 Proteins significantly regulated in *ΔhflKC* grown in TB anaerobic

Protein	Function	Log_2 (Fold change)[a]
Respiratory proteins		*ΔhflKC* vs *WT*
ISPG	Oxidoreductase, Isoprenol biosynthesis	-3.53
UBIT	Anaerobic ubiquinone biosynthesis	-1.52
UBIE	Ubiquinone biosynthesis	-1.17
NARG	Oxidoreductase, nitrate reductase	1.43
AIDB	Putative acyl-CoA dehydrogenase	1.39
NARH	Oxidoreductase, nitrate reductase	1.33
Other proteins		
AG43	Antigen 43	-3.43
FLHD	Flagellar transcriptional activator	-3.06
ASNA	Asparagine synthetase A	-2.09
HISP	lysine/arginine/ornithine ABC transporter	-1.72
RBSR	DNA-binding transcriptional repressor	-1.63
ISCR	DNA-binding transcriptional activator	-1.39
YDCI	DNA-binding transcriptional dual regulator	-1.32
YDHC	Putative transporter	-1.30
FIEF	Ferrous-iron efflux pump	-1.28
FLIL	Flagellar biosynthesis protein	-1.20
ILVB	Acetolactate synthase	-1.10
FTSB	Cell division protein	-1.08
NARJ	Molybdenum-cofactor-assembly chaperone	3.45
FIMH	Minor component of type 1 fimbriae	3.03
DCEB	Glutamate decarboxylase B	2.74
FIMG	Minor component of type 1 fimbriae	2.22
YEHZ	Glycine betaine-binding protein	1.98
YDJN	Uncharacterized protein	1.97
DCEA	Glutamate decarboxylase A	1.96
GADC	Glutamate/gamma antiporter	1.65
ACPH	Acylaminoacyl-peptidase	1.57
YMGG	Uncharacterized protein	1.51
HDEA	Acid stress chaperone	1.48
SLP	Starvation lipoprotein, acid resistance	1.33
INTA	Prophage integrase	1.26
YRDB	Uncharacterized protein	1.25
YNBE	Uncharacterized protein	1.22
HYAF	Hydrogenase-1 operon protein	1.17
MDTF	Multidrug efflux pump	1.06
FIMF	Minor component of type 1 fimbriae	1.04
IVY	Inhibitor of vertebrate lysozyme	1.04
PPA	Inorganic pyrophosphatase	1.04

HDEB	Acid stress chaperone	1.03

[a]Values in grey indicate no significant change.

Table S 3 Abundance of fatty acids identified in *ΔhflKC* and WT

Fatty acid	*ΔhflKC*	WT	Fatty acid	*ΔhflKC*	WT
LPC 30:8	208966.8	199864.7	PE 30:1	350780402.0	272563795.5
LPE 13:0	41865808.9	35065018.3	PE 32:1	667712.0	522073.0
LPE 14:0	445216.2	248281.4	PE 31:2	5466972.6	818722.6
LPE 14:0	266974.0	240611.4	PE 31:2	2089153.1	315955.5
LPE 15:0	859217.6	209745.2	PE 34:5	18249.6	82885.7
LPE 15:0	291271.0	73562.6	PE 30:0	145609725.6	125987061.0
LPE 16:0	10498444.5	12461773.9	PE 30:0	5932328.2	719896.1
LPE 16:0	820234.6	773207.2	PE 32:1	315281663.6	88143156.4
LPE 16:1	4030591.5	6204793.2	PE 30:2	4527747.8	3332292.1
LPE 16:1	1205834.1	1568178.3	PE 30:2	320739.4	274965.7
LPE 17:0	1707702.2	634616.3	PE 35:3	563256.7	113957.9
LPE 17:0	1707702.2	634616.3	PE 30:1	104627993.0	81524628.1
LPE 17:1	10499678.3	2716361.5	PE 31:1	292767834.3	96312607.4
LPE 17:1	3036928.6	730854.4	PE 31:1	240206701.7	42657380.1
LPE 18:1	4070689.0	4918138.9	PE 31:1	623139.2	173345.8
LPE 18:1	2316230.6	2150893.5	PE 32:0	32970409.5	51765421.0
LPE 19:1	658778.8	137411.8	PE 32:1	1543308655.9	2073059619.9
LPE 19:1	128906.1	137411.8	PE 33:0	2571060.3	1879756.1
LPE 20:4	611046.8	571013.7	PE 33:0	1428928.1	470301.6
LPE 40:10	1224652.2	715816.7	PE 33:1	1058532796.9	521405345.8
PC 32:1	112422.0	869089.2	PE 34:0	1084591.0	2632513.6
PE 27:0	4920181.7	1058809.5	PE 35:1	33048157.9	14072201.4
PE 28:1	10560207.7	6120745.1	PE 35:1	1004004.2	500638.5
PE 28:1	1166640.3	3796504.1	PE 36:3	454138.9	342989.5
PE 28:1	3251218.7	1911235.8	PE 32:2	129406840.6	227720637.0
PE 29:0	1698699.3	630590.0	PE 32:2	5317631.9	1992976.2
PE 30:1	46090856.4	37588080.9	PE 32:2	3010573.4	3039320.2
PE 26:0	3438973.1	2584091.8	PE 32:2	576550.9	598820.2
PE 28:0	23437904.0	13987355.0	PE 33:2	162767016.1	84643898.6
PE 29:1	11721405.9	1869213.8	PE 33:2	28650860.3	8672290.9
PE 29:1	2714548.3	609591.6	PE 33:2	312704.5	132112.0
PE 29:0	9980721.2	3254980.2	PE 34:2	296221966.8	330899304.7
PE 30:0	45793506.0	51629257.5	PE 33:1	235684081.2	92792558.4

PE 30:1	115860118.0	114387677.5	PE 34:1	466343224.0	844382649.7
PE 31:1	111041597.6	17027443.3	PE 34:1	46277205.1	12299456.1
PE 31:2	1580379.5	221265.7	PE 35:1	23182549.0	12810801.2
PE 31:0	10738776.0	6944635.9	PE 36:1	816091.1	265354.9
PE 31:0	3482885.8	971445.9	PE 34:2	77756423.3	9464786.0
PE 31:1	81163023.8	42673402.2	PE 34:2	19999236.6	7471227.6
PE 32:1	111142115.5	28809270.9	PE 34:3	777995.8	468605.0
PE 30:2	2915461.3	2756363.3	PE 35:2	101387820.3	48781481.8
PE 30:2	113844.0	114486.7	PE 35:2	12139587.0	4471611.2
PE 31:2	2506879.4	700061.5	PE 35:3	88541.7	42943.4
PE 32:0	9329078.8	28250888.2	PE 35:4	37577.3	39436.6
PE 32:1	627553985.7	1093662882.6	PE 36:1	4906589.3	7641453.6
PE 32:1	72498.1	149301.4	PE 36:2	98098176.9	133687374.2
PE 33:0	772470.5	1556568.4	PE 36:2	5943149.0	1410388.0
PE 33:1	561114756.5	193681416.6	PE 36:2	1491331.4	463080.7
PE 34:5	18294.1	226343.6	PE 37:2	4585351.1	1824754.2
PE 32:2	40289105.3	101875922.0	PE 54:14	7384.3	1757002.9
PE 32:2	2699478.7	717398.6	PE 42:11	870420.2	346759.4
PE 32:2	720492.7	903963.5	PE 38:2	217516.0	95671.8
PE 33:2	58208426.7	31249586.1	PE 38:5	53723.6	282903.3
PE 33:2	10044010.6	4718784.1	PE 25:0	351700.9	253223.1
PE 34:2	144631541.0	165729306.9	PE 34:3	235698.4	293810.2
PE 35:2	76019483.0	23888122.9	PG 31:1	3255143.8	2094738.8
PE 33:1	43424897.2	34069832.7	PG 33:0	1588626.9	1269250.4
PE 35:1	7315983.5	5665284.1	PG 28:0	577800.4	717749.9
PE 34:2	35130290.7	3272187.5	PG 30:0	5403785.2	6263309.2
PE 34:2	8571780.7	2286960.3	PG 30:1	3294843.2	4519971.6
PE 35:2	3750734.5	1562089.4	PG 30:1	268579.0	425998.9
PE 34:1	129960494.7	300803652.8	PG 31:1	8917771.8	6783645.1
PE 34:1	21298209.8	4164252.7	PG 30:1	1151096.0	1396425.7
PE 35:1	15013561.8	5241704.2	PG 32:0	7744797.9	10540723.1
PE 36:2	24834663.9	43868020.2	PG 32:0	1898146.5	3040604.9
PE 36:2	2676261.8	210464.2	PG 32:1	146858057.9	254726961.3
PE 37:2	2119072.1	600149.4	PG 32:1	8991413.2	3854021.2
PE 40:8	36113521.5	32866641.5	PG 32:1	1454859.0	974756.1
PE 42:11	951033.3	579885.6	PG 32:1	329171.3	509788.6
PE 30:1	3058597.3	3031658.9	PG 34:0	580771.0	1346125.5
PE 30:1	1008437.6	440686.9	PG 34:1	3576389.0	1880979.0
PE 31:1	2724750.3	1605365.1	PG 32:2	3008454.1	6313065.6
PE 32:0	461879.7	1062375.3	PG 33:2	3202266.3	2613817.2
PE 32:1	10106893.0	12794878.0	PG 33:2	1062861.9	569104.6
PE 32:2	1060352.2	1829284.5	PG 34:2	66384718.5	172847758.6
PE 33:1	2596125.3	2302065.3	PG 34:1	196790992.7	266176026.0
PE 33:2	1516027.4	1226746.3	PG 34:1	5108848.4	1121204.0
PE 34:1	4227584.4	4914934.7	PG 35:1	17486613.7	8729657.2

PE 34:1	1397271.2	291160.1	PG 34:2	2495704.4	615730.7
PE 34:2	2972087.5	1920210.2	PG 34:2	756367.5	1119655.6
PE 34:2	1885492.9	1733892.5	PG 35:2	27785132.9	22843499.5
PE 34:2	1956665.2	193215.4	PG 35:2	9934540.5	7259736.3
PE 35:1	1280597.1	336399.3	PG 34:1	45086849.4	138273695.4
PE 36:2	1068648.0	1555636.1	PG 35:1	6132775.3	3386872.0
PE 16:1	273957.8	117132.2	PG 36:1	64745688.1	145756510.1
PG 31:1	1788882.9	1725980.9	PG 36:2	104231595.0	145834510.0
PG 31:1	1283282.1	2288006.4	PG 37:2	5647695.5	3733220.5
PG 28:0	122935.0	267766.1	PG 37:2	2709142.3	1761559.9
PG 30:0	647358.8	1916548.2	PG 33:1	64216251.4	34814341.1
PG 32:1	577973.6	2084464.9	PG 33:1	29280438.8	18436607.2
PG 32:1	14154203.4	76068504.6	PG 33:1	3225990.5	2632756.5
PG 32:1	1099505.6	881132.5	PG 33:1	1385093.5	2108788.7
PG 33:2	738011.2	1041213.4	PG 33:1	309475.3	167324.2
PG 32:0	9164007.3	20639833.1	PG 31:0	5913604.5	3993671.8
PG 32:0	1065902.2	3274128.0	PG 33:0	1176271.2	623980.2
PG 34:0	11159459.2	36160400.7	PG 29:0	862537.5	517063.9
PG 32:2	601063.9	6480245.2	LPG 13:0	165093347.9	165949326.1
PG 35:2	2158850.4	4514642.2	PE 26:1	383188.8	107467.1
PG 30:1	495496.1	1523726.9	PE 27:0	10787675.1	2850983.0
PG 30:1	193521.1	661911.5	PE 28:1	15590882.8	7843978.7
PG 34:2	879573.8	116628.7	PE 28:1	7557632.3	2818672.6
PG 35:2	6270728.6	14737900.5	PE 28:1	1436734.9	3230294.6
PG 37:2	584297.7	464225.9	PE 26:0	6573786.8	3651468.9
PG 32:1	3669461.8	6567173.9	PE 27:1	410164.6	29457.9
PG 33:1	13914361.7	12056191.8	PE 27:1	288061.3	118549.3
PG 33:1	5146975.9	7211519.6	PE 29:0	31606518.2	8426496.5
PG 33:1	4307813.9	5285273.1	PE 29:0	4073186.9	661835.1
PG 34:1	13141402.2	71129208.8	PE 29:1	19885247.7	2764431.6
PG 34:1	689253.0	213430.9	PE 29:1	6727584.9	930446.2
PG 35:1	527584.6	532584.1	PE 29:1	807527.6	296830.8
PG 36:2	16904315.0	52703971.4	PE 30:1	2143454.1	1744182.4
PG 35:1	1522542.7	1960815.4	PE 31:0	30931403.2	11061994.4
PG 31:0	6250106.0	6532943.0	PE 31:0	9121020.7	2113331.9
PG 33:1	3310952.8	3258382.2	PE 31:0	415429.1	94051.0
LPC 36:10	1702642.1	1524824.3	PE 28:0	57794074.7	31652535.9
LPE 13:0	25282293.9	19737103.7	PE 28:0	758620.7	186027.4
LPE 14:0	280990.0	181473.5	LPE 17:1	1682012.9	595228.8
LPE 14:0	207679.0	124456.5	LPE 18:0	177943.8	190093.5
LPE 15:0	606633.2	126665.7	LPE 18:1	3156925.9	2874930.7
LPE 15:0	251478.7	38518.0	LPE 18:1	1414651.0	1279968.6
LPE 16:0	6201155.9	6708294.9	LPE 19:1	367102.7	61817.0
LPE 16:0	602396.2	402915.5	LPE 20:4	387502.9	289255.8
LPE 16:1	3278328.9	3592915.9	LPE 38:10	38048032.3	26099045.8

LPE 16:1	793044.0	858164.9	LPE 38:10	14320993.9	9126409.6
LPE 17:0	864592.9	263957.0	LPE 40:10	4538667.4	1998798.3
LPE 17:0	82022.8	86964.8	LPE 19:1	99647.1	97821.9
LPE 17:1	6174913.9	1457631.3			

Table S 4 Proteins significantly regulated in IspG knockdown grown in TB

Protein	**Function**	**Log_2 (Fold change)[a]**
Respiratory proteins		YYdCas9 + pMI112 0.2uM aTc vs YYdCas9 + pgRNA
NARG	Nitrate Reductase A Subunit Alpha	-7.99
NIRB	Nitrite Reductase	-5.83
NARH	Nitrate Reductase A Subunit Beta	-5.25
NIRD	Nitrite Reductase	-5.15
LLDD	L-lactate dehydrogenase	-4.62
ISPG	Oxidoreductase involved in isoprenol biosynthesis	-4.20
YFCG	Disulfide Bond Oxidoreductase	-2.84
HYBA	Hydrogenase 2 Iron-Sulfur Protein	-2.77
GLPC	Anaerobic Glycerol-3-Phosphate Dehydrogenase Subunit C	-2.65
NAPA	Periplasmic Nitrate Reductase Subunit	-2.47
SDHD	Succinate:Quinone Oxidoreductase, Membrane Protein	-1.85
GLPB	Anaerobic Glycerol-3-Phosphate Dehydrogenase Subunit B	-1.67
GLPA	Anaerobic Glycerol-3-Phosphate Dehydrogenase Subunit A	-1.54
PUTA	Oxidoreductase, proline dehydrogenase	-1.52
MQO	Malate:Quinone Oxidoreductase	-1.36
STHA	Oxidoreductase, NAD(P)+ transhydrogenase	-1.28
MAO2	Malate dehydrogenase	-1.27
ALDA	Lactaldehyde dehydrogenase	-1.25
FRDB	Fumarate Reductase Iron-Sulfur Protein	-1.21
FRDA	Fumarate reductase flavoprotein subunit	-1.15
ENTA	2,3-dihydro-2,3-dihydroxybenzoate dehydrogenase	-1.12
SUCC	Succinyl-CoA synthetase subunit β	-1.12
SDHB	Succinate dehydrogenase iron-sulfur subunit	-1.09
SUCD	Succinyl-CoA synthetase subunit α	-1.03
SDHA	Succinate dehydrogenase flavoprotein subunit	-0.98
DHSD	Oxidoreductase, succinate dehydrogenase cytochrome b	-0.96
YEIQ	Putative Oxidoreductase	-0.95
DADA	D-amino acid dehydrogenase	-0.90
UBIE	Ubiquinone biosynthesis	-0.88
FADE	Acyl-CoA dehydrogenase	-0.79
CYOA	Cytochrome bo(3) ubiquinol oxidase subunit 2	-0.78

DHG	Quinoprotein glucose dehydrogenase	-0.70
NRDI	Dimanganese-Tyrosyl Radical Cofactor Maintenance Flavodoxin	-0.70
CYOB	Cytochrome bo(3) ubiquinol oxidase subunit 1	-0.69
ODO1	Oxidoreductase, 2-oxoglutarate dehydrogenase	-0.67
YKGF	L-lactate dehydrogenase complex protein	4.12
YKGE	L-lactate dehydrogenase complex protein	2.59
SRLD	Sorbitol-6-phosphate 2-dehydrogenase	1.92
ADHE	Fused acetaldehyde-CoA dehydrogenase	1.60
FHUF	Ferric-siderophore reductase	1.58
CYDB	Cytochrome bd-I ubiquinol oxidase subunit 2	1.41
DHNA	NADH:quinone oxidoreductase II	1.18
CYDA	Cytochrome bd-I ubiquinol oxidase subunit 1	1.16
AIDB	Putative acyl-CoA dehydrogenase	1.12
IDND	L-idonate 5-dehydrogenase	1.08
YGHA	NADP(+)-dependent aldehyde reductase	1.04
POXB	Pyruvate dehydrogenase (quinone)	1.01
HISX	Histidinol dehydrogenase	0.97
LDHD	D-lactate dehydrogenase	0.97
ADHP	Ethanol dehydrogenase	0.93
YGHU	Oxidoreductase, organic hydroperoxide reductase	0.88
CURA	NADPH-dependent curcumin reductase	0.86
NQOR	NAD(P)H:quinone oxidoreductase	0.79
GLRX2	Reduced glutaredoxin 2	0.76
GATD	Galactitol-1-phosphate 5-dehydrogenase	0.67
AHPF	Oxidoreductase, alkyl hydroperoxide reductase	0.62
YDGJ	Putative oxidoreductase	0.61

Table S 5 Significantly regulated proteins in *ΔarcB* grown in TB

Protein	**Function**	**Log_2 (Fold change)[a]**
Respiratory proteins		*ΔarcB* vs WT
NIRB	Nitrite reductase (NADH) large subunit	-5.72
NAPA	Periplasmic nitrate reductase subunit	-4.21
QUEG	Epoxyqueuosine reductase	-3.68
DMSB	Dimethyl sulfoxide reductase subunit B	-3.42
CYDA	Cytochrome bd-I ubiquinol oxidase subunit 1	-2.70
CYDB	Cytochrome bd-I ubiquinol oxidase subunit 2	-2.63
UBIT	Anaerobic Ubiquinone Biosynthesis	-2.56
YAHK	Aldehyde reductase, NADPH-dependent	2.02
HISX	Histidinal/histidinol dehydrogenase	2.03
PUTA	Oxidoreductase proline to glutamate	2.07
GPR	L-glyceraldehyde 3-phosphate reductase	2.08
FADJ	3-hydroxyacyl-CoA dehydrogenase	2.08

NUOH	NADH:quinone oxidoreductase subunit H	2.10
ACDH	Acetaldehyde dehydrogenase	2.22
NUOM	NADH:quinone oxidoreductase subunit M	2.32
YCAK	Putative oxidoreductase	2.37
YBIC	Hydroxycarboxylate dehydrogenase B	2.45
HCAD	Putative 3-phenylpropionate	2.51
IDH	Isocitrate dehydrogenase	2.54
MQO	Malate:quinone oxidoreductase	2.55
POXB	Pyruvate oxidase	2.61
MDH	Malate dehydrogenase	2.66
CURA	NADPH-dependent curcumin/dihydrocurcumin reductase	2.89
ADHE	Bifunctional aldehyde-alcohol dehydrogenase	2.93
SDHB	Succinate:quinone oxidoreductase, iron-sulfur cluster binding protein	3.03
SDHA	Succinate:quinone oxidoreductase, FAD binding protein	3.07
DHSD	Succinate:quinone oxidoreductase	3.15
ODO2	Dihydrolipoyltranssuccinylase	3.20
SUCD	Succinyl-CoA synthetase subunit alpha	3.28
ALDA	Aldehyde dehydrogenase A	3.31
SUCC	Succinyl-CoA synthetase subunit beta	3.34
DADA	D-amino acid dehydrogenase	3.52
IDND	L-idonate 5-dehydrogenase	3.82
ABDH	Gamma-aminobutyraldehyde dehydrogenase	3.82
LLDD	L-lactate dehydrogenase	4.04
FADE	Acyl-CoA dehydrogenase	4.12
GABD	Succinate-semialdehyde dehydrogenase	4.24
YKGE	Putative lactate utilization oxidoreductase	4.40
LHGO	L-2-hydroxyglutarate dehydrogenase	4.53
SRLD	Sorbitol-6-phosphate 2-dehydrogenase	5.14
SODC	Superoxide dismutase (Cu-Zn)	5.15
YKGF	Putative amino acid dehydrogenase with NAD	5.35
ASTD	Aldehyde dehydrogenase	6.07
Other proteins		
YEER	inner membrane protein	-5.89
NIRD	Nitrite reductase (NADH) small subunit	-5.17
TDCB	Catabolic threonine dehydratase	-5.00
NIRC	Nitrite transporter	-4.99
YFDC	Unknown function	-4.28
AG43	Biofilm formation	-4.20
ADEP	Adenine:H (+) symporter	-3.93
PLAP	Putrescine:H (+) symporter	-3.41
YGIQ	Unknown function	-3.33
YGHG	Lipoprotein	-3.31
MEND	Menaquinone pathway	-3.22

ACFD	Putative lipoprotein	-2.86
CODB	Cytosine transporter	-2.75
RECN	DNA repair protein	-2.64
YDCP	23S rRNA 5-hydroxycytidine C2501 synthase	-2.63
QSEC	Sensor histidine kinase	-2.59
FEOB	Fe 2 (+) transporter	-2.45
CSPB	Cold shock-like protein	-2.43
FTNB	Putative ferritin-like protein	-2.43
CSPA	Cold shock protein	-2.42
PYRE	Orotate phosphoribosyltransferase	-2.41
YBFE	Unknown function	-2.39
FIS	DNA-binding transcriptional dual regulator	-2.37
TADA	tRNA adenosine (34) deaminase	-2.35
YDIY	Unknown function	-2.33
YJJI	Unknown function	-2.24
BCSE	c-di-GMP-binding protein	-2.24
EPMA	Enlongation factor P	-2.23
GHXP	Guanine/hypoxanthine transporter	-2.19
DEAD	ATP-dependent RNA helicase	-2.16
HYPD	Hydrogenase maturation factor	-2.12
FADL	Long-chain fatty acid transport protein	-2.09
RLMG	rRNA base methyltransferase	-2.06
RFAY	Lipopolysaccharide core heptose (II) kinase	-2.06
KDPB	K (+) transporting P-type ATPase subunit	-2.06
RAPA	RNA polymerase-binding ATPase and RNAP recycling factor	-2.06
RHLE	ATP-dependent RNA helicase	-2.05
FEOA	Ferrous iron transport protein A	-2.03
ANSP	L-asparagine transporter	-2.02
LDCI	Lysine decarboxylase 1	8.63
CSID	Glutarate dioxygenase GlaH	8.50
ASTC	Succinylornithine transaminase	7.46
YEAG	Protein kinase	5.46
ACTP	Acetate/glycolate:cation symporter	5.41
RPOS	RNA polymerase sigma factor	5.37
RMF	Ribosome modulation factor	5.30
POTF	Putrescine ABC transporter periplasmic binding protein	5.11
FADB	Fatty acid oxidation complex subunit alpha	5.03
GABT	4-aminobutyrate aminotransferase	4.83
PSIF	Phosphate starvation-inducible protein	4.83
ACSA	Acetyl-CoA synthetase	4.77
LLDR	DNA-binding transcriptional dual regulator	4.74
PTHA	Sorbitol-specific PTS enzyme IIA component	4.56
YGAM	Unknown function	4.56
YEBF	Secreted protein	4.49

UGPC	sn-glycerol 3-phosphate ABC transporter ATP binding subunit	4.43
PTHC	PTS system glucitol/sorbitol-specific EIIC component	4.22
PTHB	PTS system glucitol/sorbitol-specific EIIB component	4.13
YKGG	Unknown function	4.12
PUUA	Glutamate-putrescine ligase	4.09
METE	Novo methionine biosynthesis	4.06
YDCS	Bifunctional polyhydroxybutyrate synthase	4.05
YDIH	Unknown function	4.03
YJHG	D-xylonate dehydratase	3.97
FADA	3-ketoacyl-CoA thiolase	3.93
ASTA	Arginine N-succinyltransferase	3.93
CISY	Citrate synthase	3.83
FUCA	L-fuculose-phosphate aldolase	3.81
DPPF	Dipeptide ABC transporter ATP binding subunit	3.81
AMY2	Alpha-amylase	3.69
YDEN	Unknown function	3.63
OTC1	Ornithine carbamoyltransferase	3.61
PAAK	Phenylacetate-CoA ligase	3.58
UGPB	sn-glycerol 3-phosphate ABC transporter periplasmic binding protein	3.57
PAAJ	Beta-ketoadipyl-CoA thiolase	3.56
MGLA	ATP-binding component of a D-galactose	3.53
GLCC	DNA-binding transcriptional dual regulator	3.49
BFR	Bacterioferritin	3.49
LSRF	3-hydroxy-2,4-pentadione 5-phosphate thiolase	3.38
BLUF	Temperature-regulated antirepressor	3.35
MGLC	ATP-binding component of a D-galactose	3.20
IDNK	D-gluconate kinase, thermosensitive	3.19
YFFR	Unknown function	3.17
AES	Acetylesterase	3.17
YDEI	BOF family protein	3.12
FLGJ	Putative peptidoglycan hydrolase	3.10
MHPC	2-hydroxy-6-ketonona-2,4-dienedioate hydrolase	3.07
GALS	DNA-binding transcriptional dual regulator	3.06
ASTE	Succinylglutamate desuccinylase	2.99
YHJG	Unknown function	2.98
ALR2	Alanine racemase 2	2.97
AGAL	Alpha-galactosidase	2.96
ARGT	lysine/arginine/ornithine binding protein	2.90
FUMC	Fumarase C	2.88
YAHO	Unknown function	2.87
DGAL	Methyl-galactoside ABC transporter binding protein	2.86
KBAZ	Putative tagatose-1,6-bisphosphate aldolase 1 chaperone	2.86
PHSM	Maltodextrin phosphorylase	2.81

FUCK	L-fuculokinase	2.75
XYLF	Xylose ABC transporter periplasmic binding protein	2.73
ALF1	Fructose-bisphosphate aldolase class I	2.72
DPPA	Dipeptide ABC transporter periplasmic binding protein	2.71
FRLB	Fructoselysine 6-phosphate deglycase	2.70
TREA	Periplasmic trehalase	2.70
DPPC	Dipeptide ABC transporter membrane subunit	2.68
YBGS	Unknown function	2.67
OTSA	Trehalose-6-phosphate synthase	2.66
SRA	Ribosome-associated protein	2.64
CSPD	DNA replication inhibitor	2.64
YIGI	Putative thioesterase	2.61
FUMA	Fumarase A	2.61
YNIA	Putative kinase	2.59
YEBV	Unknown function	2.58
MTFA	Mlc titration factor	2.55
OSMY	Periplasmic chaperone	2.53
PGPC	Phosphatidylglycerophosphatase C	2.50
TALA	Transaldolase A	2.49
YTFQ	Galactofuranose ABC transporter binding protein	2.48
PHOH	ATP-binding protein PhoH	2.48
YJHH	Putative 2-dehydro-3-deoxy-D-pentonate aldolase	2.44
YDCI	DNA-binding transcriptional dual regulator	2.43
PTKA	PTS system galactitol-specific EIIA component	2.42
YQHA	Unknown function	2.40
HISQ	Histidine transport permease	2.38
ELAB	Unknow function	2.36
CLSC	Cardiolipin synthase C	2.36
YBAY	Unknown function	2.36
GCSP	Glycine decarboxylase	2.34
PAAB	Phenylacetyl-CoA 1,2-epoxidase subunit B	2.33
RBBA	Ribosome-associated ATPase	2.32
ARAF	Arabinose ABC transporter periplasmic binding protein	2.32
MALQ	4-alpha-glucanotransferase	2.30
PTKB	PTS system galactitol-specific EIIB component	2.30
CUTA	Copper binding protein	2.29
TRG	Methyl-accepting chemotaxis protein	2.28
IDNO	5-keto-D-gluconate 5-reductase	2.27
ECNB	Bacteriolytic entericidin B lipoprotein	2.27
YEGP	Unknown function	2.26
TAM	Trans-aconitate 2-methyltransferase	2.26
ACNA	Aconitate hydratase 1	2.23
CFA	Cyclopropane fatty acyl phospholipid synthase	2.22
FADI	3-ketoacyl-CoA thiolase	2.22
TKT2	Transketolase 2	2.22

PTTBC	PTS system trehalose-specific EIIBC component	2.21
GLGB	1,4-alpha-glucan branching enzyme	2.18
TNAA	Tryptophanase	2.18
OPPB	Murein tripeptide ABC transporter	2.18
GARL	Alpha-dehydro-beta-deoxy-D-glucarate aldolase	2.17
MALE	Maltose binding protein	2.13
YEGR	Unknown function	2.12
YODC	Unknown function	2.10
FLGM	Anti-sigma factor for FliA	2.06
TAR	Methyl-accepting chemotaxis protein	2.03
DPPD	Dipeptide ABC transporter ATP binding subunit	2.03
GATY	Tagatose-1,6-bisphosphate aldolase 2	2.02
OMPF	Outer membrane porin F	2.02
TREC	Trehalose-6-phosphate hydrolase	2.01

[a]Values in grey indicate no significant change.

Table S 6 Significantly regulated proteins in *ΔhflKC ΔarcB* grown in TB

Protein	**Function**	**Log_2 (Fold change)[a]**
Respiratory proteins		*ΔhflKC_ΔarcB* vs *ΔarcB*
YAHA	Aldehyde Reductase, Nadph-Dependent	-2.62
UBIT	Anaerobic Ubiquinone Biosynthesis	-2.57
UXAB	Tagaturonate Reductase	-2.53
ISPG	Oxidoreductase involved in isoprenol biosynthesis	-2.33
UBIE	Ubiquinone biosynthesis	-1.64
PUTA	Oxidoreductase, proline dehydrogenase	-1.08
CYSI	Sulfite Reductase, Hemoprotein Subunit	1.13
AEGA	Putative Oxidoreductase	1.13
RCLA	Cupric Reductase	1.14
DKGA	Methylglyoxal Reductase	1.16
GLRX2	Reduced Glutaredoxin 2	1.23
HDHA	7-Alpha-Hydroxysteroid Dehydrogenase	1.30
YAHK	Aldehyde reductase	1.43
YQJG	Glutathionyl-Hydroquinone Reductase	1.46
ABDH	Ethanol Dehydrogenase/Alcohol Dehydrogenase	1.48
ALDB	Aldehyde Dehydrogenase B	1.67
OSMC	Osmotically Inducible Peroxiredoxin	1.81
POXB	Pyruvate Oxidase	1.84
CURA	Nadph-Dependent Curcumin/Dihydrocurcumin Reductase	1.87

CATE	Oxidoreductases, Catalase-Peroxidase	2.03
NQOR	Nad(P)H:Quinone Oxidoreductase	2.11
ADHP	Ethanol Dehydrogenase	2.89
YGHA	Nadp(+)-Dependent Aldehyde Reductase	3.98
YBDR	Putative Zn(2(+))-Dependent Alcohol Dehydrogenase	4.95
FIXB	Putative Electron Transfer Flavoprotein	5.12
Other proteins		
PLAP	Putrescine:H (+) Symporter	-5.04
YHCN	Unknown function	-3.98
THIC	Phosphomethylpyrimidine synthase	-3.47
PFLD	Putative formate acetyltransferase 2	-2.82
CODB	Cytosine transporter	-2.25
FLGA	Flagellar basal body P-ring formation protein	-2.16
LDCI	lysine decarboxylase 1	-1.99
FLHD	DNAbinding transcriptional dual regulator	-1.86
CRFC	Regulator of diguanylate cyclase	-1.85
FLHC	DNA-binding transcriptional dual regulator	-1.83
FLGI	Flagellar P-ring protein	-1.75
FHUE	Ferric coprogen outer membrane receptor	-1.72
FIU	Iron catecholate outer membrane transporte	-1.70
AER	Aerotaxis receptor	-1.65
CIRA	Iron-catecholate outer membrane transporter	-1.55
PTOCB	Maltose phosphotransferase	-1.54
ADEC	Adenine deaminase	-1.52
FLGL	Flagellar hook-filament junction protein 2	-1.51
FLHE	Flagellar protein	-1.49
FLIK	Flagellar hook-length control protein	-1.47
CLSC	Cardiolipin synthase C	-1.42
YDIY	Acid-inducible putative outer membrane protein	-1.40
MOTB	Motility protein B	-1.33
YECR	Unknown function	-1.33
PTTBC	Rehalose phosphotransferase	-1.32
NANA	N-acetylneuraminate lyase	-1.28
SDAC	L-Serine:H (+) symporter	-1.25
YBIJ	Unknown function	-1.24
FLGE	Flagellar hook protein	-1.23
FLIJ	Flagellar biosynthesis protein	-1.22
OMPF	Outer membrane porin F	-1.21
YDDA	ABC Transporter family protein	-1.20
TNAA	Tryptophanase	-1.20
FLIM	Flagellar motor switch protein	-1.19
YJIY	Pyruvate:H (+) Symporter	-1.17
FLIH	Flagellar biosynthesis protein	-1.17

YBJX	Unknown function	-1.16
FLGD	Flagellar biosynthesis, Initiation of hook assembly	-1.14
FLGF	Flagellar basal-body rod protein	-1.13
FLIS	Flagellar biosynthesis protein	-1.13
TRG	Methyl-accepting chemotaxis protein	-1.13
FLIO	Flagellar biosynthesis protein	-1.13
TREC	Trehalose-6-phosphate hydrolase	-1.12
TSR	Methyl-accepting chemotaxis protein	-1.11
PSUG	Pseudouridine-5'-phosphate glycosidase	-1.11
CSTA	Pyruvate transporter	-1.10
YHJE	Inner membrane metabolite transport protein	-1.10
FLGJ	Putative peptidoglycan hydrolase	-1.10
TRUC	tRNA pseudouridine (65) synthase	-1.09
FLIC	Flagellar filament structural protein	-1.07
PUTP	Sodium/proline transporter	-1.05
DCTA	Aerobic C4-dicarboxylate transport protein	-1.04
BGLR	Beta-glucuronidase	-1.03
PQQL	Periplasmic metalloprotease	-1.02
GLPT	sn-glycerol 3-phosphate:phosphate antiporter	-1.00
GARD	Galactarate dehydratase	-1.00
FSAB	Fructose-6-phosphate aldolase 2	-1.00
DGAL	Methyl-galactoside ABC Transporter	-1.00
GM4D	Mannose 4,6-Dehydratase	7.33
YBHP	Unknown function	4.96
YHBO	Protein/Nucleic acid deglycase 2	4.51
YEGS	Lipid Kinase	4.02
UDG	Glucose 6-dehydrogenase	3.88
OTSB	Trehalose-6-phosphate phosphatase	3.24
YGDI	Uncharacterized Lipoprotein	3.01
YBGS	Unknown function	2.93
PHNB	Unknown function	2.88
YPFG	Unknown function	2.85
OSMY	Periplasmic chaperone	2.65
IDI	Isopentenyl-diphosphate delta-isomerase	2.55
MDTE	Multidrug Efflux Pump Membrane Fusion Protein	2.42
YCAC	Putative Hydrolase	2.34
MANB	Phosphomannomutase	2.30
SRA	Ribosome-Associated Protein	2.29
YCIF	Unknown function	2.26
YEAG	Protein Kinase	2.26
YGAM	Unknown function	2.26
OTSA	Trehalose-6-phosphate synthase	2.24
YGAC	Unknown function	2.24
YFDC	Unknown function	2.22
TKT2	Transketolase 2	2.22

DOSC	Diguanylate cyclase	2.19
IVY	Inhibitor of vertebrate lysozyme	2.17
DCEA	Glutamate Decarboxylase A	2.13
YDEI	Unknown function	2.05
TALA	Transaldolase A	2.03
ELAB	Tail-anchored inner membrane protein	1.99
YEGP	Unknown function	1.96
CBPA	Curved DNA-binding protein	1.88
BFR	Bacterioferritin	1.87
YJBJ	Putative stress response protein	1.87
YCCJ	Unknown function	1.85
YAIA	Unknown function	1.84
ALF1	Fructose-bisphosphate aldolase class 1	1.83
PHNO	Aminoalkylphosphonate N-acetyltransferase	1.83
YEHZ	Glycine betaine ABC transporter periplasmic	1.79
HDEB	Periplasmic acid stress chaperone	1.78
MSYB	Acidic protein	1.76
ECNB	Bacteriolytic entericidin B lipoprotein	1.76
GCS2	Carboxylate-amine ligase	1.76
WZC	Protein-tyrosine kinase	1.74
YDHS	Unknown function	1.74
PSIF	Phosphate Starvation-Inducible Protein	1.73
DPS	Dna protection during starvation protein	1.68
GADC	L-glutamate:4-aminobutyrate antiporter	1.66
OSME	Osmotically-inducible lipoprotein	1.66
YBIO	Moderate conductance mechanosensitive channel	1.62
YAHO	Unknown function	1.62
YGIW	Cellular response to hydrogen peroxide	1.60
YBAY	Uncharacterized Lipoprotein	1.59
MLIC	Membrane-bound lysozyme inhibitor	1.58
YEBF	Unknown function	1.57
FIC	Putative adenosine monophosphate	1.56
TAM	Trans-aconitate 2-methyltransferase	1.56
HCHA	Protein/Nucleic acid deglycase 1	1.56
DCEB	Glutamate decarboxylase B	1.55
CSIR	DNA-binding transcriptional repressored Protein	1.53
YNHG	D-Transpeptidase	1.48
TREA	Periplasmic trehalase	1.43
RMF	Ribosome modulation factor	1.43
INAA	Putative lipopolysaccharide kinase	1.42
YOBB	Unknown function	1.36
YHHA	Unknown function	1.36
YBJP	Unknown function	1.34
SLP	Starvation lipoprotein	1.32
YMGG	Unknown function	1.27

YHJG	Asma family protein	1.27
NHOA	Arylamine N-acetyltransferase	1.25
YQJE	Unknown function	1.24
YDIH	Unknown function	1.23
YODC	Unknown function	1.22
YQJD	Unknown function	1.22
YNIA	Putative Kinase	1.19
AG43	Biofilm formation	1.17
YJDJ	Putative N-acetyltransferase	1.13
YGAU	K (+) Binding Protein	1.12
YDCS	Putative ABC transporter periplasmic binding	1.11
YOAC	Unknown function	1.09
CSIE	Stationary phase-inducible protei Csie	1.09
CYSP	Thiosulfate/Sulfate AbBC Transporter Periplasmic Binding Protein	1.08
PFKB	6-Phosphofructokinase 2	1.05
GABT	4-aminobutyrate aminotransferase	1.03

[a]Values in grey indicate no significant change.

Acknowledgements

First and foremost, I would like to express my heartfelt gratitude to Prof. Dr. Victor Sourjik. Throughout the course of my Ph.D., he has been an exceptional supervisor, and I deeply appreciate all the discussions and scientific advice that led to the accomplishment of this work. This, would not have been possible without his guidance, motivation, and support. I am particularly grateful for the excellent working environment in AG Sourjik.

I extend my sincere thanks to the members of my thesis advisory committee, Prof. Dr. Martin Thanbichler and Dr. Andreas Diepold, for their valuable contributions and suggestions during our annual meetings. Special thanks go to my examiners: Prof. Dr. Martin Thanbichler, who also kindly reviewed this thesis, Dr. Andreas Diepold, and Prof. Dr. Lennart Randau.

I take this moment to acknowledge Dr. Jing Yuan and Dr. Gabriele Malengo for sharing their expertise and experience throughout the experiments involving protein purification and microscopy analysis. I would also like to express my gratitude to the dedicated technicians in our group, who ensured the smooth progress of this thesis by consistently providing fresh media, clean glassware, and all other necessary materials. Special thanks go to Jörg Kahnt from the proteomics facility at MPI Marburg, who was always kind and willing to collaborate in protein abundance quantification.

My warmest thanks go to all the Ph.D. students and post-docs in Sourjik's group for their valuable feedback during our lab meetings, for creating a welcoming place to work, and for the wonderful friendships that have flourished. I also want to extend my great thanks to Rogelio, Ananda, Camila, and Nataliya for their work proofreading this thesis.

Lastly, I would like to thank Dr. Dušica Radoš for her guidance and support during my Ph.D. journey. And also thanks to IMPRS students of 2019.

Constantemente me pregunto por qué dejamos las cosas más importantes para el final? Muchas veces, durante las largas noches mientras escribía este documento, venían a mi mente las palabras exactas con las que quería expresar mi gratitud. Ahora que debo escribirlas, ahora que el tiempo empieza a contar, todas las emociones e ideas se revuelven, y en el silencio intento encontrar nuevamente esas palabras con las que quiero expresar mi gratitud y todo mi amor.

En primer lugar, debo agradecer a Dios, quien ha utilizado este proceso en mi vida para acercarme a Él y conocerlo mejor. Hoy confieso que hace muchos años, sentada en una banca de la Iglesia de Cartagena a la edad de 14 años, le pedí a Dios que me permitiera estudiar en un buen colegio. Nunca imaginé los planes que Él tenía para mí! Esta tesis es el testimonio más vivo de que hablar con Dios es posible y que los anhelos de tu corazón llegan a tu vida en el momento indicado.

Mi familia lo es todo para mí, y hoy dedico esta tesis doctoral a cada uno de ellos, comenzando por mi abuelita Gabriela, a quien aún recuerdo cuando nos levantaba por las mañanas para ir al colegio con el sonido de fondo de un radio viejo. A mis padres, Héctor Pérez y Olga Lucía López, que con su esfuerzo, consejos y amor han hecho posible cada etapa en mi vida. Mis hermanos, Carlos Andrés y Héctor Augusto, a quienes amo con todo mi corazón y de los que me siento muy orgullosa por los padres que son. Mis sobrinos, Jerónimo, Gabriela y Nico (y aquellos en camino), a quienes más extrañé en este proceso y a quienes quiero que, a través de la culminación de esta tesis, sepan que el amor, el esfuerzo y la constancia pueden superar cualquier obstáculo. Sobrinos, no hay que temer a lo desconocido, hay que ser valientes y continuar. También quiero agradecer a mis tíos, quienes durante este proceso me ayudaron de diversas maneras y a quienes también les agradezco desde lo más profundo de mi corazón.

Infinitas gracias a todos mis amigos en Marburgo. Gracias por brindarme tanto amor, por siempre darme un abrazo, una voz de aliento, una sonrisa y una compañía en los momentos que más lo necesité. Gracias a Mari y su familia, a Rogelio y al "cartel de Marburgo" quienes hicieron la hora de los almuerzos el momento más divertido. A Dani, Chiraf, Ibis, Memduha y a todas las chicas de "Un café con Jesús". Son innumerables las historias y momentos que guardo en mi corazón. Gracias a mis flatmates, Sophie, Mila y Jannis, por enseñarme la cultura alemana y hacer que mi tiempo con ellos fuera muy divertido.

Aquí no solo culmino my tesis, éste ha sido un tiempo que con sus altibajos, me ha ayudado a crecer. He descubierto nuevas pasiones e intereses, he cambiado mi manera de pensar y de ver el mundo. Ahora estoy agradecida y lista para continuar con mi camino.

Erklärung

Hiermit erkläre ich, dass ich die vorliegende Dissertation mit dem Titel:

“Role of SPFH proteins in aerobic respiration in *Escherichia coli* “

selbstständig verfasst, keine anderen als die im Text angegebenen Hilfsmittel verwendet und sämtliche Stellen, die im Wortlaut oder dem Sinn nach anderen Werken entnommen sind, mit Quellenangaben kenntlich gemacht habe.

Die Arbeit wurde in dieser oder ähnlicher Form noch keiner Prüfungskommission vorgelegt.

Marburg, den _____._____._____

_____

María Isabel Pérez López